OPTICAL CHARACTERIZATION OF POLYCRYSTALLINE SEMICONDUCTORS FOR PHOTOVOLTAIC APPLICATIONS

by

Muhammed Hasan Aslan

A thesis submitted to the Faculty and Board of Trustees of the Colorado School of Mines in partial fulfillment of the requirements of the degree of Doctor of Philosophy (Applied Physics).

Golden, Colorado

Date: 1/29/99

Signed: ______________________
Muhammed Hasan Aslan

Approved: ______________________
Reuben T. Collins

Golden, Colorado

Date: 29 Jan 99

____
Dr. Don L. Williamson
Professor and Head,
Department of Physics

ABSTRACT

II-VI polycrystalline materials are under active investigation for application in solar cell technology. Optical characterization techniques are useful, economic and nondestructive for monitoring the quality of II-VI devices. Photoluminescence (PL) is one of the optical characterization techniques that is widely used to control the quality of II-VI solar cells by researchers. Particularly, PL can be used to measure the alloy composition, x, of a number of direct band gap polycrystalline compounds. Besides PL, Time-Resolved PL (TRPL) measurement methods which are based on luminescence phenomena can also be used to characterize the optical properties of the II-VI solar cell. TRPL technique allows the life time of the minority carriers to be determined.

The interdiffusion of CdTe/CdS during annealing process and $CdCl_2$ treatment plays a significant role in the operation of the solar cells. Present work studies the S diffusion into CdTe near the CdS interface. The CdTe thin films are produced by electrochemical deposition technique and the CdS is deposited by chemical bath deposition.

The characterization methods used to determine the optical and structural properties are PL, X-Ray Diffraction (XRD), TRPL, Auger Electron Spectroscopy and Atomic Force Microscopy (AFM). We have used chemical etching techniques in

conjunction with PL to study the effects of annealing temperature and $CdCl_2$ treatment on the S diffusion into CdTe. After etching process, measurements made from the CdTe side of the samples by Photoluminescence (PL) and X-Ray Diffraction (XRD) show the presence of two distinct $CdTe_{1-x}S_x$ phases within the CdTe film. Interdiffusion occurs during annealing step following a $CdCl_2$ treatment. We have profiled the S composition as a function of depth by sequentially etching the film followed by PL and XRD measurements. We find that as we approach the CdS interface, the ternary phase becomes more dominant. For samples annealed at 350 °C S concentration in the ternary phase is 1-2% near the interface. At 410 °C, which corresponds to the optimal annealing temperature for high efficiency devices, the S concentration increases from <0.1% at back face to 4-5% near CdS/CdTe interface. The 460 °C annealed sample shows around 5% S content throughout the CdTe layer. Auger Electron Spectroscopy (AES) measurements have been made to confirm these results. Measurements also made from the glass side of the sample by PL give us the opportunity to speculate about Te diffusion into CdS and changing of CdS structure at different temperatures.

TABLE OF CONTENTS

LIST OF FIGURES

LIST OF TABLES

ACKNOWLEDGMENTS

I would like to xpress my deep gratitude to Dr. Reuben T. Collins for the years of technical guidance, educational guidance, and personal help, without which I could not have achieved this work.

I wish to thank Dr. Dean H.Levi for his technical advice and for allowing me to use his TRPL and PL setup. I would like to thank Dr. Timohty R Ohno and his students, Brian Roy and Chris Kelso, for helping me to take the AES data. I would also like to thank Dr. Richard K.Ahrienkel and Dr. Victor Kaydonov for their ideas and discussions.

I deeply appreciate Dr. David Albin for providing me his materials and Dr. Don Williamson for providing financial support. I am very thankful to Jack Kintner, a master instrument maker, who made parts for my equipment.

My thanks extend to Mary Herndon, Joseph Beach , John Flory ,Wenjie Song and Jason Verley for their friendship and support.

I appreciate Dr.Tim Cross serving as the chair of my thesis committee and Mark Linne as a member of my thesis committee.

I acknowledge Gebze Institute of Technology for the financial support of my study.

DEDICATION

This thesis is dedicated to my wife, Zarlast who helped me to go through this period of intense work as well as my son, Muhammed Emir, and my parents, Güngör and Müslüm.

CHAPTER 1
INTRODUCTION

1.1 Introduction

Photovoltaic solar cell technologies that convert electromagnetic radiation into electricity are one of the most promising renewable energy sources. The most common solar cell type is based on a single pn junction. Tandem solar cells which contain more than one pn junction and have very high efficiencies (~35% (1)) have also been developed. Some of the advantages of solar cells include the following:

- they use an inexhaustible electromagnetic radiation source, the sun
- they pollute the environment much less than fossil fuel based technologies
- they don't need major maintenance
- they are modular
- they are portable.

However, they also have some disadvantages:

- the cost of energy is high compared to existing technologies
- providing power for large areas (towns, villages, etc) would involve physically large solar forms

- since they produce energy during daylight, the energy needs to be stored for night and cloudy day use.

PV power sources are presently used in applications such as satellites, calculators, watches, and road signals. These are examples of power needs in remote locations where carrying or storing power is much more expensive than in conventional applications. This feature makes PVs cost attractive. These present usages provide a guide for the next opportunities for PVs which is in third world-countries, such as Saudi Arabia, Egypt, Morocco, etc., where both building fossil fuel plants and distributing power (for example in the middle of a desert or a jungle) is expensive. Also, since PV panels can be constructed and installed in a shorter time than a large power plant, using PV technology can help solve the energy-shortage problem for such countries, which are in immediate need of additional power. Furthermore, if, in the future, the cost of PV power can be reduced sufficiently it could become an environmentally safe power source in mainstream residential and industrial applications throughout the world.

After understanding the importance of the photovoltaic systems as an alternative energy source which is becoming cost competitive with traditional energy sources (oil, gas, and nuclear power), some governments around the world began to attach importance to research on solar cells, which are a type of photovoltaic devices. The governments are still supporting the projects and programs for developing photovoltaic solar cell technologies.

The environment is another reason to develop renewable energy technologies. As an energy source, fossil fuels emit gasses that pollute the atmosphere. For example, automobile exhaust is a serious source of air pollution in large cities. Sulfur contributes to acid rain, and CO_2 as a potential connection to global warming is being investigated. Because of environmental concerns, research on renewable energies will undoubtedly grow in the next century.

1.2 Band structure of a semiconductor

This thesis is concerned with optical studies of the layers that make up thin film solar cells. In particular, the materials, which we will focus on, are the CdTe and CdS layers in thin-film CdTe-based solar cells. CdTe and CdS are direct-bandgap semiconductors. To understand and interpret optical properties of these materials requires an understanding of their band structures.

When atoms are brought together to form a crystalline solid, the electronic orbital of the individual atoms begin to overlap, and these discrete energy levels broaden into energy bands. Fig. 1.1a is a schematic diagram of the energy bands of an undoped at low temperature or T=0 K semiconductor. Here, the valence band is completely filled with electrons, while the conduction band, which is the next highest energy band, is unfilled. Since each band contains two times as many energy levels as the number of unit cells in the crystal, the atoms making up a unit cell of a semiconductor must have an even number of valence electrons. The energy gap between the bottom of the conduction band

and top of the valence band is referred to as the band gap. If a photon with an energy larger than the band gap is incident on a semiconductor, it can be absorbed by an electron from the valence which is excited to the conduction band, as shown in Fig. 1.1b.

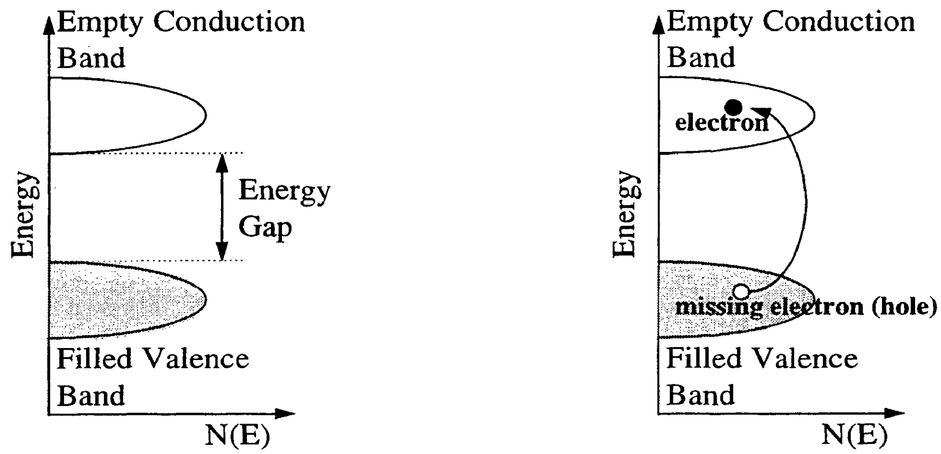

Figure 1.1 a) Illustration of energy bands of a semiconductor. b) Optical excitation of an electron in the valence band to the conduction band.

In this situation, the valence band can either be viewed as a sea of electrons with one vacant state, or, as is commonly viewed, as an empty band filled with one hole which is equivalent to the missing electron. When an electron in the conduction band recombines with a hole in the valence band, this is called electron-hole recombination. If this recombination occurs with the emission of a photon, it is called luminescence.

By exciting electron-hole pairs (ehp) optically, and studying the photoluminescence emitted under various conditions, a great deal can be learned about semiconducting materials. The material's quality, band gap, minority carrier lifetime, defect energy levels, etc. can all be characterized and understood using this technique. It is particularly well suited to studies of solar-cell materials since an understanding of the optical properties of these materials is essential to improving their performance. Much of this thesis involves photoluminescence studies of thin-film PV materials.

1.3 Photovoltaics (PV)

The photovoltaic effect is a phenomena in which an electric potential is generated when light or radiation is absorbed in a semiconductor or semiconductor junction. Solar cells typically induce use of a pn junction to generate a photovoltage or current. To understand the PV effect, we will consider a pn homojunction as shown fig. 1.2

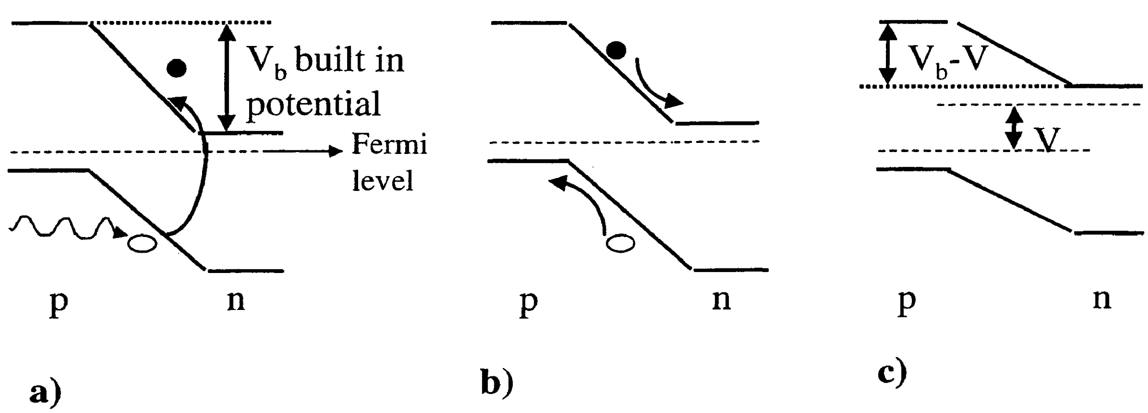

Figure 1.2 a) A photon with energy greater than the energy gap is absorbed to create electron-hole pairs. b) The electron-hole pair is separated by the built-in electric field. c) A potential difference is created by the charge separation.

After the absorption of photons with energy greater than the energy gap (fig.1.2a), electron-hole pairs are created in the depletion region adjacent to the pn junction. These charge carriers move in opposite directions under the influence of the built-in field (fig.1.2b) in the depletion region. That is, electrons move to the n region of the pn junction, and holes move to the p region. Thus, charge separation occurs. Due to this charge separation, a potential difference, V, called a photovoltage develops across the pn junction (fig.1.2c). For this situation, in which no current flows, the potential difference is called the open-circuit voltage (Voc). More detail about the current-voltage relationship can be found in reference (2).

A solar cell is basically a pn junction. Cells can be made from pn homojunctions, where n and p-type layers are composed of the same semiconductors, and pn heterojunctions, made up of different n and p-type materials. The operation of the heterojunction solar cell is the same as the pn homojunction solar cell in terms of photogeneration of carriers and diffusion or drift of carriers taking place in the junction. Heterojunction materials, however, provide a solar-cell designer a much greater degree of flexibility. When semiconductors with different band gaps are brought together to build a junction, there are likely to be discontinuities in the energy bands as the Fermi levels line up at equilibrium as shown in Fig.1.3. V_{o1} and V_{o2} and depletion widths on each side can be found by solving Poisson's equation. V_{o1} and V_{o2} are the amount of built-in potential on each side, and V_o is the built in contact potential. More details about solving Poisson's equation can be found in the Ref. (3).

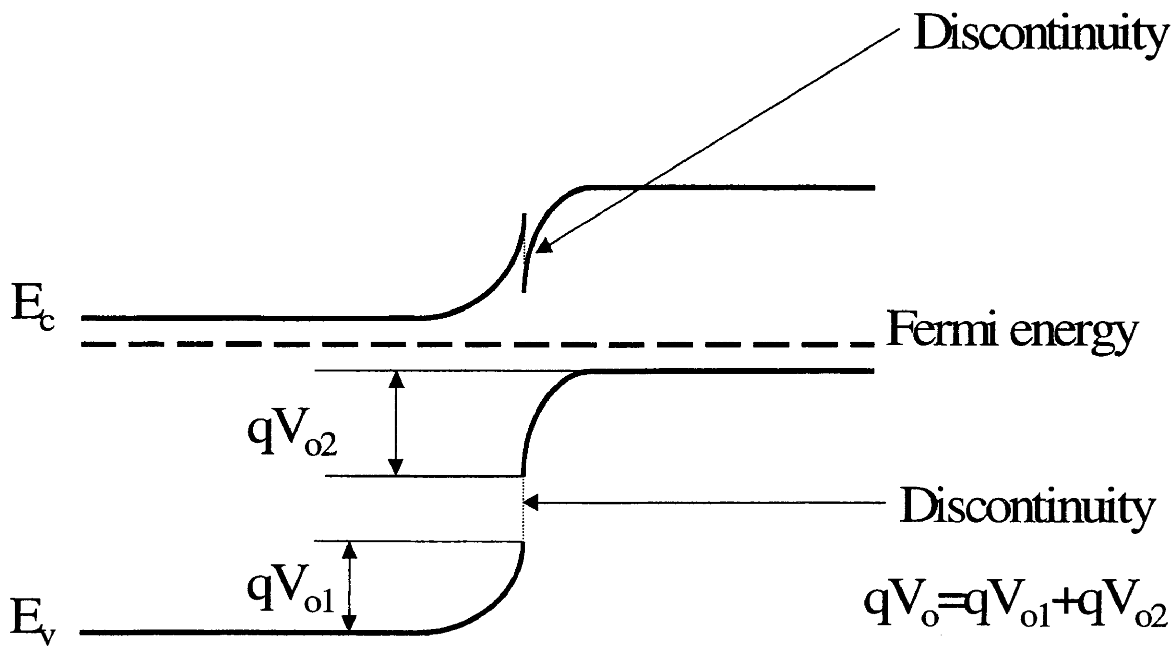

Figure 1.3 A pn heterojunction shows band discontinuities

In a heterojunction solar cell, the wider-gap material can be used to avoid photogeneration and recombination in certain regions. For this reason, the wide-gap semiconductor (the case of CdTe/CdS cells, CdS width E_g > 2.4 eV at room temperature and 2.58 at 4.2 K (4)) is made so wide that most of the photons in the solar spectrum pass through without being absorbed. This kind of material becomes a window layer. The semiconductor that has a small band gap is used as an absorber, and it can be made the only absorber in the heterojunction solar cell.

1.4 Thin-film CdS/CdTe solar cells

There are several competing materials in PV technologies. Single crystal Si and GaAs based solar cells have been commercially available since the 1980's. They are generally used in the form of small modules. These solar cells are also fairly expensive sources of power compared to fossil fuels. For these reasons, a great deal of recent effort in PVs has been directed at thin-film solar cells. This is because they require very little semiconductor material, use low-cost deposition techniques, and can be manufactured much less expensively than the crystalline solar cells in large area modulus.

$CuInSe_2$ (CIS), CdTe and amorphous-Si (a-Si:H) are the most promising materials for the fabrication of thin-film solar cells. Cells made of a-Si:H have actually been manufactured for many years and are available commercially. Efficiency of a-Si:H, however, tends to be limited to 10%-12% (5). On the other hand, CIS and CdTe have high absorption coefficients, 10^5 cm^{-1}, suitable band gaps, 0.95 eV for CIS, and 1.51 eV for CdTe (6), which we chose to use in our study, and good stability. Because of these particular properties, thin film technologies using $CuInSe_2$ and CdTe are being investigated to improve their performance and decrease PV costs. Lately, scientists from NREL have achieved 17.7% efficiency in lab-prepared $CuInSe_2$ thin-film solar cells (7). Since the theoretical efficiency of (n)CdS/(p)CdTe has been reported to be 27.5% (8) and 16% has been achieved in the lab. (9), this is also a very attractive material and is potentially important.

The typical (n)CdS/(p)CdTe solar-cell design is shown in fig.1.4. The antireflection coating is used to keep the solar cell from reflecting light back away from the cells. The substrate is generally made of glass to reduce cost. A transparent-conductive-oxide layer (TCO) is deposited on the glass to act both as a window layer and electrical contact. In typical cells, this is tin oxide (TO) or indium tin oxide (ITO). The highest efficiencies (>10%) have been achieved with TO layers in conjunction with thin n-type CdS (10-12). The CdS forms the n-type region of a pn heterojunction with the next layer, p-type CdTe. The thickness of the n-type CdS layer is typically 100-200 nm and the thickness of CdTe is 1-5μm. It is possible for n-type CdS to be deposited by one of several deposition techniques, such as chemical spray (13), chemical bath deposition (CBD) (14), close-space sublimation (CSS) (9) and thermal evaporation (15).

To form the n-type CdS/p-type CdTe solar cell, CdTe is deposited on the n-type CdS. There are several deposition techniques being investigated, such as atomic layer epitaxy (16), chemical vapor deposition (17), chemical spray deposition (18), close-space sublimation (9), and electrodeposition (11). As shown in fig.1.4, the CdS/CdTe thin-film solar cell is a pn heterojunction diode.

As deposited-CdTe is often an n-type material. To make it a p-type material and promote grain growth, the films are annealed at around 400°C in the presence of oxygen. After CdTe deposition and before annealing, a $CdCl_2$ coating can be applied to the CdTe surface to obtain larger CdTe grain size (19).

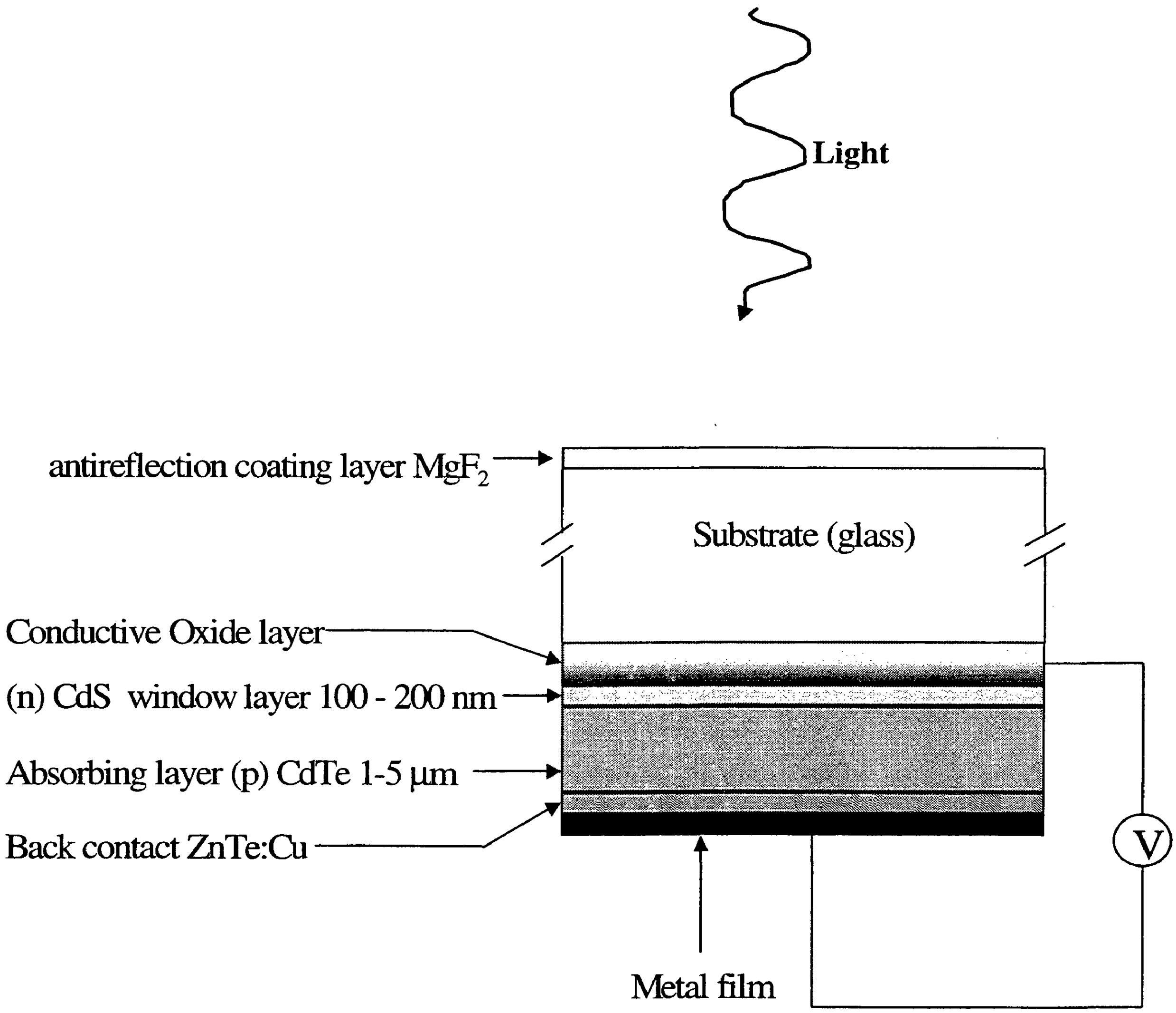

Figure 1.4 A CdS(n)/CdTe(p) solar cell

1.5 Electro-Optical properties and structure of CdTe

CdTe has a direct band gap with 1.51 eV at room temperature and 1.606 eV at liquid helium temperature. The 1.51eV band gap is close to the optimum band gap for absorption of the solar spectrum. Due to the direct band gap properties, the absorption coefficient is so high that most of the incident radiation with an energy higher than the band gap is absorbed within a few ($\sim 2\mu m$) microns of the CdTe surface.

In this thesis, we used the X-Ray Diffraction spectroscopy in order to support the results of photoluminescence measurements which were performed on the CdTe/CdS solar cells. To interpret the structural properties of CdTe, the crystal structure of this material needs to be understood. Cadmium is one of the IIB elements, and Tellurium belongs to VIA group in the periodic table. The compound CdTe has an average of 4 electrons per atom in the last shell. The stable CdTe structure is zinc-blend (cubic, fig.1.5) and its lattice-constant is 6.481Å. According to Ref. (20), the ternary phase $CdTe_{1-x}S_x$ formed due to S diffusion in to CdTe mostly has a zinc-blend structure for CdTe rich CdTe/CdS solar cell.

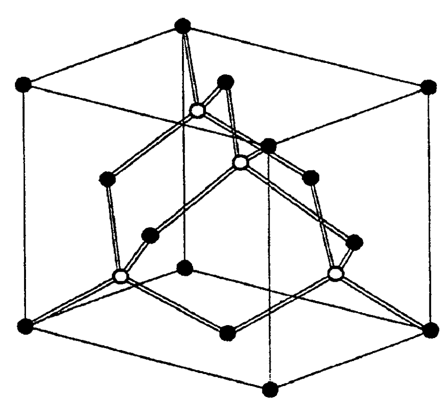

Figure 1.5 A illustration of zinc-blend structure

CHAPTER 2
BACKGROUND

2.1 Optical characterization

The key word for optical characterization is light or electromagnetic radiation. Electromagnetic radiation affects the charged particles in a semiconductor (e.g. the electrons and holes in the valence and conduction bands). Therefore optical characterization techniques such as x-ray diffraction, x-ray photoelectron spectroscopy, ellipsometry, surface analysis by laser ionization, photoluminescence etc. which use wavelengths from the ultraviolet to infrared range are very powerful tools to examine structural and electronic aspects of semiconductors.

In this study, experimental studies were performed by using photoluminescence. Photoluminescence can characterize different layers of the device easily and sensitively. From the standpoint of this thesis, the importance of photoluminescence is its ability to analyze the intrinsic (band gap) and extrinsic properties (density of impurities, type of impurities and defects) of semiconductors determining whether a semiconductor will be useful or not for a specific application. Understanding these properties can help to create better devices and to monitor the material quality. There are two key phenomena to make measurements by using photoluminescence techniques; absorption and recombination.

2.2 Optical absorption of above band gap light

As mentioned above, when a photon with an energy hν which is greater than the band gap energy E_g, impinges on a semiconductor its energy can excite electrons located in the valence band to the conduction band leaving a hole in the valence band. In this way, electron-hole pairs are created. The whole process is called optical absorption. The electron–hole pairs which are created by optical absorption are also called excess carriers. Since the momentum of a photon is small and both momentum and energy must be conserved in the absorption process, as well as no other particle such as phonon, etc, is involved in the process, the transitions will occur vertically in momentum or k-space (fig.2.1.),

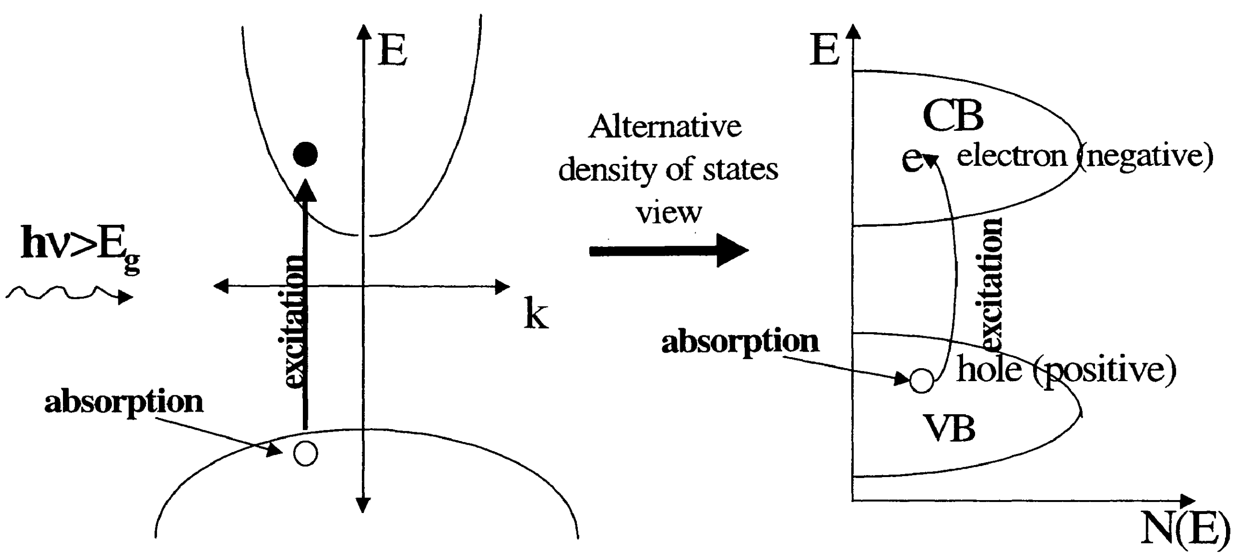

Figure 2.1 An illustration of absorption and excitation in a semiconductor

If a beam of photons with $h\nu > E_g$ is sent into a semiconductor, a certain fraction of photons will be absorbed and the rest will be transmitted. The ratio of absorbed to transmitted photons at the material depends on the properties of material, wavelength of photon and thickness of the material. This ratio can be formulated with differential eq. (1)

$$-\,dI(x)/\,dx = \alpha I(x) \tag{1}$$

and solution to this equation is

$$I(x)=I_o \exp[-\alpha x] \tag{2}$$

where α is called the absorption coefficient and has units of cm^{-1} and I is the intensity as a function of depth. If a photon has energy less than E_g, it cannot excite an electron from the valence band to the conduction band. Thus there is negligible absorption of photons for $E<E_g$. The absorption coefficient will vary with the photon wavelength as shown in fig. 2.2.

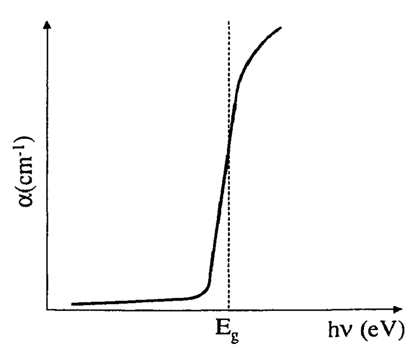

Figure 2.2. A general picture of absorption coefficient, α, versus incident light energy, $h\nu$, for a semiconductor material where E_g is the band gap of semiconductor.

In this thesis, for different excitation energies, the absorption coefficients of CdTe were calculated by using eq.(3)

$$\alpha = 4\pi k/\lambda \tag{3}$$

where λ is the wavelength of the excitation source and k is the extinction coefficient which is obtained from ref.(21). More theoretical details about eq.(3) can be found in Ref. (2)

2.3 Recombination

After the absorption process, the electrons and holes that are generated as excess carriers recombine. This process can either be radiative, in which a photon is emitted, or non-radiative. The radiative recombination is in some sense, the inverse of the absorption process.

2.3.1 Radiative recombination

When an excited electron recombines with a hole and gives off its excess energy as light, the emission is called luminescence. Radiative recombination can generally occur in five types of different transitions which are band to band, free excitonic, bound excitonic, donor-acceptor, band to acceptor (or donor) and deep level.

2.3.1.1 Band to band

As we explained in the previous section, the generation process involves optical absorption and the creation of electrons and holes or free carriers in the band states. At room temperature, the free carriers can then recombine radiatively directly from the conduction band to valence band. This is called a band to band transition fig.2.3. As temperature is reduced, the occupancy of band states decreases relative to defect states, and band-to-band transition became statistically less likely.

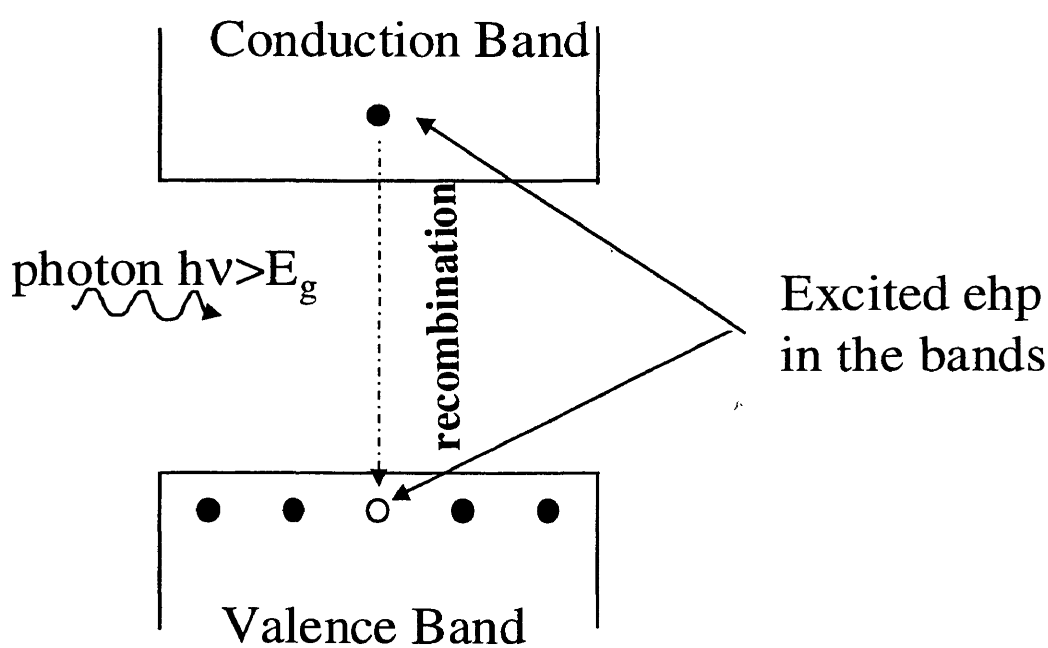

Figure 2.3 Band-to-band transition

2.3.1.2 Free Exciton

A free exciton is a hydrogen-like atom system consisting of a free electron and hole attracting each other due to the coulombic force. The ionization energy of an exciton is

$$E_x = \frac{m^* e^4}{2h^2 \varepsilon^2 n^2} \tag{4}$$

(n=1,2,3...) where n is an integer and for the ground state (n=1), it is approximately 10 meV for a typical semiconductor. m^* is reduced effective mass of the electron and hole system given by

$$m^* = \frac{m_e^* m_h^*}{m_e^* + m_h^*} \tag{5}$$

Since the effective mass of an electron and hole are larger than the reduced mass, the binding energy of an exciton is smaller than the acceptor and donor energy level discussed below. According to eq. (4), as n varies, we can get an infinite number of excited exciton states near the band gap energy (fig.2.4a). where excitation energy is being referred to the edge of the conduction band.

In direct band gap materials, free excitons recombine by emitting photons or light that have energy

$$h\nu = E_g - E_x \tag{6}$$

where E_x is the binding energy of the exciton (fig2.4b). This transition can generally be observed in sufficiently pure materials at low temperature.

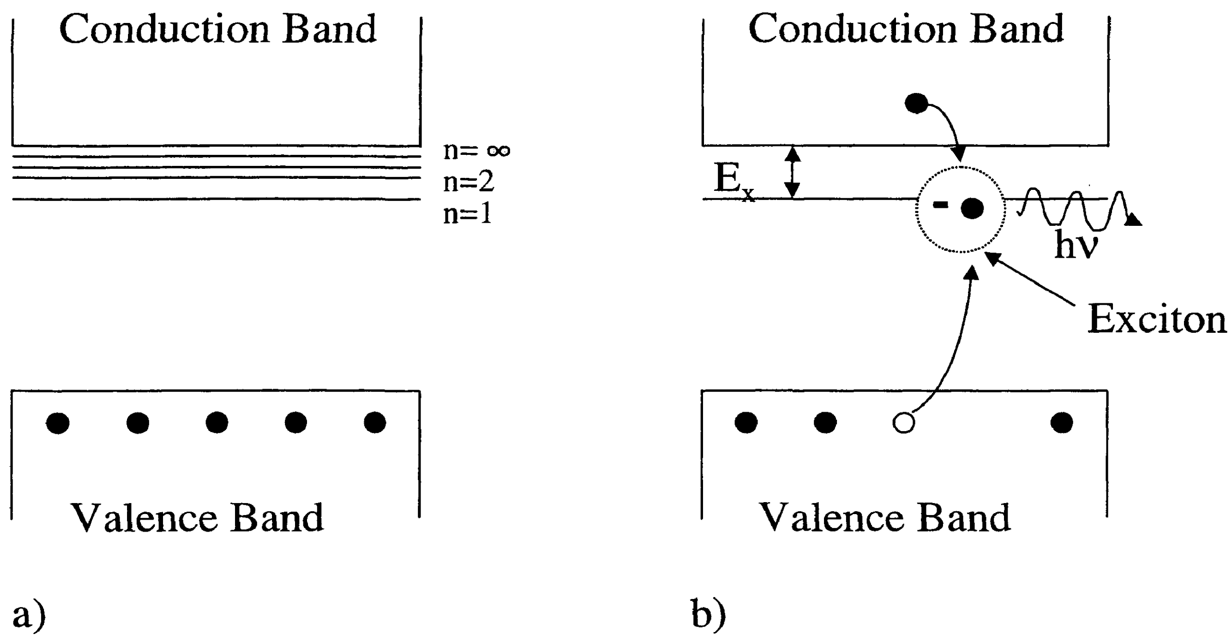

Figure 2.4 a) Exciton energy levels. b) Exciton recombination

2.3.1.3 Bound exciton

After introducing impurities into a semiconductor crystal, we create impurity states which are located below the conduction band and above the valence band in the crystal. If the impurity atom donates an electron to the crystal and forms a donor state below the conduction band then this impurity atom is called a donor. If the impurity atom accepts an electron from the atoms of the crystal, it forms an acceptor state above the valence band.

For example, following the absorption of light and the generation of electron and hole pairs, a neutral acceptor can capture an electron from the valence band and create a negatively charged acceptor. A free exciton can then bind to the acceptor and electron to form a bound exciton. When the bound exciton recombines it loses its energy as a photon (fig.2.5). This transition is called exciton bound to acceptor or more generally bound exciton transition. Similarly an exciton can be captured by a donor and the transition is called exciton bound to donor. Binding energy is generally a bit larger than for a free exciton.

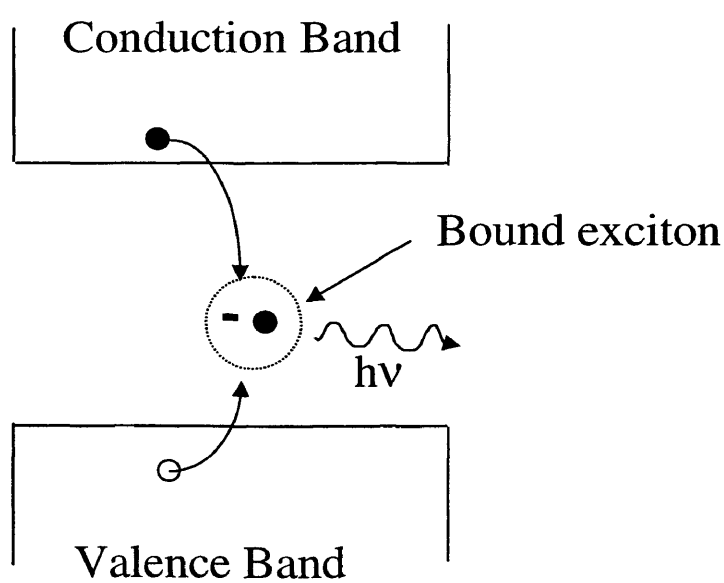

Figure 2.5 Bound exciton recombination

2.3.1.4 Donor-Acceptor

In a semiconductor that includes donor and acceptor impurities, an electron located on a neutral donor can recombine with a hole located on a neutral acceptor. When this recombination occurs, a photon is emitted with energy

$$h\nu=E_g-(E_a+E_d) \tag{7}$$

where E_a and E_d are acceptor and donor energy levels (this assumes a large distance between donor and acceptor). For very close spacing between impurities, a coulombic force arises because the donor and acceptor which are initially neutral but in their final state are charged and the emission energy is

$$h\nu=E_g-(E_a+E_d)+e^2/\varepsilon r \tag{8}$$

where r is the distance between a donor and acceptor for coulombic attraction, which modifies the emission energy (fig.2.6).

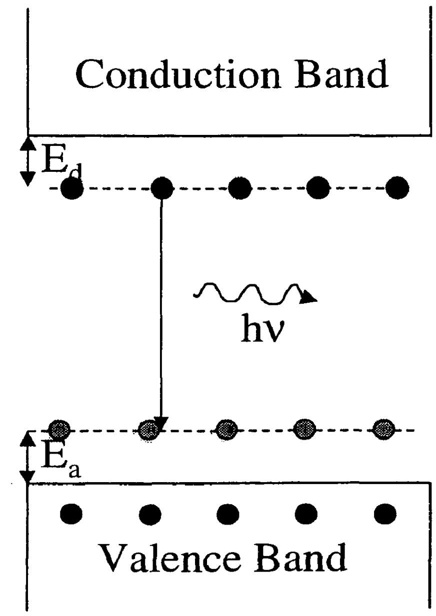

Figure 2.6 A donor and acceptor transitions

2.3.1.5 Band to impurity level

Recombination processes that involve impurity levels are often classified as shallow level transitions and deep level transitions. Following the absorption process, the recombination may occur between conduction band and donor level or between acceptor level and valence band (fig.2.7a). These tend to be very low energy. Transitions can also exist between the conduction band and acceptor level or between donor level and the valence band (fig2.7b.)

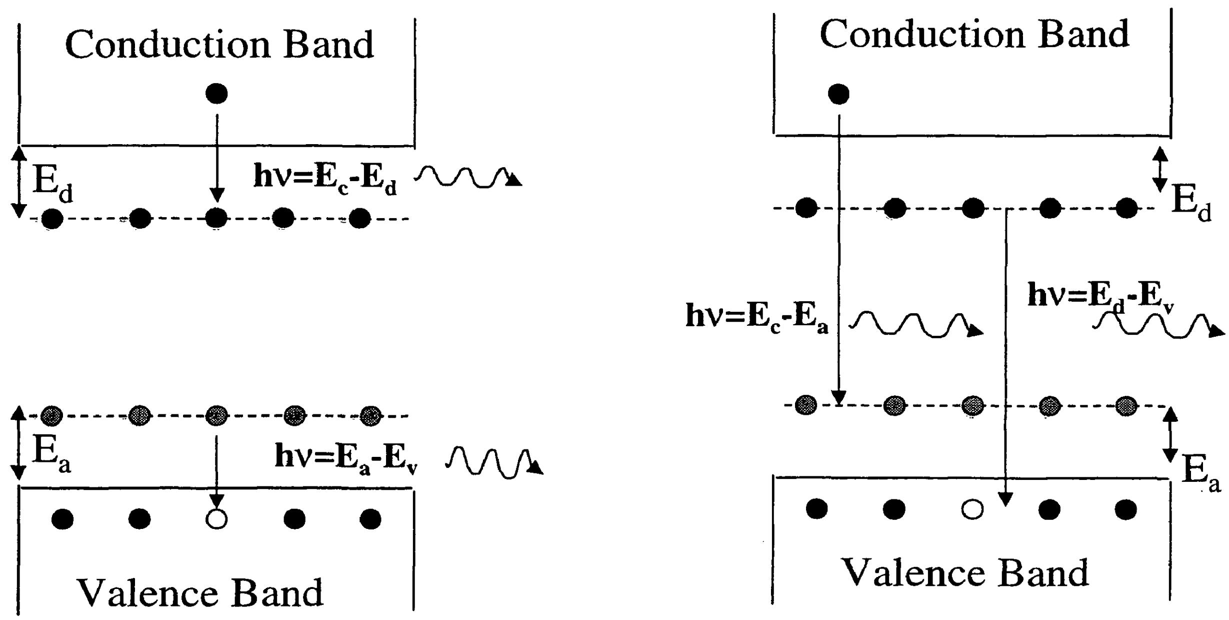

a) b)

Figure 2.7 Band to impurity level transitions

2.3.2 Non Radiative

After creating electron and hole pairs, recombination can also occur as non-radiative transitions. The experimental study of non-radiative transitions is extremely difficult due to the absence of photon emissions that can give very clear information about the recombination center. Three common non-radiative transitions include Auger recombination, surface recombination and non-radiative recombination through defects.

In the Auger effect, when the electron recombines with the hole, the released energy is absorbed immediately by another electron instead of emitting light. Sometimes the surface of a semiconductor can have a high concentration of deep and shallow levels, which contains a continuum of states. These levels may act as recombination centers. If the free electrons and holes are within a diffusion length of the surface, they can recombine via the continuum states non-radiatively. Moreover, a semiconductor can have defects that produce continuum states.

2.4 Photoluminescence (PL)

Luminescence refers to the emission of light by a material. The detection and analysis of this emission is used as an analytical tool due to its sensitivity and simplicity. When luminescence is excited by photons (usually a laser), this kind of luminescence is called photoluminescence.

Photoluminescence is a nondestructive optical characterization technique; therefore it can be used in many fields such as environmental research, pharmaceutical studies, biochemistry, food analysis etc. Photoluminescence is also a very powerful tool for examining properties of semiconductors and semiconductor quantum wells.

2.4.1 The Basic Principles of Photoluminescence

After an electron-hole excitation process, the system is subject to a non-radiative internal relaxation which involves interaction with crystalline or molecular vibrational and rotational modes, and the excited electron moves to a more stable excited level; for example, at the bottom of the conduction band or the lowest vibrational molecular state of a molecule as shown in fig.2.8. Similarly the hole moves to the top of the valence band.

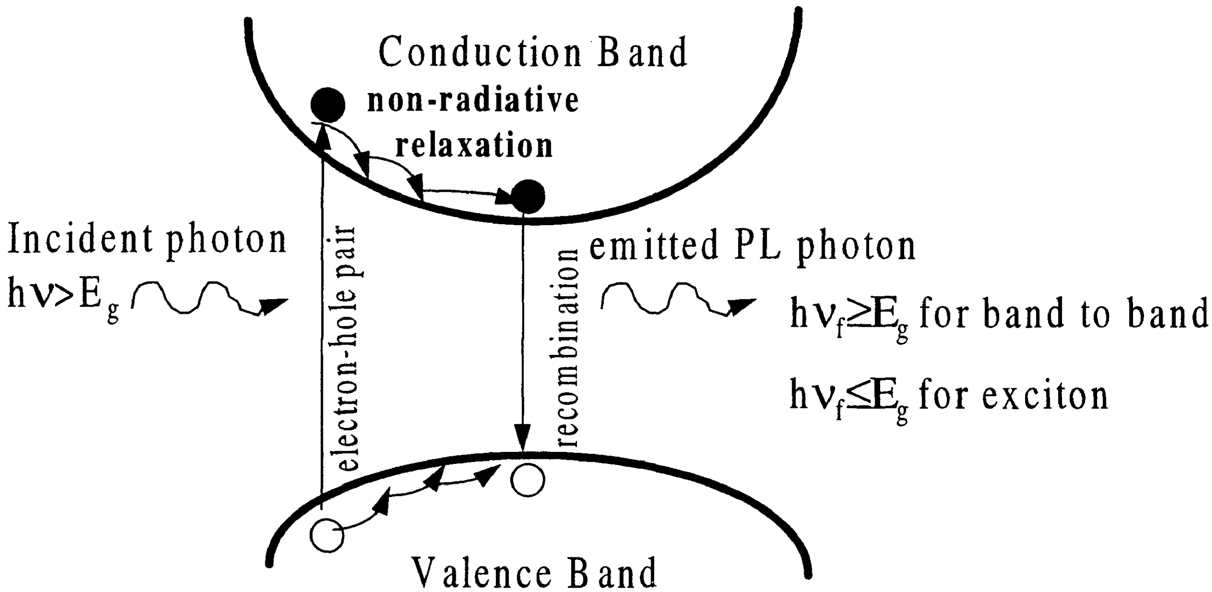

Figure 2.8 Illustration of basic PL process

As discussed in the last section, at the end of this internal relaxation process, the electrons and holes may be trapped in some localized state such as an impurity or bound exciton, etc.

After a system-dependent characteristic lifetime, which might last from picoseconds to many seconds, the electronic system will return to the ground state. During this final transition, some of the energy released is in the form of light and the rest of it is released as non-radiative transitions. The energy of this emission is smaller than the incident light. This emitted light is detected as photoluminescence and the emission spectrum of this photoluminescence is analyzed to provide information about the properties of the material.

The features of the spectrum that are generally analyzed are peak energy, peak width and peak intensity. In addition, by using pulsed excitation sources, such as mode-locked lasers, time resolved PL (TRPL) can be measured. By using a tunable excitation source such as a dye laser, PL excitation (PLE) measurements can be made. More details about TRPL will be given in next section. Table 2.1 lists sample parameters that can be explored from a continuous wave PL spectrum.

Table 2.1 The list of the spectral features of PL measurements

Spectral Features	**Sample Parameters**
Peak Energy	Identification of materials Identification of impurities Band gap/electronic levels Impurity or exciton binding energy Quantum well width Alloy composition
Peak Width	Quantum well interface roughness Carrier or doping density
Peak Intensity	Relative quality Radiative efficiency Surface damage Excited state lifetime Impurity or defect concentration

2.4.2 Instrumentation of photoluminescence

A basic experimental PL set up is shown in fig.2.9. This set up can be slightly changed according to the goal of the measurement. Four basic components make up a photoluminescence system: a light source for excitation, a sample holder, a monochromator to analyze the emission spectrum, and an optical detector with electronics.

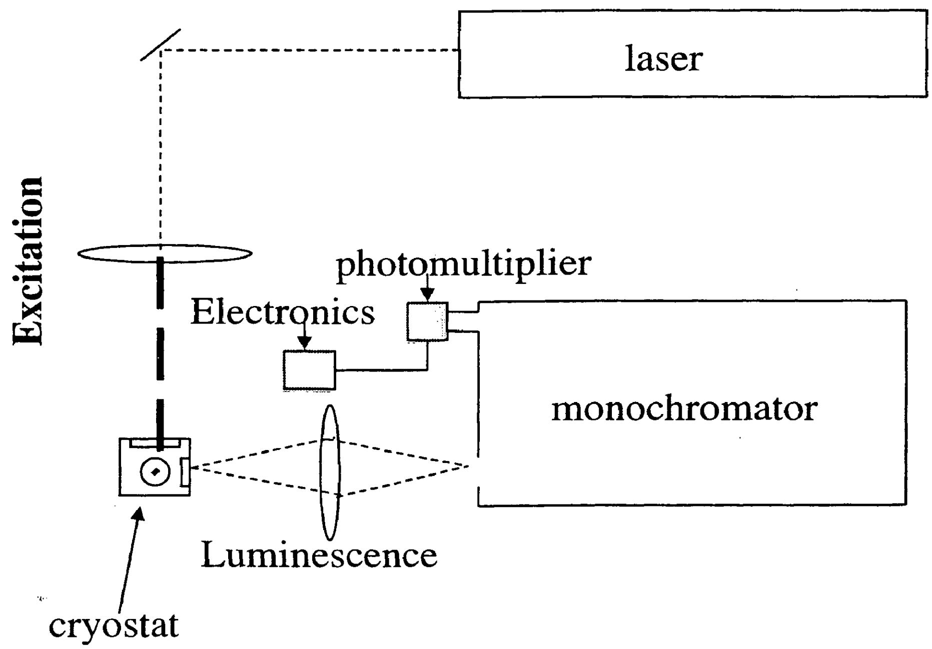

Figure 2.9 Illustration of a basic photoluminescence set up

For luminescence measurements, the most convenient excitation source is a laser with $h\nu > E_g$. The light from the laser can be directed by mirrors and lenses onto the sample mounted in a cryostat. The cryostat allows the temperature of the sample to be varied.

After excitation, the luminescence light is focused onto the entrance slit of the monochromator using a collection lens. The light is dispersed by the grating in the monochromator. Wavelength is selected by the exit slit and focused onto the detector. After this, the detector signal passes through an amplifier discriminator and then a photon counter. The signal output is then collected as a function of wavelength or energy yielding PL spectrum.

2.4.3 Time-resolved photoluminescence (TRPL)

The excess or minority carrier lifetime is a very important parameter for crystalline materials (22). The concentration of minority carriers is monitored by detecting the time dependence of the light emitted by the recombining electron-hole pairs. This is the principle of TRPL. The minority carrier density is not just a function of minority carrier lifetime, but may also depend on diffusivity and device geometry. TRPL measures the minority carrier lifetime directly and may have advantages over other lifetime measurement techniques such as, photoconductive decay, current or voltage decay. Most of these measurement techniques are connected to the minority carrier lifetime indirectly which makes it harder to analyze the data due to complicated parameter fits.

The minority carrier lifetime for a semiconductor is characterized by a PL decay time, τ_{PL}, defined by the eq.(9)

$$I_{PL} = I \exp[-t/\tau_{PL}] \tag{9}$$

where I_{PL} is PL intensity and t represents time. τ_{PL} is directly related to the lifetime of the photo-excited carriers in the material. The reader can find more detailed information about the theory of TRPL and minority carrier lifetime in Ref. (23)

A typical experimental TRPL setup contains a short pulsed excitation source, a spectrometer, a beam splitter, a photodiode, a time to amplitude converter (TAC), and a multichannel analyzer as shown in fig. 2.10.

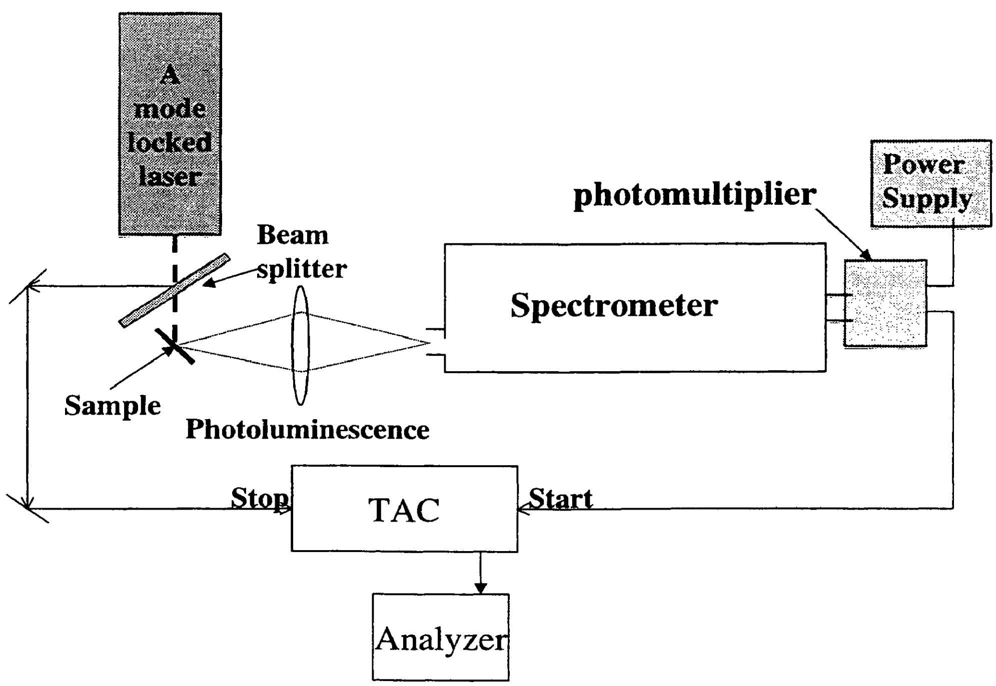

Figure 2.10 Instrumentation of a basic TRPL setup

2.5 X-Ray Diffraction (XRD)

XRD is the most widely used non-destructive technique for determining the crystalline microstructure in materials. By comparing the measured XRD pattern of a sample with cataloged XRD patterns, a huge data bank that covers every pattern of every known material (powder diffraction patterns), it is possible to identify the pattern in polycrystalline material.

In this section, we will briefly discuss the fundamental principles of XRD. The reader can find more details in ref.(24). In XRD analysis, a beam of monochromatic x-rays impinges on the sample. The radiation is scattered by the atoms of the sample. However, the scattered radiation from each atom only constructively interferes at certain angles or directions which are characteristic of the crystal lattice.

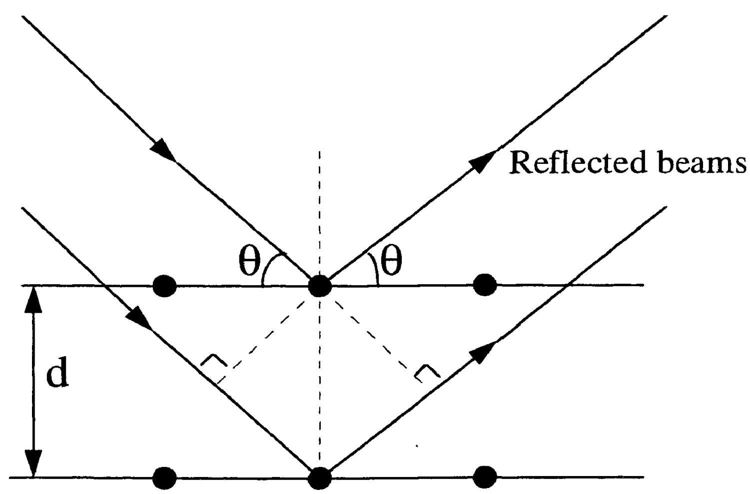

Figure 2.11 Illustration of XRD process

In this diagram (fig.2.11), we see two x-ray beams impinging with angle θ on two crystalline planes which are separated by a distance, d. Because the incident x-rays are in phase, the reflected x-rays should also be in phase, leading to a constructive inference if the difference between their paths is equal to an integer multiple of the wavelength λ of the rays. After this discussion, we can say that the condition for constructive interference is

$$n\lambda=2d\ \mathrm{Sin}(\theta) \qquad (10)$$

where n is an integer.

Eq.(10), Bragg's law, which allows the identification of different phases in a material just by measuring the position of the peaks in a XRD pattern is the heart of the XRD technique as we have used it in the work. Each set of crystal planes can allow constructive interference only at certain angles. Although we have explained Bragg's law for only two crystalline planes, it is easily shown that it can be applied for any number of parallel planes.

Experimentally measured XRD patterns for powder specimens of almost every known material are available in Joint Committee Powder Diffraction Standards (JCPDS) cards. Moreover, the values of peak intensities are identified in the JCPDS cards. The samples microstructure can possibly be determined by comparing the position of the peaks in a XRD pattern with values in JCPDS cards. In addition, by comparing the intensities with the associated intensities in the cards, it is also possible to identify if there is preferential orientation in one or more directions.

The theory of calculating peak intensities is more complex. In this work; however, we are just interested in determining the position of the peaks in the XRD pattern. Readers can find more information about this subject in ref.(24)

2.6 Auger electron spectroscopy (AES)

AES can be used to determine the elemental composition of the atomic layers in the surface region of solid samples. AES can also be useful for analyzing the composition of surfaces of thin films or interfaces. In our research, we used AES to identify the composition of S in CdS/CdTe films. An electron beam is used as a probe of the sample surface. Auger electrons are emitted, and a spectrum of emitted electron intensity is recorded.

The basic theory of the technique is that when a sample is bombarded by a probe beam, generally an electron beam, an inner shell electron of the atom absorbs the electron energy. The inner-shell electron is released and a vacancy is created in the inner shell of the atom. This vacancy is filled by an electron from an outer shell. During this process, the electron releases some energy in its transition to the inner-shell. A photon emission is one possible way to conserve energy. In addition to emission of the photon, the excess energy may also be released by the ejection of an outer-shell electron in a non-radiative process. This ejected electron from the outer-shell is called an Auger electron and it has a characteristic energy. The detection and measurement of the energy distribution of Auger electrons provides a direct identification of the atom from which it was emitted.

For example, if a solid sample is bombarded by an electron beam of 3 keV, the 1s, or K shell, electron of the atom with an energy E_{1s} becomes ionized. A vacancy will be created in the K shell (fig.2.12). The K shell vacancy is going to filled by the transition of an electron from one of the 2s or L subshells with E_{2s} binding energy. This ejected electron is called the secondary electron. The excess energy of the secondary electron can be released by x-ray radiation but most of the time, this energy can eject an electron from 2p or L_{23} shell with E_{2p} binding energy, which is called the Auger electron (fig.2.12). According to the energy conservation law, the kinetic energy of an outgoing Auger electron can be determined from

$$E_{kin}=E_{1s}-E_{2s}-E_{2p} \tag{11}$$

and the complete process is called KLL Auger transition.

According to one of the numerous available charts of Auger electron energies of the elemental Cd, which is one of the components of CdTe and CdS, the $M_{45}N_{45}\,N_{45}$ Auger transition is most likely to occur. The energy of M_{45} shell is 405eV and N_{45} is 9.3eV (25). When we formalize the kinetic energy of an Auger electron for this transition, we will obtain

$$E_{kin}=E_M - E_N - E_N \tag{12}$$

By using the eq.(12), we calculate that the kinetic energy is 386.4eV and this quantity matches with the number for Cd material in the Auger Handbook, which covers the known kinetic energies of the Auger transitions for all elements in the periodic table.

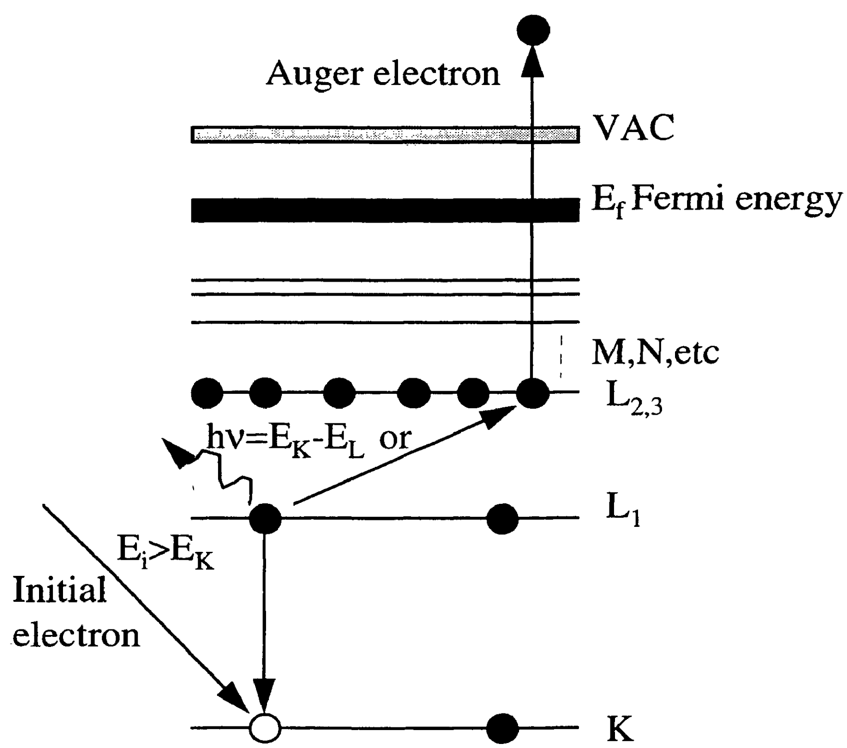

Figure. 2.12 An illustration of the KLL Auger transition

CHAPTER 3
EXPERIMENTAL METHODS

3.1 Sample fabrication

The fabrication of CdS/CdTe solar cells is well developed, and these cells are commercially available. However, there are still problems which can affect the efficiency of the cells. Many researchers who do research on CdS/CdTe solar cells have concentrated on issues which relate to fabrication of the CdS layer, the characterization of CdTe deposition, interdiffusion between CdS and CdTe, post-deposition processes (e.g. annealing and $CdCl_2$ treatment), and the deposition process of a back contact on CdTe. The issue we studied is sulfur diffusion into CdTe from CdS during the post-deposition process.

The fabrication process of a CdS/CdTe thin-film solar cell is as follows:

1. Substrate preparation
2. CdS deposition
3. $CdCl_2$ and heat or annealing treatments on CdS layer
4. CdTe deposition
5. $CdCl_2$ and heat or annealing treatments on CdTe layer
6. Back contact deposition.

We will briefly discuss each of these steps as performed on the samples used in this study in the sections below.

Substrate preparation: Tin Oxide (TO) films which were predeposited on soda-lime glass plates were used as the substrate in the CdTe-based solar cells produced by the CdTe solar-cell group at CSM. The thickness of TO is between 0.4μm-0.5μm on 1 mm thick glass. Since TO has a very high band gap and melting point, it is believed that the post-deposition process during solar-cell fabrication will not affect the TO, and therefore, the efficiency of the cell. The TO-coated soda-lime glass has to be cleaned by using soap and DI water before being used in the deposition of CdS process.

In our research, we also used NREL (National Renewable Energy Laboratory) fabricated CdTe based thin film solar cells. In these solar cells, TO coated 7059 glass plates received from Solarex Corporation are used as substrates. The thickness of the TO layers is the same as CSM fabricated solar cells.

CdS deposition: The second step in the fabrication process is CdS deposition. In CSM samples, CdS was deposited by an ultrasonically-assisted chemical-bath deposition (CBD) technique. In this technique, the recipe for the chemical solution is the main parameter. Much research has been done on different chemical solutions (26-31). In our case, the chemical solution consists of cadmium salts ($CdSO_4$, $CdCl_2$), ammonia, and thiourea ($(NH_2)_2CS$) as the source of the sulfur. Reports on concentrations of the reaction mixture for producing CdS and controlling the reaction rate can be found in Ref. (26-31). Depending on the reaction rate involved in the solution recipe, and after the desired film thickness has been achieved, substrates coated with CdS are removed from the bath and rinsed by flushing them with cool DI water. In CSM samples, CdS was deposited by using the Chu et.al. chemical recipe. The chemical reaction of this mixture is well understood (27). The growth rate versus time for this process is shown in fig.3.1. The measured grain size of as-deposited CdS varies from 67-530Å (32). The

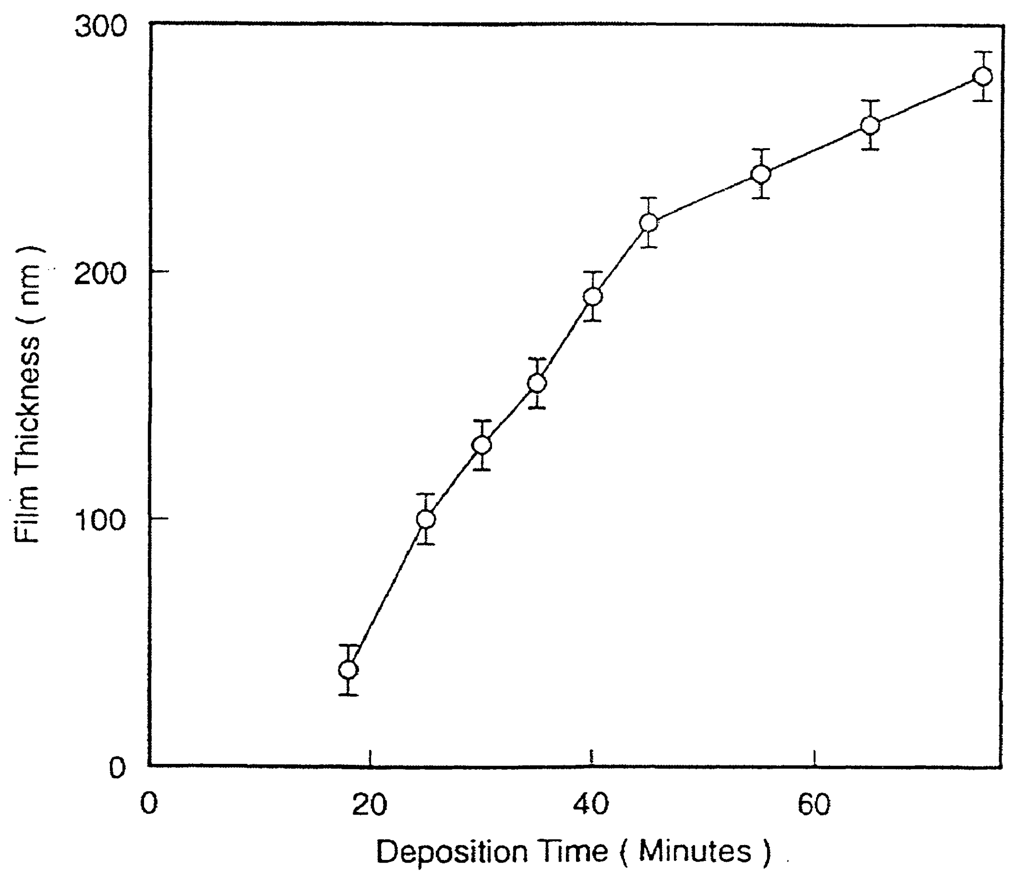

Figure 3.1 The grow rate of CdS versus deposition time Zhu et al.(32)

as-deposited thickness of CdS is typically near 0.2μm. After the annealing process, discussed in the next paragraph, CdS thickness is between 0.12 to 0.13μm.

$CdCl_2$ and heat treatment on the CdS layer: The standard $CdCl_2$ treatment on CdS is done by applying for one minute a 2.4 M $CdCl_2$ and DI water solution in the form of a mist, which is made by an ultrasonic nebulizer. The deposition system of the standard $CdCl_2$ treatment is shown in Fig.3.2. The nebulizer has a container filled with $CdCl_2$ and is connected to a chamber by two pipes. A separate heating unit sits under the chamber. One of the pipes provides an air supply to the chamber; the $CdCl_2$ mist reaches the chamber through the other pipe, which is located on the ceiling of the chamber. To treat the sample with $CdCl_2$, the sample is placed under the mist supply pipe. The chamber is heated to125°C, and then the sample is coated with $CdCl_2$ for one minute. After being coated, the sample is left in the chamber in order to evaporate the water until the temperature of the chamber decreases to 62.5°C. The sample is then removed from the chamber. For the heating or annealing treatment, the sample is then put in a furnace at 450°C in a nitrogen atmosphere for 45-50 minutes. After that, the sample is left in the furnace until the temperature drops to room temperature. The sample is then removed and rinsed with DI water. All of these processes complete the $CdCl_2$ heat treatment of the sample. The sample is now ready for CdTe deposition.

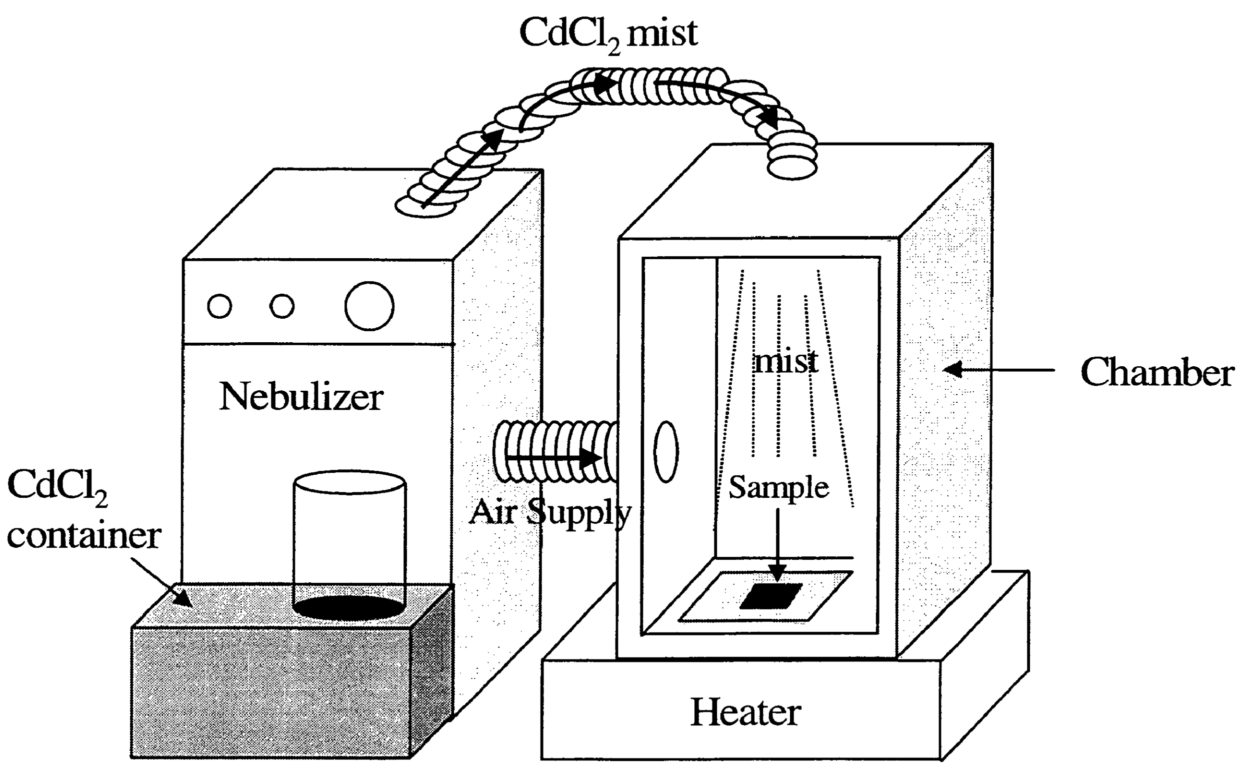

Figure 3.2 The deposition system for the $CdCl_2$ treatment.

CdTe deposition: The electrochemical deposition technique used by CSM to deposit CdTe has been well documented in Ref.(33). The typical growth rate of CdTe is around 1μm/hour (34) and grain size is between .25 to .28 μm Ref.(33). We also used CdTe samples deposited by Close Space Sublimation (CSS) technique. These samples are fabricated by the CdTe group at NREL. We will not discuss details about the CSS technique, but readers can find information about this deposition technique in Ref.(35). The next step will describe $CdCl_2$ heat treatment on CdTe layer.

$CdCl_2$ and heat treatment of CdTe layer: As deposited CdTe is n-type, to create p-type CdTe, the CdTe layer has to be annealed, or heat treated, and in addition to the annealing process, $CdCl_2$ treatment helps to create bigger CdTe grain size. The $CdCl_2$ treatment process is the same as the treatment made on the CdS layer. After $CdCl_2$ deposition, the sample is put in a furnace at 410°C for 45 minutes in air. This was found to be a necessary annealing temperature for optimal cell performance. The sample is then removed from the furnace and left to cool to room temperature. After the $CdCl_2$ and annealing treatment, the measured grain size of CdTe increases between 0.5 to 1.0 μm and even higher Ref.(33). The same effects of the $CdCl_2$ heat treatment can also be seen with CSS-deposited CdTe layer.

For CSS deposited CdTe, the deposition process for $CdCl_2$ was different. The $CdCl_2$ powder was mixed with methanol in quantities just above saturation. The solution was stirred using a spinbar and heated at temperatures between 80 °C and 100°C. After approximately one hour, the $CdCl_2$ was dissolved. The as-deposited CdS/CdTe sample was dipped into the $CdCl_2$ solution for specific length of time. In this study, samples were dipped for 10 minutes.

Back-contact deposition: To complete the fabrication of a solar cell, the next step would be a back-contact deposition on the annealed and $CdCl_2$ treated CdTe layer. The back contact may be obtained either by using a direct formation of a p^+, layer such as CdTe:Te (36), ZnTe:Cu(37), or HgTe(38) or by using contact materials such as Cu/Au(39). In this thesis, a back contact was not deposited on the samples and all measurements were made on the exposed CdTe layer.

3.2 Etching of the CdS/CdTe samples

To examine the S diffusion into the CdTe, the layer was thinned by using a Br-Methanol (CH_3OH) etch. The etching rate is about 1μm/min with a (1.5ml:200ml, Br to Methanol) recipe. The etching process was performed in a 250ml beaker at room temperature. The etch process involved masking a portion of the sample surface using black wax which is resistant to the Br-Methanol etching solution. The sample was then etched. At the end of the etching, the sample was rinsed with methanol to remove the etch from the surface of the sample. The mask on the sample surface was then removed by using trichloroethane to dissolve the black wax. After that, the sample was rinsed with acetone to remove the trichloroethane and again rinsed with methanol to clean the surface. After completing the etching process, we had one part of the sample surface which was etched (or thinned) but the other part was not. This process was repeated on the unetched surface to create a series of etch steps. The height difference between the etched and non-etched surfaces, or the step height, was measured using a profilometer. In later etchings, we used kapton tape, which is also resistant to Br- Methanol, instead of black wax. Fig. 3.3 shows a profile created in this way.

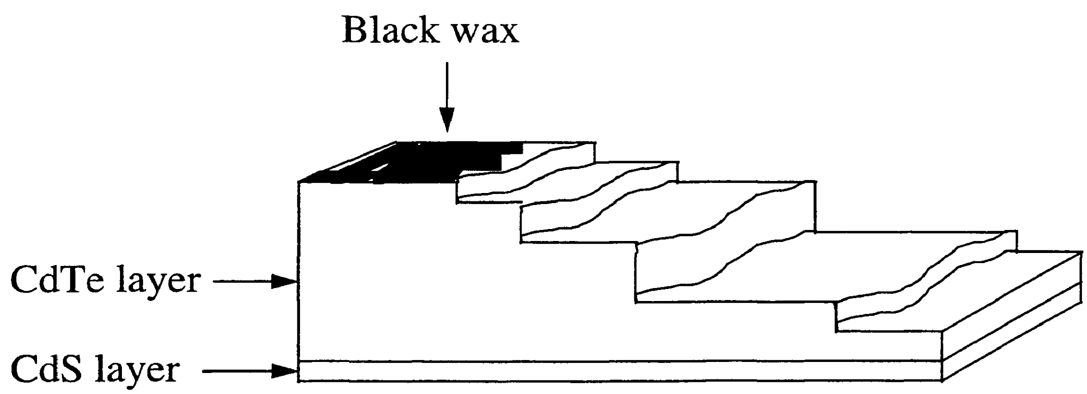

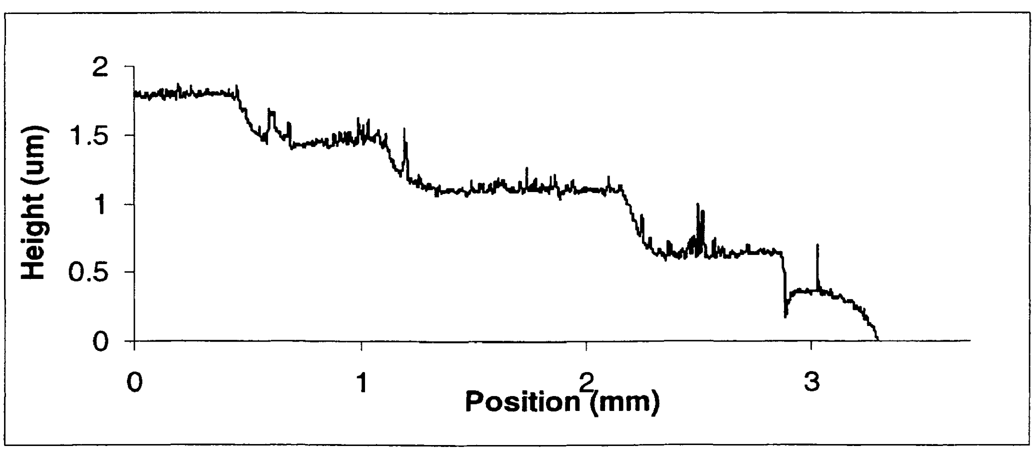

Figure 3.3 The profile of the CdTe layer using Br-Methanol etch

In this thesis, a second etching method was also used for x-ray studies. Here, a series of etching steps was applied to the entire piece of sample sequentially, and measurements were made after each etch step.

3.3 Instrumentation setup

3.3.1 Instrumentation setup for Photoluminescence (PL)

Fig.3.4 shows our photoluminescence setup. This setup contains

- Ar-Ion and He-Ne lasers as excitation sources
- A cold finger dewar in order to hold the sample and perform experiments at low temperature
- A vacuum system to create a vacuum level of around 10^{-7} torr inside the dewar and protect the sample from contamination and water condensation
- A SPEX model 1301, double pass grating spectrometer, as a dispersive element for spectral analysis of photoluminescence
- A cooled GaAs photocathode photomultiplier tube with a cutoff in the long wavelength response at 860 nm
- A photon counter as a readout system and a computer to acquire and store spectral data.

This system also includes laser line filters for 632.8 nm He-Ne and Ar-Ion laser lines in order to eliminate laser plasma lines that fall within the spectral region of interest.

In addition to plasma line filters, the luminescence system has other filters that are capable of preventing the exciting light from entering the spectrometer. Neutral density filters are used to control the excitation power.

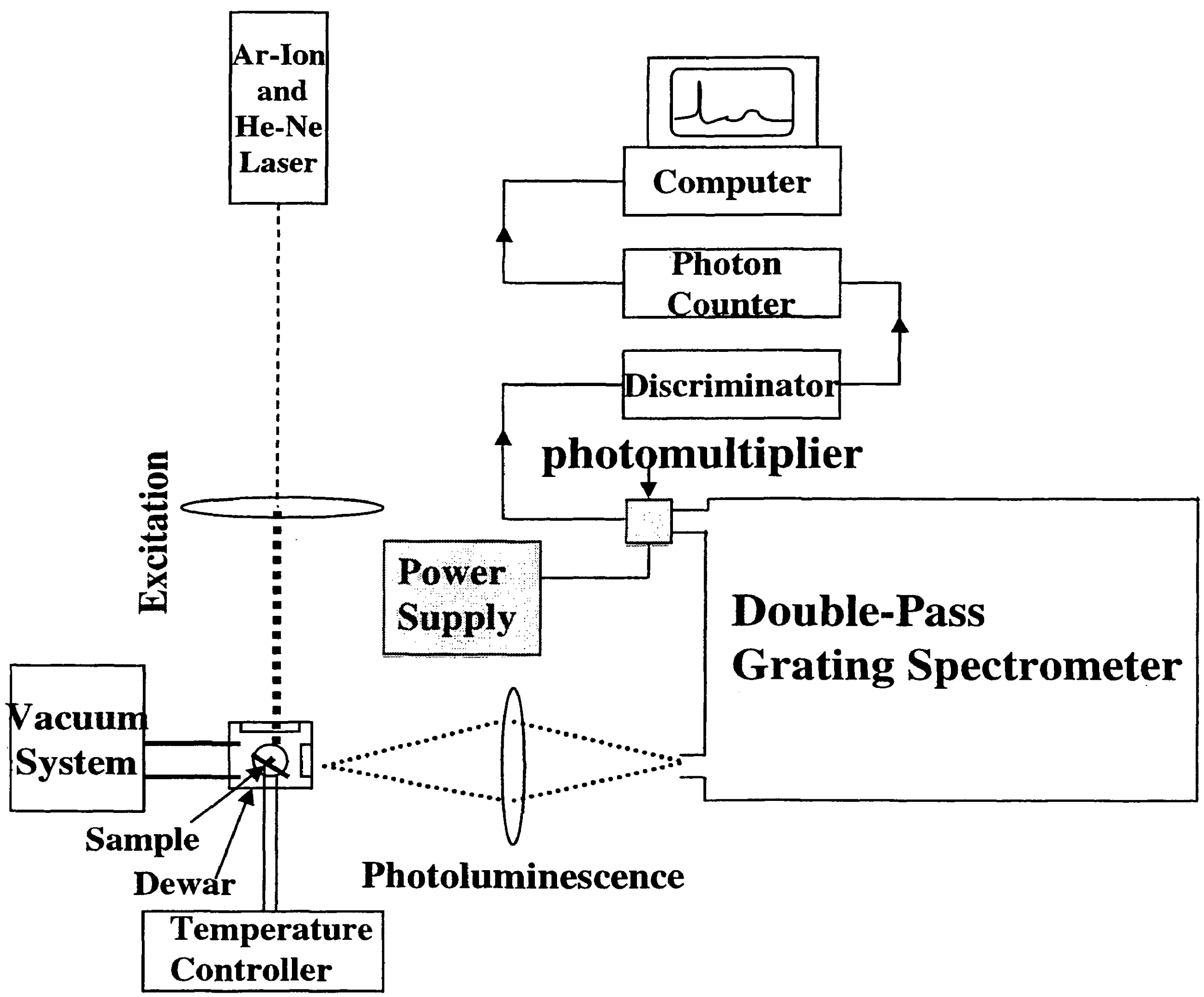

Figure 3.4 Instrumentation of our PL experimental setup

3.3.2 Instrumentation setup for Time-Resolved Photoluminescence (TRPL)(NREL)

The NREL TRPL experimental apparatus is shown in Fig.3.5. This setup has

- A laser system which contains a mode-locked Nd-YAG laser, which is used to pump a cavity-dumped dye laser. This is used as a source of excitation pulses at 600 nm wavelength. Pulses have 5-10 psec. fullwidth at half-maximum.
- A Spex. Model 1672s, spectrometer, is used to analyze the photoluminescence signals
- These signals are detected by a micro-channel plate (MCP) detector, Hamamatsu model E 3059, which can detect a single photon.
- The electric pulse, generated by a PL photon, goes to the TAC and produces a stop message at the TAC. On the other hand, the signal that the photodiode producer is also sent to the TAC and this electric pulse produces a start message at the TAC. The voltage difference between start and stop electric pulses is proportional to the time between triggering and detection.
- This voltage is sent to the multichannel analyzer as an output pulse of the TAC.
- The multichannel analyzer counts the output of TAC for different voltages
- These counts are stored and displayed in the computer to build up a spectrum of PL intensity vs, time after the pulse.

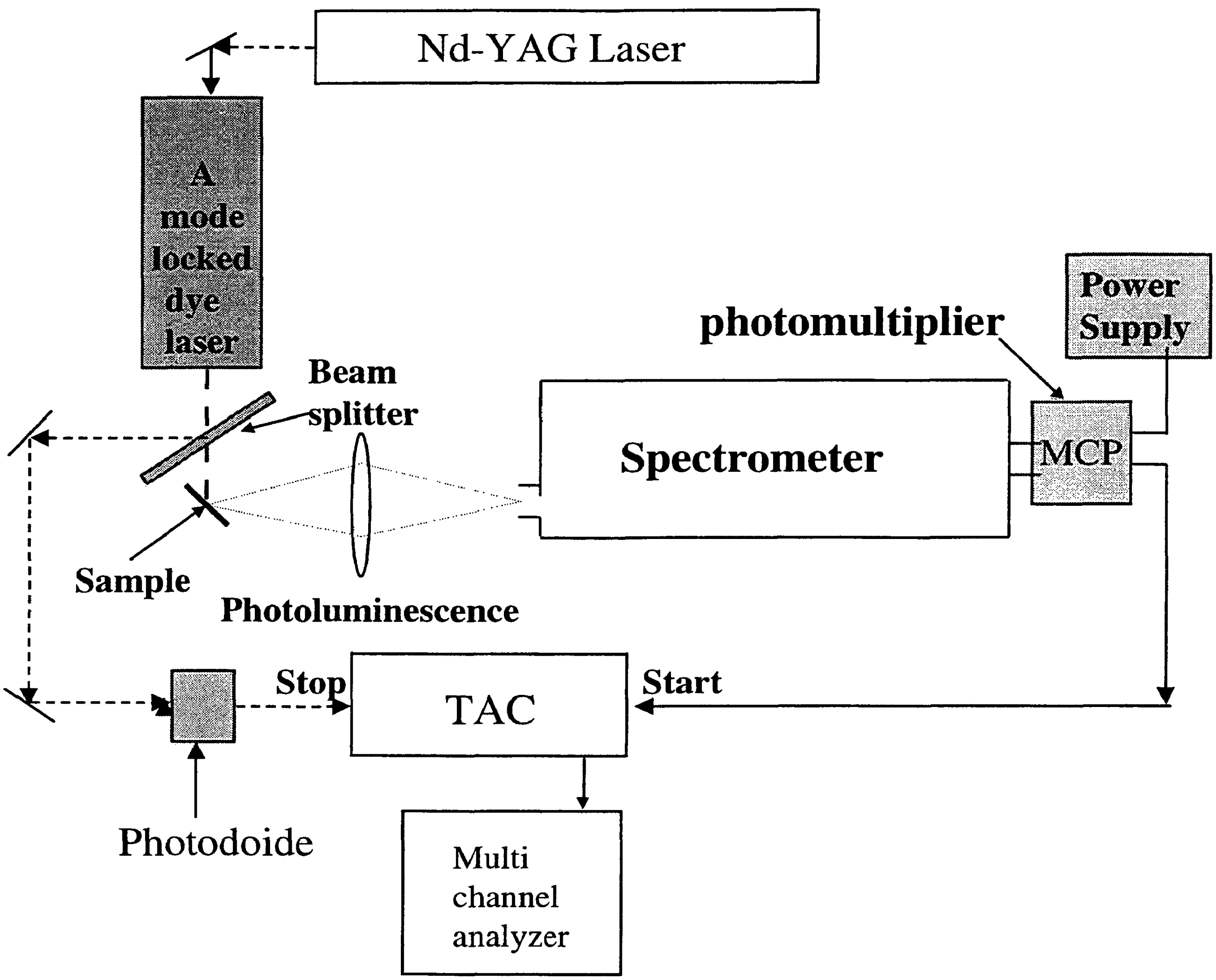

Figure 3.5 The TRPL experimental setup (NREL)

CHAPTER 4
RESULTS AND DISCUSSION

4.1 Examination of S diffusion into CdTe solar cell

As discussed above, interdiffusion between the n-type CdS window layer and the p-type CdTe layer occurs and influences the performance of the CdTe solar cell. For this reason we have explored S diffusion into CdTe near the n-type interface of CdS by using PL, XRD, and Auger Electron Scanning measurements. The degree of interdiffusion between the CdS and CdTe layers depends on the technique used to grow CdS and CdTe layers. For this interdiffusion study, CdS is deposited by chemical-bath deposition on Tin-oxide coated soda-lime glass and then treated with $CdCl_2$ before annealing it at 450°C, for approximately 45-50 minutes in N_2. A CdTe layer is then deposited by electrodeposition on the annealed CdS. After this, a $CdCl_2$ treatment has been applied to the surface of CdTe and the sample is annealed again in dry air. The optimal annealing temperature for maximum efficiency in our samples is 410°C. Interdiffusion of CdTe and CdS occurs during this annealing (40-43). To complete the fabrication of the solar cell, a back contact needs to be deposited. However, complete cells were not needed in our experiments so no back contact was deposited.

To examine the S concentration in the CdTe layer, the CdTe layer is sequentially thinned by using a Br-methanol etch as described above. Atomic Force Microscopy (AFM) studies of etched surfaces show that this etching process did not create pinholes or enhance the grain boundary features. The sample used in XRD measurements, had a glass/TO/CdS/CdTe configuration with CdTe thickness of 5.3 μm. It was annealed at 410°C. As discussed above, a series of etch steps was applied to the entire piece of the sample sequentially removing the CdTe layer. After each etching step (5 min., 10 min., 20 min.,) an XRD measurement was performed (fig.4.1). The rate of etching was ~0.25 μm/min.

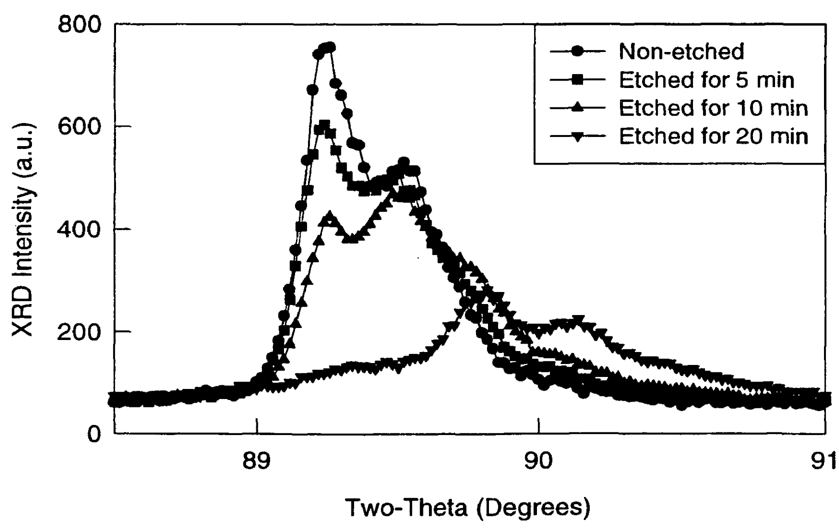

Figure 4.1 XRD measurements of the CdTe layer in a CdTe/CdS heterojunction. Traces were obtained after sequential etching in Br-methanol for 0, 5, 10, and 20 minutes

The XRD technique was used for investigating the diffusion process by directly detecting the presence of ternary phase $CdTe_{1-x}S_x$ formed during the S diffusion into the CdTe layer. XRD measurements were made on a Rigaku X-Ray diffractometer using Cu-Kα radiation. The lattice constants of CdTe and CdS are 0.6481 nm and 0.5818 nm. Thus, the $CdTe_{1-x}S_x$ ternary phase will have a smaller lattice constant than the CdTe phase. This allows the ternary phase to be identified by a shift of diffraction peaks toward a higher angle with respect to the pure CdTe phase.

PL measurements were used to characterize S diffusion by monitoring shift in the band gap with depth. The band gap of $CdTe_{1-x}S_x$ changes with x. The behavior of the band gap of the ternary phase as a function of the S molar fraction is show in fig.4.2 which has been reproduced with permission from Dave Albin (44). In the range of interest for this study, the band gap decreases with increasing S due to a bowing in the curve.

Figure 4.2 Optical band gaps data for $CdTe_{1-x}S_x$ alloy system

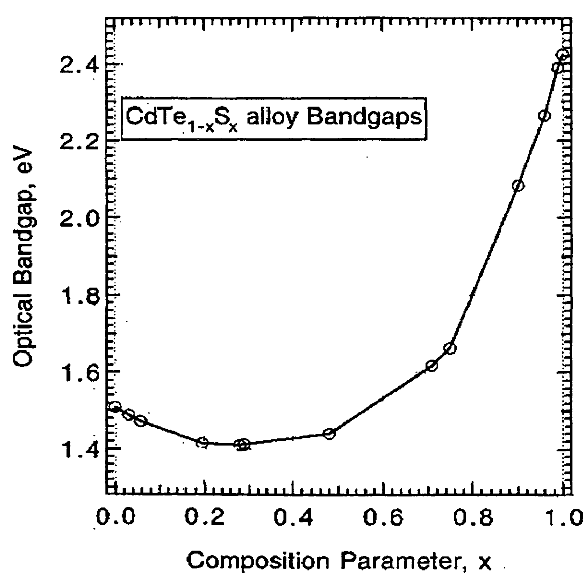

According to (20, 45), the band gap decreases with increase of S content up to $x \cong 0.25$. After this x value, the band gap increases with increasing CdS molar fraction, x. From the studies of the $CdTe_{1-x}S_x$ band gap versus CdS content at room temperature, an empirical quadratic equation was obtained relating band gap to S content (20);

$$E_g(x)=1.74x^2-1.01x+1.51 \tag{13}$$

however, at low temperature, we expect this quadratic equation to take form

$$E_g(x)=1.74x^2-1.01x+1.602 \tag{14}$$

where $E_g(x)$ is the band gap of $CdTe_{1-x}S_x$. We used also Albin's empirical equation obtained by fitting the data shown in fig. 4.2 but there was not a significant difference between the results using either fit equation.

4.1.1 XRD Results

Fig.4.1 shows the XRD patterns of annealed CdTe films etched for different times (0 min., 5 min., 10 min., 20 min.). Approximately 1.5 μm of CdTe was removed in each etching step, and longer etch corresponds to a region closer to the CdTe/CdS interface. The diffraction angle, two theta, is in the range between 88 and 92 degrees where the (531) diffraction peak of CdTe is located. A high angle diffraction peak was chosen for detailed analysis because of better depth resolution at high angles. The four patterns (fig.4.1) show a characteristic variation from surface to interface. These patterns are

1. the back surface of CdTe (unetched),
2. near the surface of CdTe (5 min. etched,),
3. the middle of the CdTe (10 min. etched)
4. near the interface of CdS/CdTe (20 min. etched).

The two peaks in the unetched spectrum represent $CuK\alpha_1$ and $CuK\alpha_2$ lines. After the 5min. and 10min. etching process, additional peaks are observed as shoulders on the pure CdTe peaks. After the 20min. etching step, this structure has shifted to higher angles, which is an indication of increasing S composition. After fitting the XRD patterns, we can find the plane spacing from the pattern, wavelength of the X-ray source and Bragg's law. Since the CdTe has zinc-blend structure and preferentially grow in (111) direction, the lattice constant can be calculated by using planar spacing formula for a cubic structure. By using the relation between S composition and lattice constant given in Ref. (45), S concentration near the CdTe/CdS interface can be estimated. Our estimation shows a 5.3% S concentration near the CdTe/CdS interface

4.1.2 Low temperature PL Results

Our typical PL spectrum, at low temperature (15 K), from the backside (or CdTe side) of the cell is shown in fig. 4.3. The band gap of crystalline CdTe at 4.2 K is 1.606 eV (4). Fig. 4.3 also includes the PL spectrum of a single crystal (111) CdTe for comparison. The peaks in the PL spectrum of the single crystal have been assigned (46) as follows:

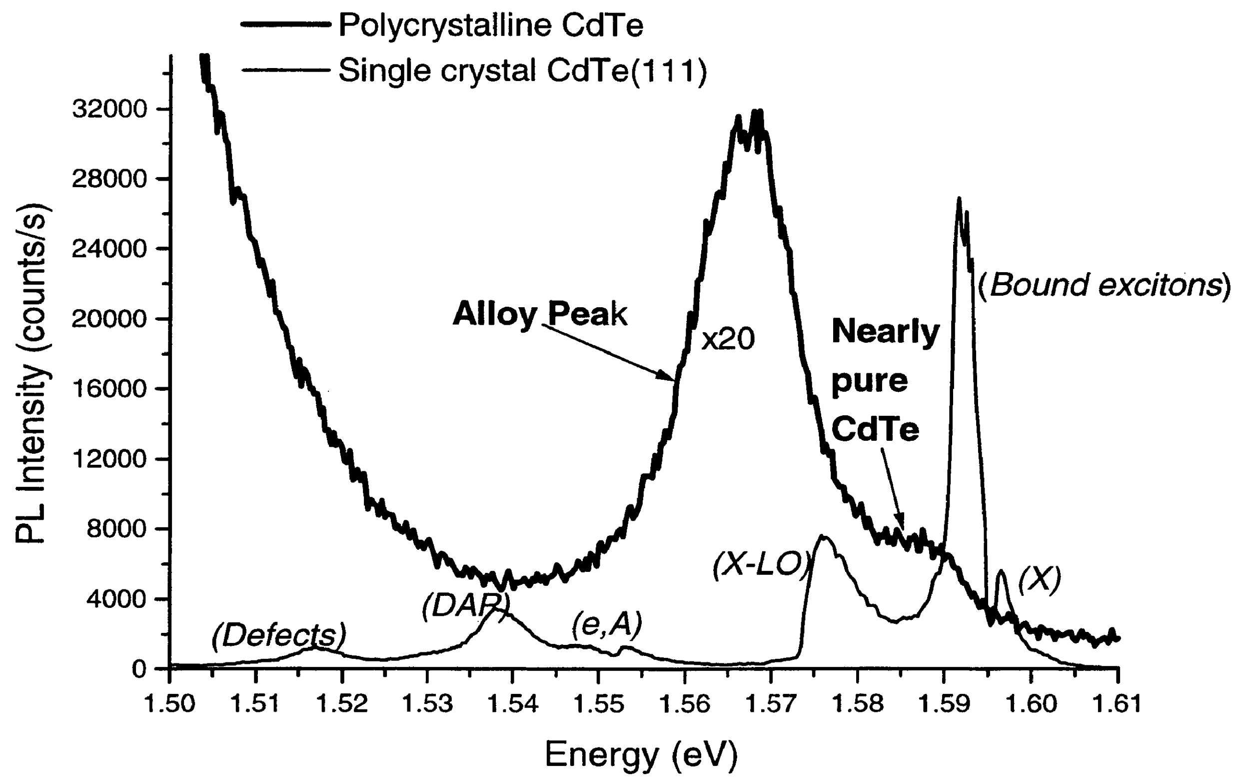

Figure 4.3 a standard PL spectrum of CdTe/CdS solar cell (thick line) and the PL spectrum of crystalline CdTe (111) (thin line)

- The peak at 1.596 eV is a free exciton (X) transition
- The peaks at 1.593, and 1.589 are from bound exciton (X,D^o,XA^o) recombination

- The peak at 1.576 eV is a phonon replica (X-LO) peak
- The very broad peak at 1.538 eV is a result of donor-acceptor pair (DAP) transition
- At slightly higher energy, 1.548 eV, than (DAP) transition is a transition between the conduction band and the neutral acceptor which produces a tail labeled (e, A)
- The peak at 1.518 eV is associated with crystal defects and deep impurity levels.

Excitonic luminescence (free and bound) in the crystalline material occurs between 1.585 to 1.596 eV at 15 K. At 15 K, the band edge is only about 1meV lower in energy than at 4.2 K [47]. According to information about energy levels of crystalline CdTe (fig. 4.4), excitonic transitions, XRD results as mentioned above and Ref. [45], we believe that in the PL spectrum, obtained from back side (CdTe side) of the cell, the

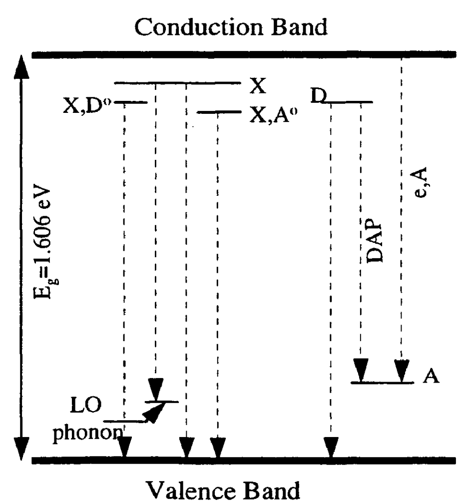

Figure 4.4 Energy level diagram for CdTe showing major luminescence transitions.

higher energy shoulder around 1.585 eV comes from nearly pure CdTe and the peak, at 1.57 eV, is an excitonic peak of $CdTe_{1-x}S_x$ coming from the ternary phase which we will call the alloy peak. The very wide peak at 1.45 eV belongs to a deep donor-acceptor defect band. This feature is commonly observed in polycrystalline CdTe. We haven't studied it in detail here.

To examine S diffusion into the CdTe layer in more detail, a series of samples that were annealed at different temperatures were etched by creating a sequence of steps of various heights into a single sample as discussed above. To do PL measurements, we chose two standard samples that had our typical configuration of glass/TO/CdS/CdTe for high efficiency devices. Two different pieces from one of the samples were annealed at 350°C, and 460°C separately following $CdCl_2$ coating. The thickness of CdTe layer of this sample was ~3.8 μm. A second sample, which had the same configuration as the other one, was annealed at 410°C (the standard anneal) and then treated with $CdCl_2$. The thickness of the CdTe layer was ~1.8 μm thick CdTe. Depth profiles after step etching and associated PL spectra are shown in figs. 4.5, 4.6, and 4.7.

Fig.4.5a shows the etch profile and fig. 4.5b shows the PL spectra of the sample annealed at 350°C. The PL spectrum obtained from the unetched region of the sample shows a peak position of 1.581eV. There are some samples which show variation in the position of this peak with it occurring at energies as high as 1.585eV. Since excitonic luminescence in the crystalline CdTe material varies from 1.585eV to 1.596eV, we again interpret this peak as belonging to excitonic transitions in CdTe. If we take a small S content, residual strain, and even internal electric fields into consideration, we can explain the variation of peak position that is slightly lower than typical of bound excitons in crystalline material. As seen in fig.4.5b, there is a very small shift, (about 7 meV) in PL energy with depth. This may imply increasing S content. If we made this assumption, the 7meV shift would correspond to 0.7% S content based on Eq.14. This amount of S content is quite low when it is compared to S diffusion of 410°C and 460°C annealed samples as discussed next.

We obtained the PL spectra for a sample annealed at 410°C. The etch profile is shown in fig.4.6a and PL profile in 4.6b. The PL spectrum from the thickest region of the sample shows two distinct peaks. This is similar to fig.4.3 and we frequently see this for 410°C anneal. The higher energy peak is close to the peak energy after the 350°C anneal and to excitonic energies in pure CdTe while the lower energy peak indicates a $CdTe_{1-x}S_x$ ternary phase structure as mentioned above. When PL measurements are made near the interface, the higher energy peak loses its intensity and even disappears at the thinnest region. On the other hand, the lower energy peak shifts to even lower energies and its intensity become stronger, which indicates increasing S concentration with increasing depth. This is consistent with XRD observations. The energy difference between the CdTe and $CdTe_{1-x}S_x$ can be used to estimate the S concentration of the ternary phase as a function of depth from the PL spectrum.

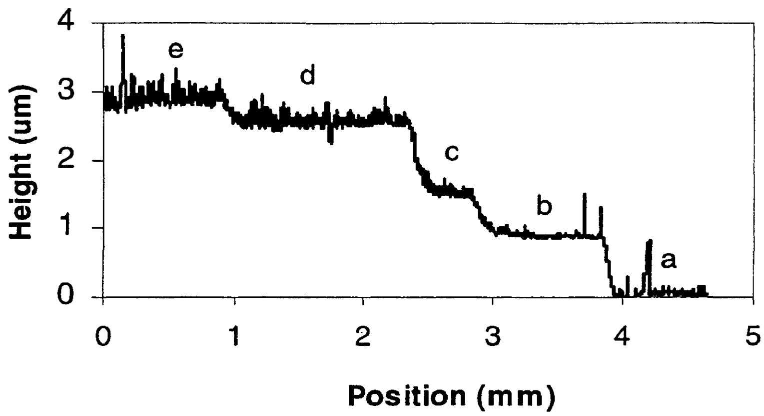

Figure 4.5a Etch profile for a 350°C annealed sample

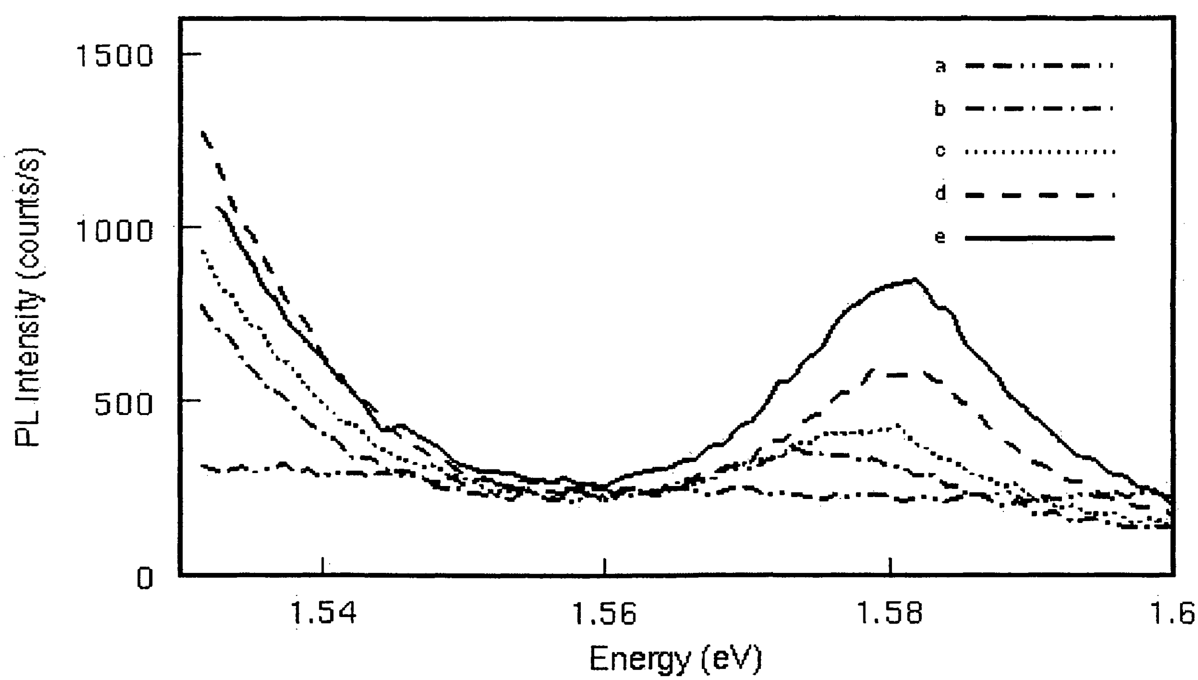

Figure 4.5b The band edge PL spectra of a 350°C annealed sample, the labeling curves (a-e) correspond to etch steps from part a on which the measurements were made

We assume the 1.585 peak correspond to E_g-E_{ex} in pure CdTe, and we rearrange Eq.14 to read

$$E_g\text{-}E_{ex}(x)=1.585-1.01x+1.74x^2 \qquad (15)$$

S composition is then estimated from this equation. We also assumed that the exciton binding energy change with S content is small which we expect. All the estimates based on Eq. 15 may include ±5% error due to uncertainty of parameters in formulas. We estimate S concentration to vary from 1.5% for the alloy peak at the CdTe side to 4% near the interface.

Fig.4.7a shows the etch profile and fig. 4.7b shows PL curves for a sample annealed at 460°C. The PL peaks are visible at lower energy, which corresponds to higher S content. This S content is consistent with estimated S concentration from PL spectra which are obtained from the thinnest region of the sample annealed at 410°C. The S concentration is estimated to be around 5% for the sample annealed at 460°C.

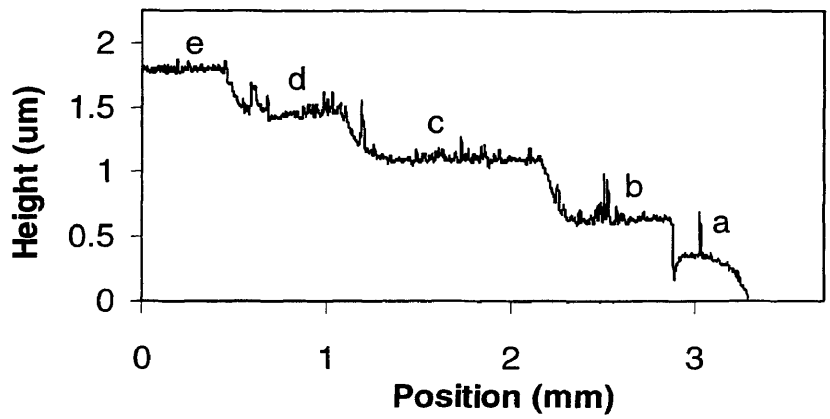

Figure 4.6a Etch profile for a 410°C annealed sample

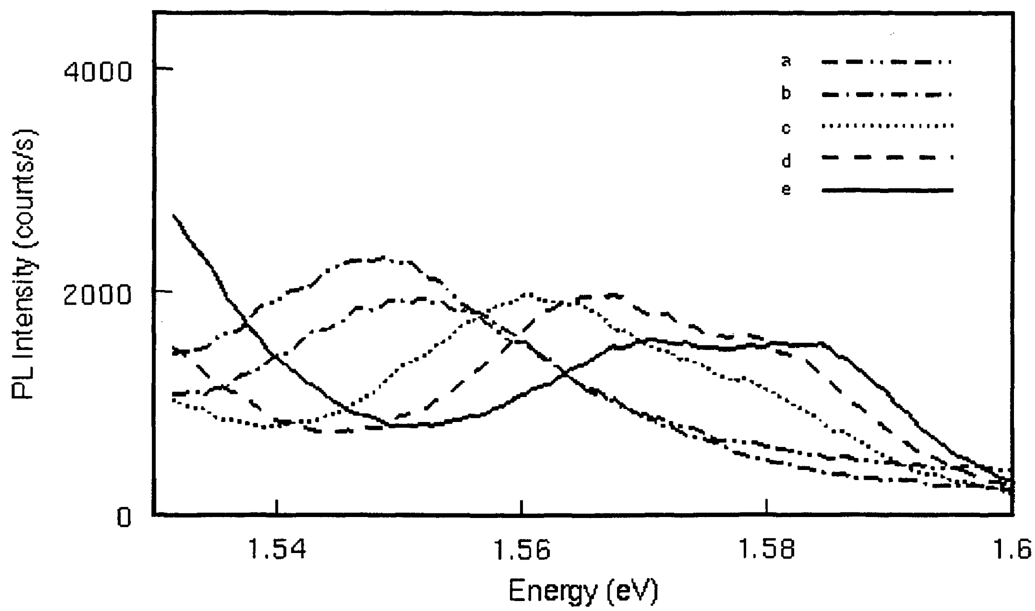

Figure 4.6b The band edge PL spectra of a 410°C annealed sample, the labeling curves (a-e) correspond to etch steps from part a on which the measurements were made

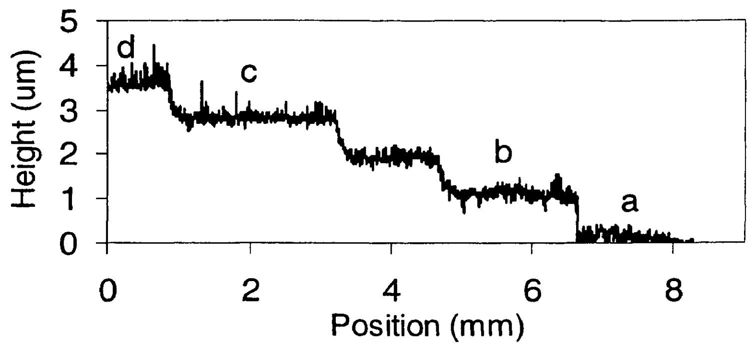

Figure 4.7a Etch profile for a 460 °C annealed sample

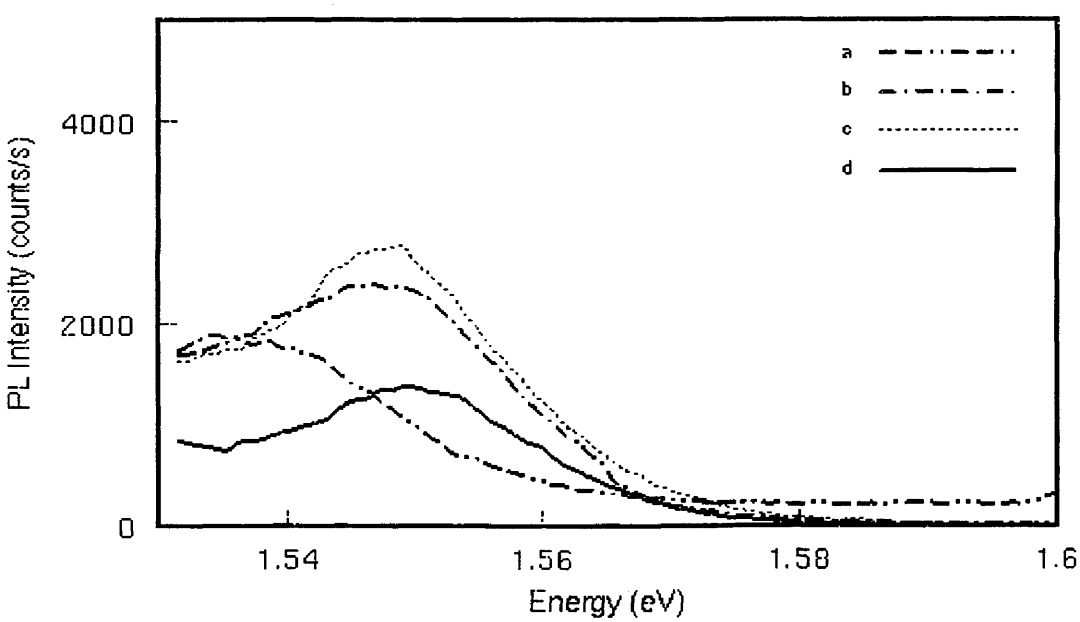

Figure 4.7b The band edge PL spectra of a 460 °C annealed sample, the labeling curves (a-e) correspond to etch steps from part a on which the measurements were made

4.1.3 Room temperature PL results

We also explored whether PL spectroscopy at room temperature could be used to analyze the S diffusion into CdTe. The PL measurements at room temperature were also performed as a function of step depth on the same samples used for low temperature PL measurements with the etch profiles shown in figs. 4.5a, 4.6a, and 4.7a. The PL spectra on each sample were obtained from both the backside (or CdTe side), and the glass side of the samples.

At room temperature, band-to-band recombination is dominated by defect state recombination. The defect density is so high that the photoexcited carriers produced by a CW laser operating at reasonable power (one that won't substantially heat the sample) recombine primarily non-radiatively and limit the ability to detect luminescence of the sample. The efficiency of emission is

$$\eta = \frac{P_r}{P_r + P_{nr}} \tag{16}$$

where P_r is the probability of radiative recombination and P_{nr} is the probability of non-radiative recombination.

Unfortunately, the mechanism of the non-radiative recombination among the defect levels in the CdTe layer of the cell is not well known. This mechanism can be very complex and have several explanations. One of the reasons may be that the charge carriers recombine at defect levels inside the band gap. These defect levels are Shockly-Read-Hall defects (SRH). The rate of recombination can be expressed (23) as

$$\frac{dn}{dt} = \frac{dp}{dt} = \frac{\sigma_p \sigma_n v_{th} N_t (pn - n_i^2)}{\sigma_n \left\{ n + n_i * \exp(\frac{E_t - E_i}{kT}) \right\} + \sigma_p \left\{ p + n_i * \exp(\frac{E_i - E_t}{kT}) \right\}} \tag{17}$$

where

- σ_p : capture cross-section for a hole in the considered defect level
- σ_n : capture cross-section for an electron in the considered defect level
- T : temperature
- v_{th} : thermal velocity of the electron or hole
- N_t : volume density of the defect states
- n : concentration of electrons
- p: concentration of holes
- n_i : intrinsic concentration of holes and electrons
- E_t : energy of the defect level inside the band gap
- E_i : energy of the intrinsic Fermi level which is in the middle of the band gap (It is very close to the middle of the band gap for CdTe)
- k : Boltzman constant.

From the SRH equation, we can see that the rate of non-radiative recombination can have maximum values for defect levels located in the middle of the band gap which means that exponential terms will be zero. On the other hand, when the defect levels approach the valence or conduction band the rate of recombination decreases. This is because of the probability of thermal excitation of a carrier to this band (electron when the defect level is close to conduction band or hole when the defect level is close to the valence band) increases and the probability of recombination decreases. In the defect levels which are close to the middle of the band gap, recombination can take place; however, the energy of these levels is low and for this reason, photons emitted by a carrier recombining through the defects will not be detected by PL. Moreover, the rate of radiative recombination can be expressed as Ref. (23)

$$\frac{dn}{dt} = \frac{dp}{dt} = B(T)np \tag{18}$$

where B(T) is a recombination coefficient as a function of temperature and it is

$$B(T) = B\left(\frac{E_g}{1.5}\right)^2\left(\frac{300}{T}\right)^{1.5}$$

where B is a constant related to effective density of states and it is 3×10^{10} for GaAs. This constant is somewhat different in CdTe since the effective masses in the conduction and valence bands which are the parameter for the effective density of states are different from GaAs. We assume, however, that this recombination rate can also be used for CdTe material. We notice that the value of B(T) increases as the temperature increases; therefore, the rate of radiative recombination decreases and the probability of the radiative recombination decreases. Hence, it is very difficult to make PL measurements at room temperature on polycrystalline CdTe with a CW laser in the same manner as we used at low temperature. In this study, instead of using the Ar-ion-CW laser, a cavity-dumped dye laser was used as an excitation source. By using the cavity-dumped dye laser, which is a pulsed excitation source, we could inject more photoexcited carriers during the pulse than by using CW-laser, while keeping the average power low enough to avoid damage to the sample. In this way, we saturate the defect states. Once the defect states are occupied with carriers, the remaining carriers are free to recombine radiatively.

Fig. 4.8 shows a PL spectrum from the glass side of a sample which has a standard configuration and was annealed at 410 °C using the standard process. There is a main peak at 1.478 eV and a shoulder at higher energy. We have used a two-peak-Lorentzian fitting function to fit the spectrum. The peak energies from the fit are at 1.467 and 1.508 eV. According to information about the band to band transition and PL results, mentioned in Ref. (48), we speculate that the shoulder could come from band to band recombination in a nearly pure CdTe phase of the sample. Its energy matches the band gap energy of CdTe which is 1.51 eV at room temperature. However, there is uncertainty in the fit energy related to the model chosen. We also used a Gaussian fit which may be more reasonable for inhomogeniously broadened lines but the Lorentzian line gives a better fit. However, within the uncertainty of our measurements, both are suitable and lead to the same conclusions. Based on our low temperature study it is tempting to assign the PL peak at 1.478 eV to band-to-band recombination from a $CdTe_{1-x}S_x$ ternary phase formed near the interface of CdTe/CdS due to S diffusion into CdTe as was done by Levi et al. in Ref. (49).

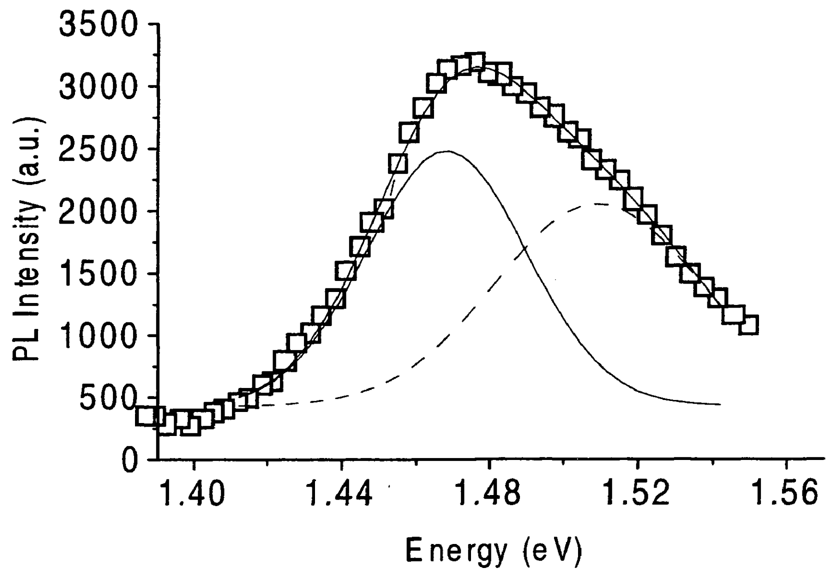

Figure 4.8 PL spectrum from glass side at room temperature

Fig.4.9 shows the PL spectrum from the back (CdTe side) of the sample. The spectrum contains a single broad maximum at 1.498 eV. This energy is 12 meV below the bandgap of CdTe; therefore we can't associate this peak with the band to band transition corresponding to a pure CdTe phase. If this peak had occurred because of any defects, by increasing the intensity of the laser we should have eventually saturated the defect and seen the peak shift to the higher energy band to band transition. In our study, we increased the intensity of the laser by as much as a factor of five; however, no shift was observed. (Since we performed the PL measurements at room temperature, the idea that this peak occurred as a result of excitonic transitions was not a part of our consideration. At room temperature the excitons are thermalized).

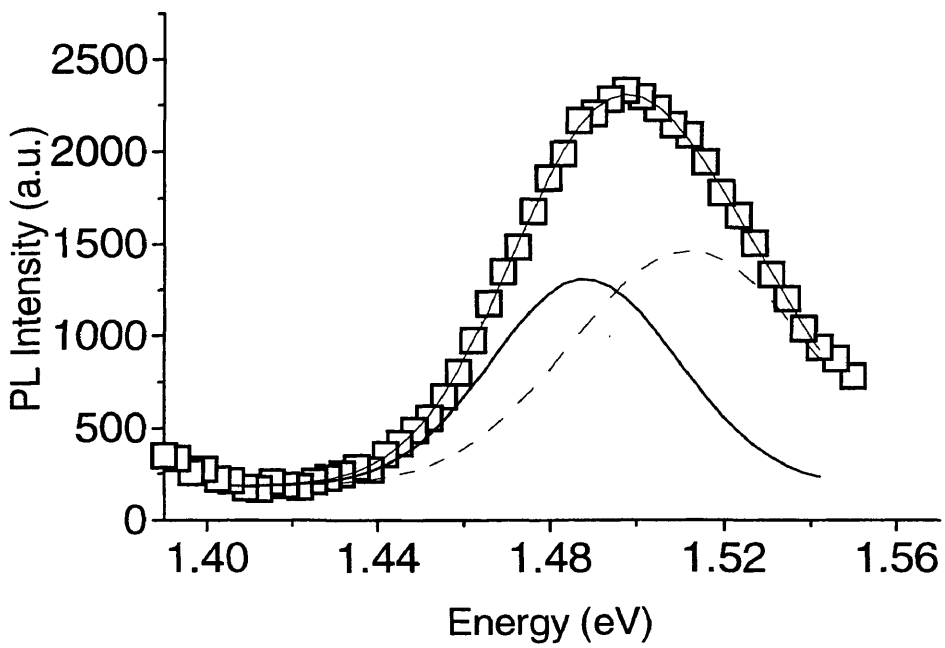

Figure 4.9 PL spectrum from CdTe side at room temperature

Because of the asymmetry of the peak, we again tried to fit this peak by using the two Lorentzian-fitting function in analogy to analysis from the glass side. We achieved fitting of the peak with two Lorentzian lineshapes with energies 1.487 eV and 1.509 eV. When we tried to fit this peak by using Gaussian functions, we were also able to fit it with two peaks and the positions of the Gaussian peaks were almost the same as the Lorentzian ones. Interestingly the peak at 1.509 eV matches the band gap energy of CdTe, and the peak at 1.487 eV matches the band gap of a $CdTe_{1-x}S_x$ alloy with 2.2% S content based on eq. 12. We, surprisingly, noticed that the higher-energy-Lorentzian peak stayed in the same position compared with the position of the Lorentzian peak of the PL spectrum obtained from the glass side, while the lower-energy- Lorentzian peak changed its position relative to the glass side. By considering the results of the PL spectra taken from CdTe side of the 350 °C, 410 °C and 460 °C annealed samples, discussed next, we speculate that what appears to be a single broad peak observed in the PL spectrum of the CdTe side may actually consist of two peaks, which belong to a nearly pure CdTe phase and the ternary phase. However this is not a definitive conclusion and it may be clarified by doing more investigation by using, for example, Near-Field Scanning Optical Microscopy (NSOM) supported PL measurements .

Fig.4.10a,b,c, and d show the room temperature fitted PL spectra taken from the CdTe side of the sample annealed at 350 °C as a function of depth (from unetched region to most etched region, respectively). The PL spectrum from the unetched region shows a peak position of 1.508 eV. Since the energy of the peak is close to the band gap energy of CdTe, this peak was again identified as a band-to-band transition. By considering spectral resolution and a small amount of the S content, we can explain the peak energy which is 2 meV below the bandgap energy of CdTe. As the PL measurements were performed closer to the interface (fig.b, c, and d), the shape of the spectrum becomes broader and the position of the maximum shifts to lower energy. As seen in fig.4.10d, the PL spectrum shows a maximum at 1.483 eV, and a clear shoulder at higher energy around 1.51eV which matches the band gap energy of CdTe. We again interpreted this shoulder as arising from nearly pure CdTe.

In addition, we have performed the two Lorentzian fit in each PL spectrum, and we can observe that the higher energy Lorentzian peak stays at almost the same position as the lower energy Lorentzian peak changes its position to lower energies with increasing depth. This can be seen more clearly in the fig. 4.10d. According to the fitting process done on the PL spectrum taken from the most etched region, the position of the shoulder was found at 1.514 eV which could again be interpreted as band-to-band recombination coming from a pure or nearly pure CdTe phase. The lower energy peak is shifted around 23 meV compared to the fit to the unetched PL spectrum. This shift may imply increasing S content. Based on eq. 13, it would correspond to 2.3% S content.

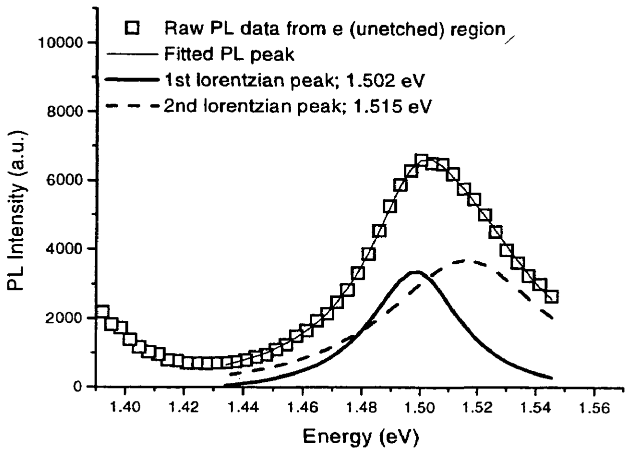

a)

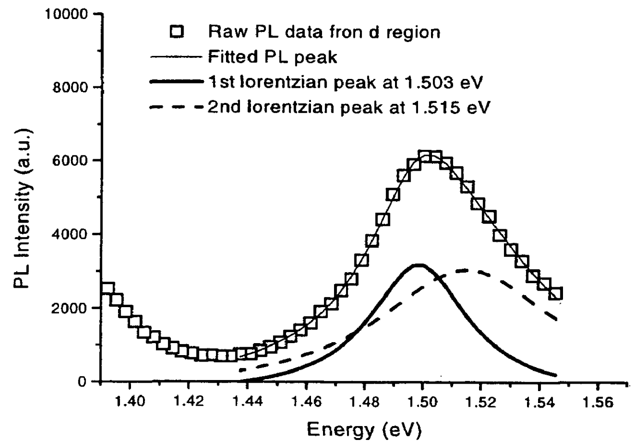

b)

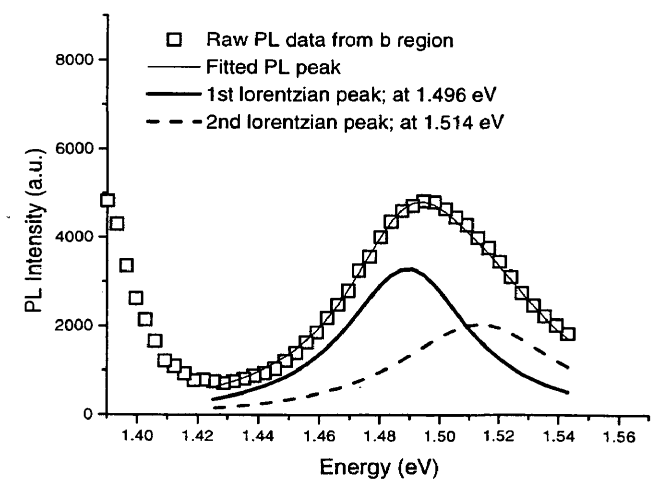

c)

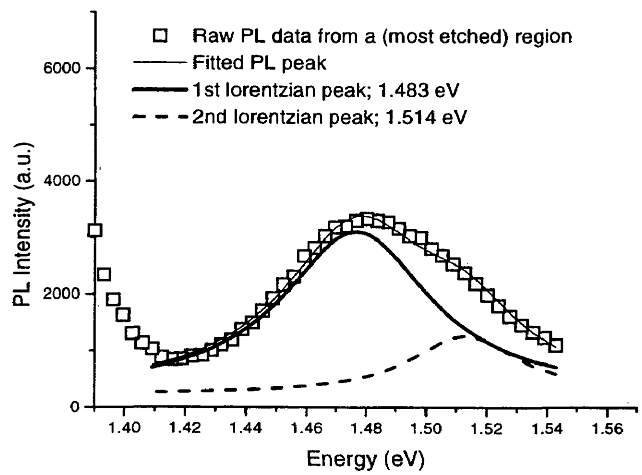

d)

Figure 4.10 PL spectra as a function of depth from 350 °C annealed sample. The location of the measurement relative to the profile in fig. 4.5a is indicated in each figure.

Fig.4.11 shows PL spectra taken from the CdTe side of the sample annealed at 410 °C. The PL spectrum from the unetched region of the sample (fig. 4.11a) shows a single broad maximum similar to fig. 4.8. PL on three of the etched regions are shown in parts b, c, and d. As we make PL measurements nearer to the interface, the PL energy decreases, and a shoulder appears at approximately 1.51 eV, The data was again fit to two peaks. The lower energy peak, which we speculate is an alloy peak, shifts to lower energy with depth, implying increasing S content with increasing depth. This interpretation is consistent with XRD, low temperature PL, and Auger results discussed next. If we assume that the interpretation is correct, the energy difference between the CdTe and $CdTe_{1-x}S_x$ can be used to estimate the S concentration of the ternary phase as a function depth. The estimate shows that the S concentration varies from 2.3% for the alloy peak at the back (CdTe) side to 5.1% near the interface. The higher peak energy obtained from the fit stays at approximately 1.51 eV as a function of depth. This result strengthens our hypothesis that the single broad spectrum consists of two peaks which belong to a nearly pure CdTe and a $CdTe_{1-x}S_x$ ternary phase.

We also obtained room-temperature PL measurements from the back (CdTe) side of the sample annealed at 460 °C (fig.4.12a, b, c, and d). The PL spectra taken from region e and d show a tail around 1.51 eV and a very broad asymmetric maximum around 1.46 eV. The PL spectra of region b and a interestingly show another shoulder around 1.44 eV as well as the shoulder at 1.51 eV and a peak at 1.46 eV.

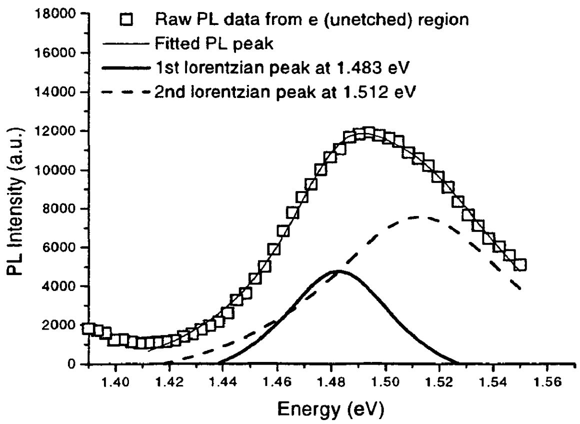

a)

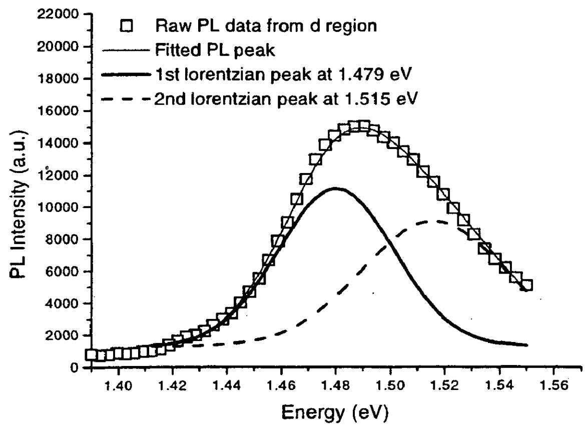

b)

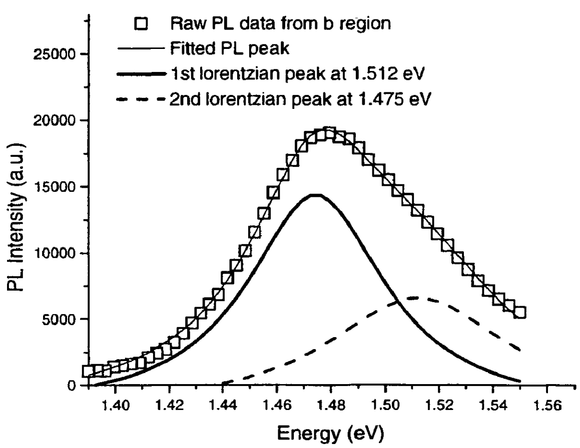

c)

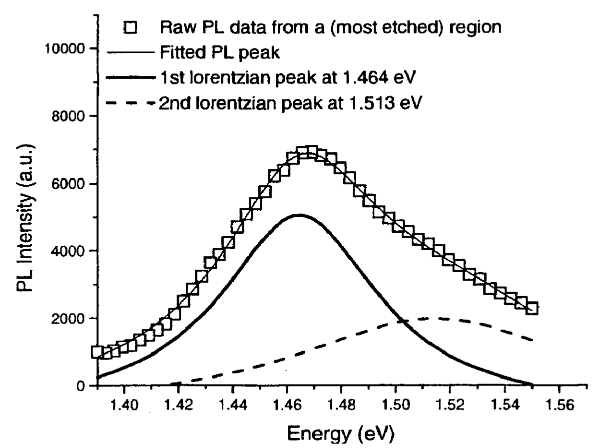

d)

Figure 4.11 PL spectra as function of depth from 410 °C annealed sample. The location of the measurement relative to the profile in fig. 4.6a is indicated in each figure.

The PL spectra of the 460 °C annealed sample does not show a systematic change like we observed in the spectra of 350 °C and 410 °C annealed samples as measurements are made from the CdTe surface to near the interface. We tried to fit the PL spectra and we achieved the best fit using three-Lorentzian peaks. Although the intensity of the Lorentzian peaks change, they stay at almost the same position in each PL spectrum. The Lorentzian peaks with around 1.508 and 1.47 eV energies match again the band gap energy of CdTe and the band gap of a $CdTe_{1-x}S_x$ alloy with 5.3% S content based on eq. 13, respectively. These peak energies also match the Lorentzian peak positions used to fit the PL spectrum taken from near the interface of the 410 °C annealed sample (fig.4.11d).

The Lorentzian peak at around 1.44 eV appeared at roughly the same energy in all the spectra for the 460 °C annealed sample. It was not observed in the fitted PL spectra of 350 °C and 410 °C annealed samples. First, if we assume this peak represents another composition of alloy, we estimate S content to be around 8%. However, since the solubility limit of S in CdTe at 415 °C is 5.8% as reported by Jensen et al. (43), it is hard to believe that this peak represents another alloy peak. For this reason, we tend to believe that this peak may come from a deeper defect level in the cell.

Fig. 4.13 shows S concentration vs. depth as result of the PL measurements at low temperature and room temperature. The S concentration estimated from room temperature PL matches the values of concentration estimated from low temperature PL reasonably well. In the 460°C anneal, we have estimated S from the 1.47 eV feature which is most likely associated with a $CdTe_{1-x}S_x$ phase.

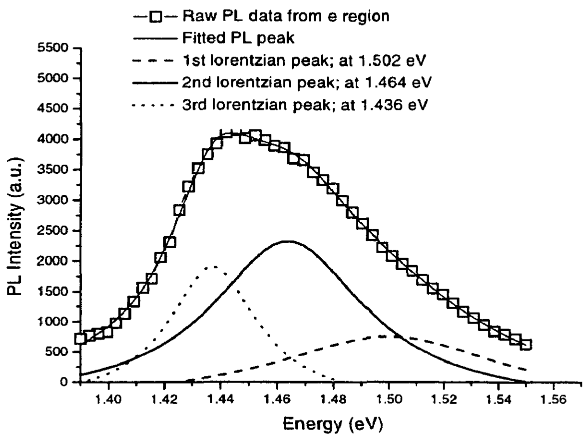

a)

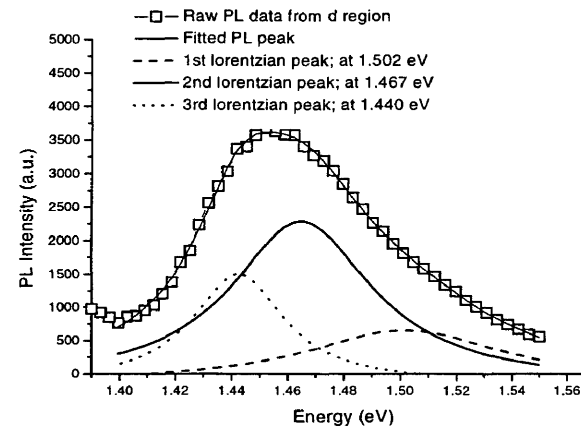

b)

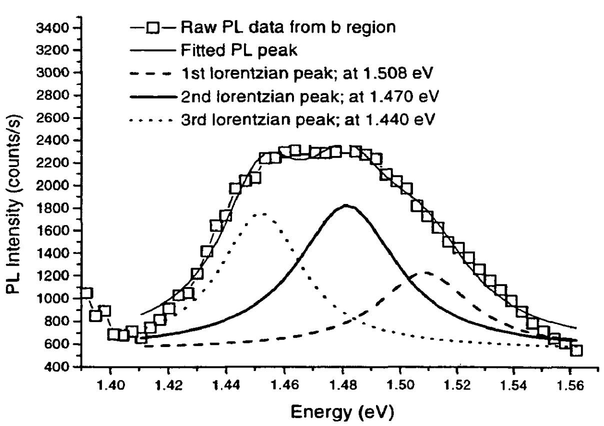

c)

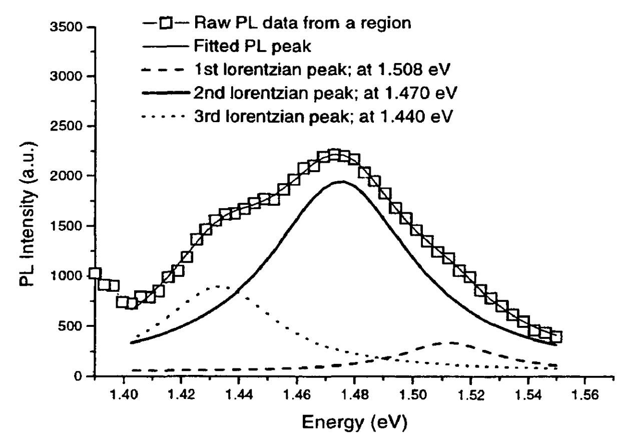

d)

Figure 4.12 PL spectra as function of depth from 460 °C annealed sample. Regions are identified consistent with the depth profile in fig. 4.7a

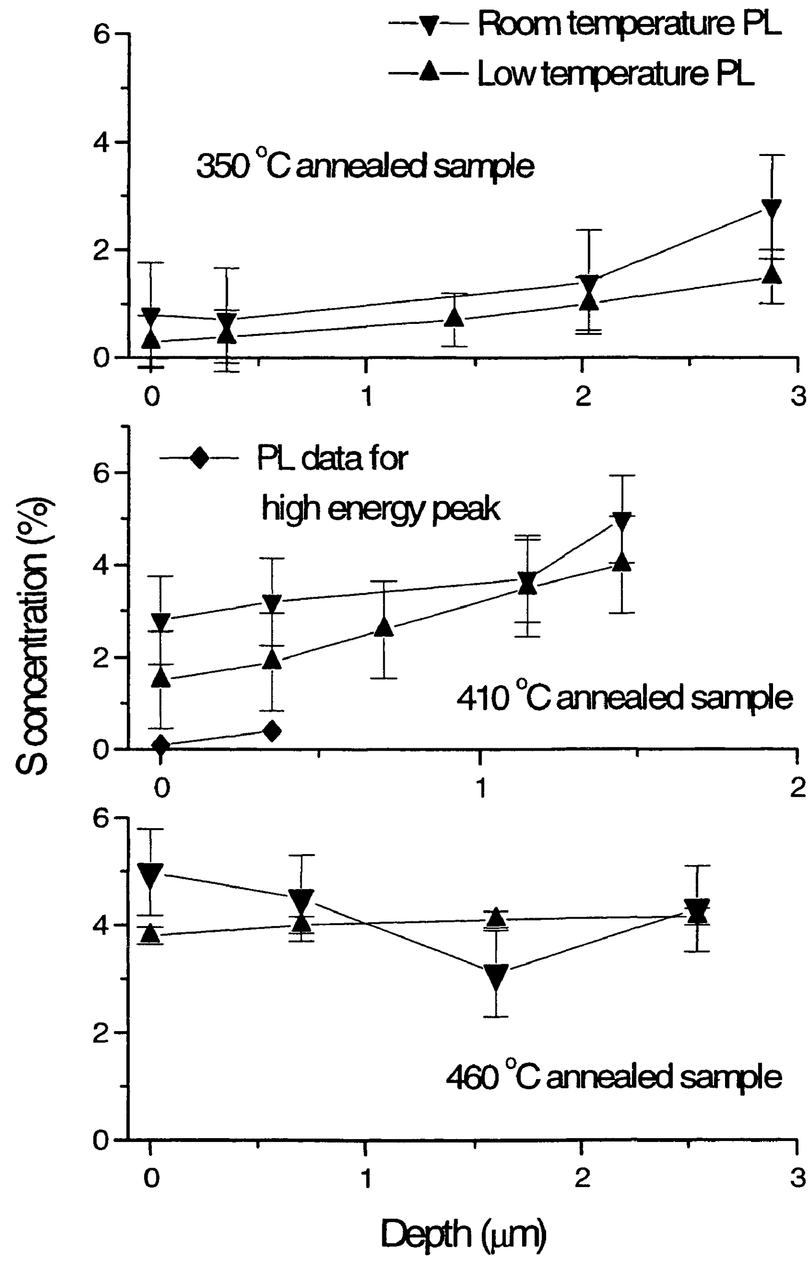

Figure 4.13 The comparison of room temperature PL and low temperature PL determination of S composition vs. depth

4.1.4 AES Results

AES analysis was also used to determine the sulfur composition on the same electrodeposited CdTe samples studied using XRD and PL measurements. Measurements were again taken as a function of step height. The analysis of these samples was performed using the following procedure

- The samples were sputtered for 30 seconds using an electron beam operating at 3kV. The sputter rate was approximately 400 Å/min, thus, 200 Å of the film was removed during the sputtering. Fig. 4.14 shows that sputtering removed the carbon and oxygen contamination from the surface.
- The Auger analysis was performed on this sputtered region by using a 5kV electron-beam
- To prevent S diffusion from the CdS layer into the CdTe layer as a result of the highly focused heat source from a stationary electron beam, the beam was rastered back and forth across the CdTe surface. If the beam remains stationary, the localized heat causes the sulfur to leach out of the CdS layer and give erroneous concentration.
- The atomic concentrations of S, Cd, and Te were determined by recording the emission spectrum.

This procedure was followed at each step height of the samples annealed at 350 °C, 410 °C, 460 °C. The atomic concentration data as a function of etch depth is shown for every sample in tables 4.1, 4.2, and 4.3. Fig. 4.15 shows a comparison of Auger and low temperature PL determined S content. Auger results are in agreement with PL measurements within experimental error (fig4.15).

Table 4.1 Atomic concentrations of S, Cd, and Te for 350 °C annealed sample.

REGION	% S	%Cd	% Te
a	2.4	46.0	51.6
b	2.1	45.9	51.9
c	0.3	46.1	53.5
d	0.1	46.3	53.4
e	0.2	45.6	54.0

Table 4.2 Atomic concentrations of S, Cd, and Te for 410 °C annealed sample.

REGION	% S	%Cd	% Te
a	2.6	45.9	51.3
b	4.2	46.4	49.2
c	1.3	46.2	52.4
d	0.9	46.9	52.1
e	0.7	46.1	53.0

Table 4.3 Atomic concentrations of S, Cd, and Te for 460 °C annealed sample.

REGION	% S	%Cd	% Te
a	5.1	46.0	48.8
b	3.4	46.7	49.8
d	2.6	47.8	47.8

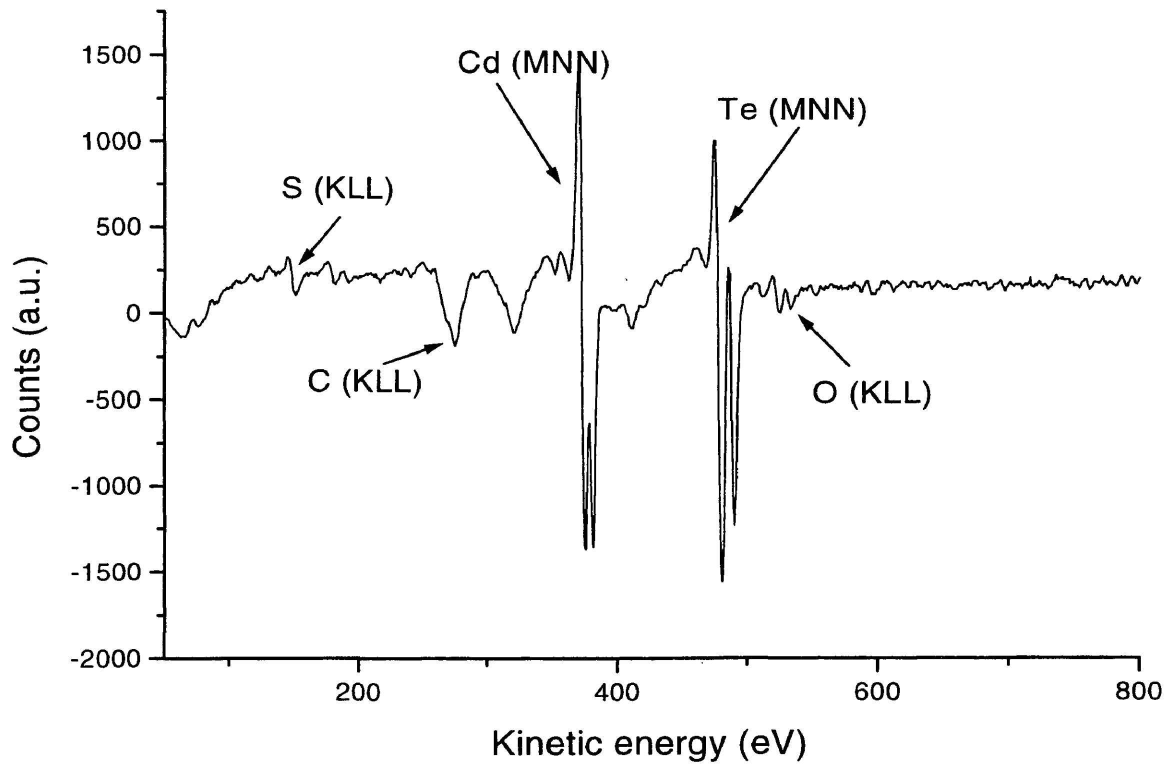

Figure 4.14 AES scan of Cd, Te, and S after sputtering

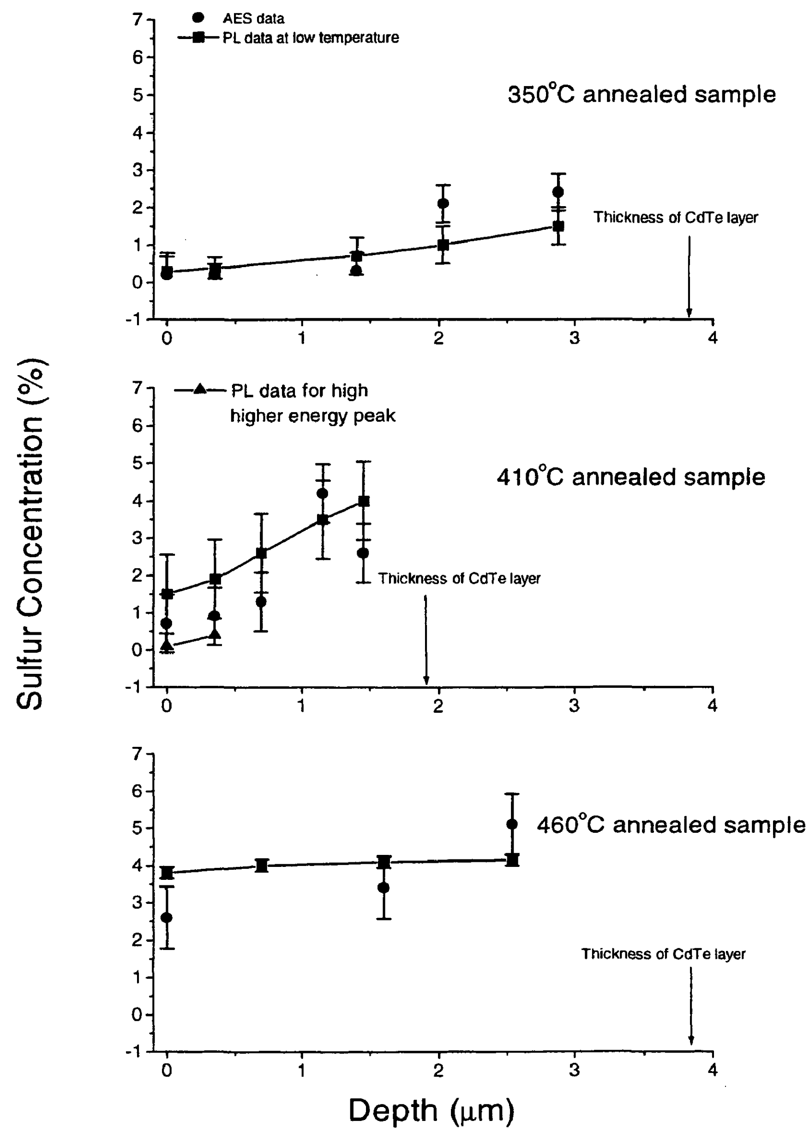

Figure 4.15 The comparison of PL and AES determined S composition vs. depth

4.1.5 Examination of the effects of annealing temperature on S diffusion into CdTe/CdS solar cells.

To study the interdiffusion that occurs during the annealing process, we made PL measurements on a sample that was annealed sequentially at 250°C, 350°C, 410°C, and 460°C. After each annealing step, a PL measurement was done from the CdTe side. Fig. 4.16 shows the PL spectra for these four annealing conditions.

At 250°C annealing temperature, the PL measurement does not show any near-band edge luminescence. The heat treatment may not be enough to eliminate the crystalline defects near the surface, which cause a decrease in the radiative recombination rate and make it difficult to observe excitons. After annealing at 350 °C, a 1.585 eV energy peak was obtained. The energy is very near the excitonic energies expected for pure CdTe phase. We identified it as an excitonic peak in CdTe with no (or very low) S concentration. The sample was then annealed at 410°C. The PL spectrum again shows two peaks, one of which is pure CdTe at higher energy and the other peak shows ternary $CdTe_{1-x}S_x$ at lower energy. These peaks also have an excitonic nature. It is obvious that S diffuses into CdTe at this annealing temperature; the estimated S composition for the ternary material was 2.2%. After annealing at 460 °C, the PL spectrum only exhibits $CdTe_{1-x}S_x$ ternary phase with x=5.2%. These results show us that S diffusion into CdTe increases as the annealing temperature increases.

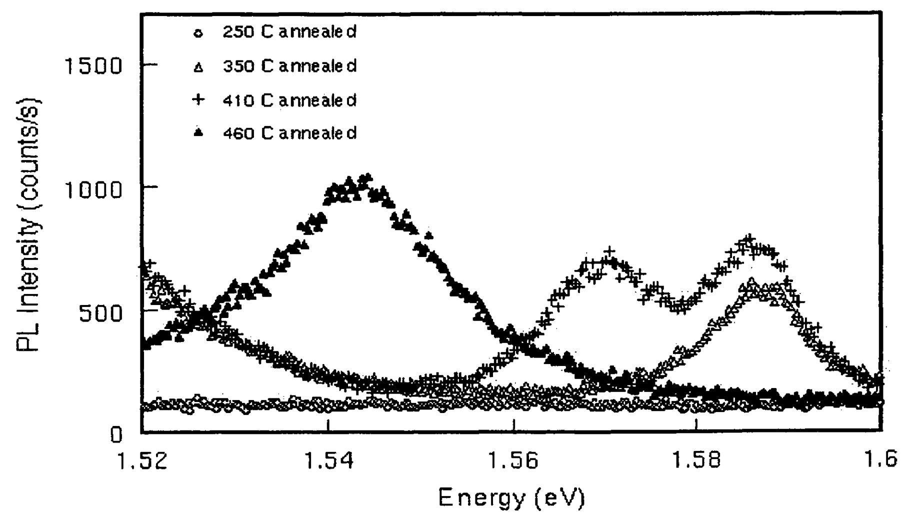

Figure 4.16 A PL spectra of the sample which were annealed at 250°C, 350°C, 410°C and 460°C.

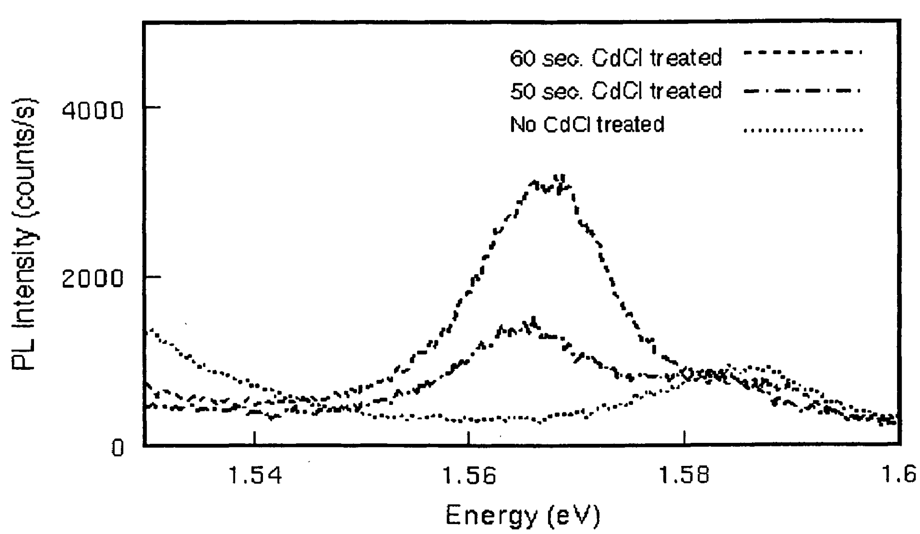

Figure 4.17 A PL spectra of the sample treated with different amount of $CdCl_2$

4.1.6 Examination of $CdCl_2$ effects on S diffusion into CdS/CdTe solar cells

The $CdCl_2$ treatment in the fabrication of CdTe/CdS solar cell is a critical step for achieving a high efficiency (> 10%) solar cell. $CdCl_2$ treatment has an important impact on the S diffusion into CdTe. In this investigation, three pieces from a typical sample configuration were used. Before annealing the pieces at 410°C, they were treated with varying $CdCl_2$ exposure times (60 sec., 50 sec., and no $CdCl_2$). Fig. 4.17 shows their PL spectrum. The PL measurements were taken from the backside of the samples.

As can be seen in fig.4.17, the intensity of the $CdTe_{1-x}S_x$ peak varies with the amount of the $CdCl_2$. The PL spectra without $CdCl_2$ only show a pure CdTe peak located at 1.585 eV. In the 50 sec. $CdCl_2$ treated piece, the PL spectrum is dominated by the ternary phase indicating S diffusion into CdTe. According to fig.4.17, the intensity of the ternary phase peak relative to the CdTe peak is getting stronger as the $CdCl_2$ exposure time increases, which may indicate that $CdCl_2$ promotes interdiffusion. This statement is in an agreement with discussion in (40, 42). Note the energy of the ternary peak does not change substantially with $CdCl_2$, hence composition does not change.

4.2 TRPL measurements of the effect of annealing temperature on minority carrier lifetime

We have studied minority-carrier lifetime in CdS/CdTe thin-film solar cells in order to determine if there is a relationship between minority-carrier lifetime and S diffusion into CdTe. For this work, we performed room temperature TRPL measurements on the samples that were used for PL (at room and low temperatures), AES, and XRD measurements as discussed above. We made TRPL from the glass side of the samples and on each etched step of the CdTe side.

Prior to the TRPL measurements, room temperature PL spectra were recorded on all samples using a pulsed dye laser operating at 600nm. TRPL measurements were then made with the spectrometer held fixed at the peak wavelength of the PL spectrum. The PL spectra from the CdTe side of the samples annealed at 350°C, 410°C, and 460°C were shown in section 4.1.3 (figs. 4.10, 4.11 and 4.12). The PL spectra at room temperature taken from the glass side of the same samples are shown in fig. 4.18

Since polycrystalline CdTe has a very high absorption coefficient at 600 nm, photogenerated carriers are created within the first micron of the material. In addition carrier diffusion length is less than 1μm in this material. Thus, the data from glass or CdTe side are representative of material on that side and are independent of one another.

Fig. 4.19 shows standard TRPL responses. We determined the minority carrier lifetime by deconvulating the TRPL response from the system response and then fitting the TRPL transient with a two-exponential function.

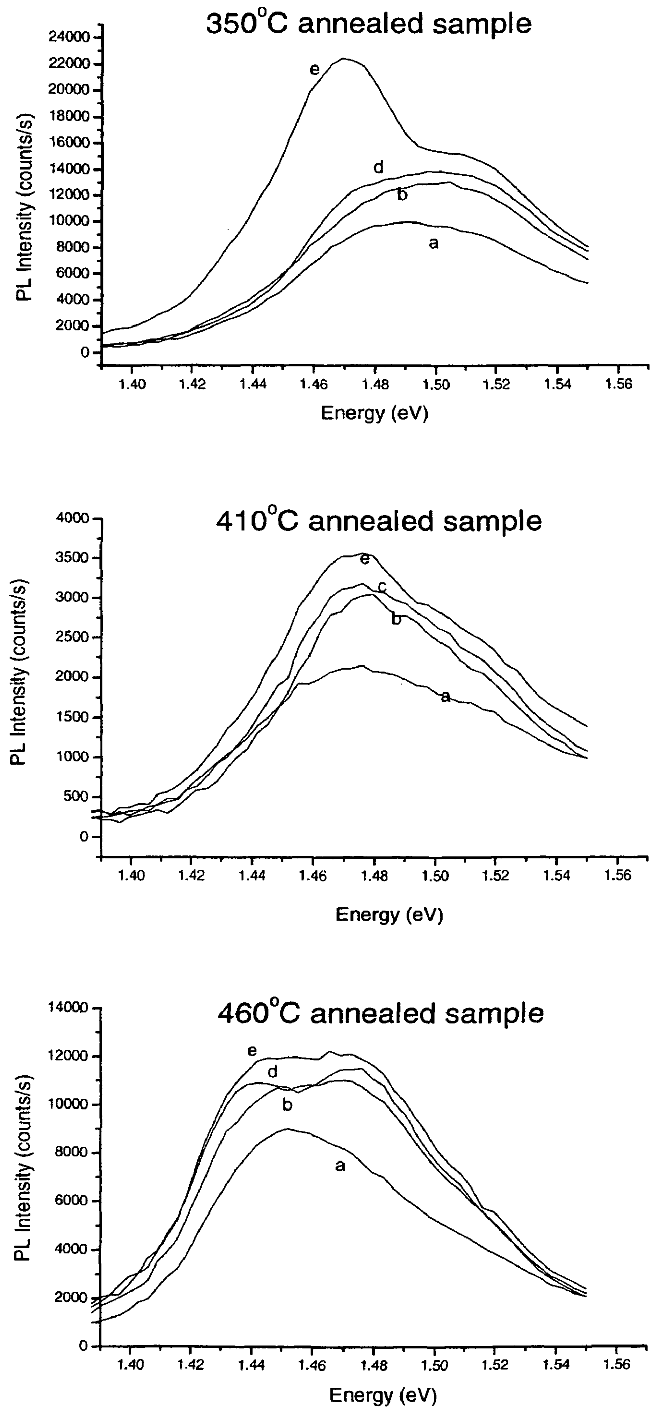

Figure 4.18 The room temperature PL spectra from the glass side of the samples annealed at 350 °C, 410 °C, and 460 °C. The letters a-e identify the step on which PL was collected

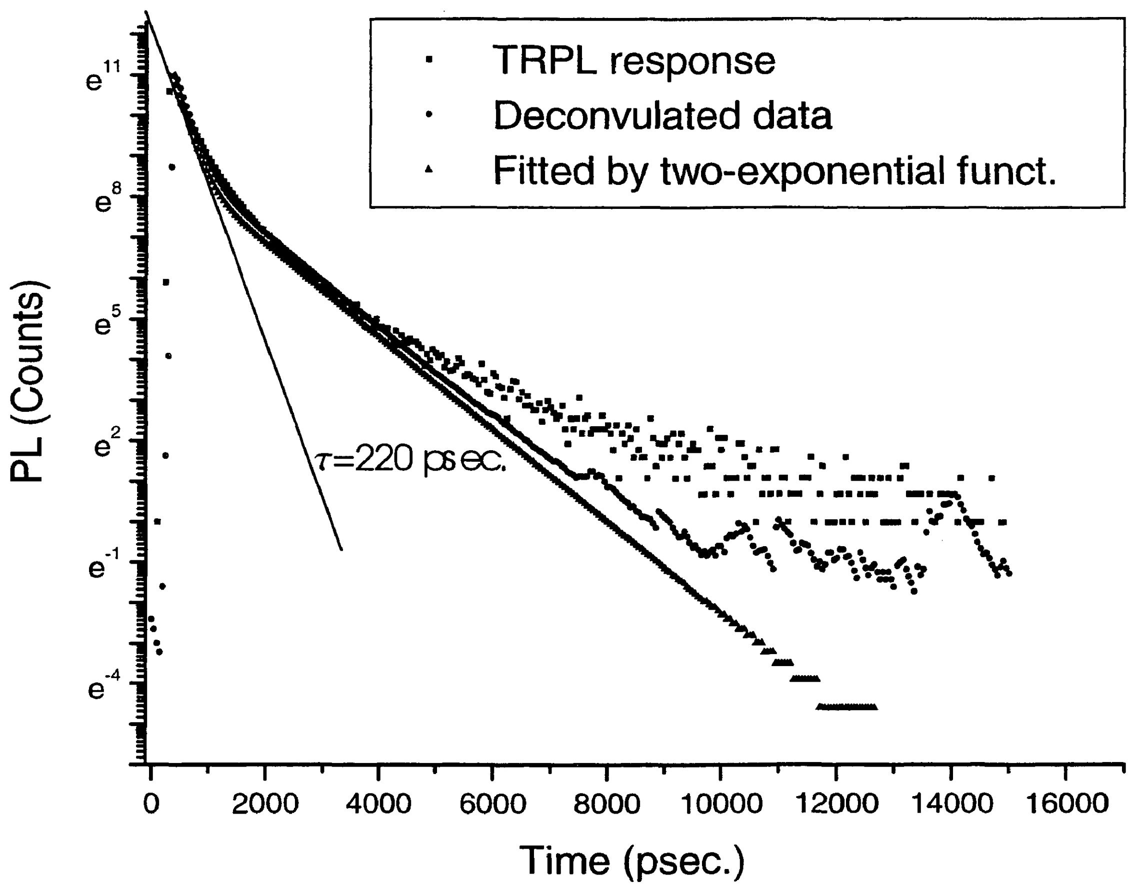

Figure 4.19 An illustration of a typical TRPL response and the best fitting of the deconvulated data

It is believed that the initial part of the transient is primarily due to radiative recombination (50). For this reason, the lifetime was obtained from this part of the curve. It is also believed that the tail of the curve (longer times) may be caused by recombination of electrons which are first trapped in a shallow defect level, then re-emitted to the conduction band, where they finally recombine with holes and emit light (50).

Fig. 4.20 shows the minority-carrier lifetime of the samples annealed at 350°C, 410°C, and 460°C as a function of step height. As seen in fig. 4.20, the lifetime measurements taken from the CdTe side of the sample did not vary significantly with depth. The lifetime was also generally less from the CdTe side than the glass side. However, as the CdTe is thinned, (for the samples annealed at 410°C and 460°C) the lifetime measured from glass side decreases, eventually becoming comparable to the lifetime measured from CdTe side. We feel that this probably does not reflect some change in quality of the sample with depth. Instead, we suggest that this can be due to the influence of surface recombination at the etched CdTe surface. As the sample is thinned, the surface moves closer to the interface, and the lifetime from the glass side is influenced and drops. As a result, we can say that the technique of preparing material by creating etched steps in a single sample is not suitable for TRPL measurements. A way to test this and possibly improve the technique would be to find a suitable surface passivation.

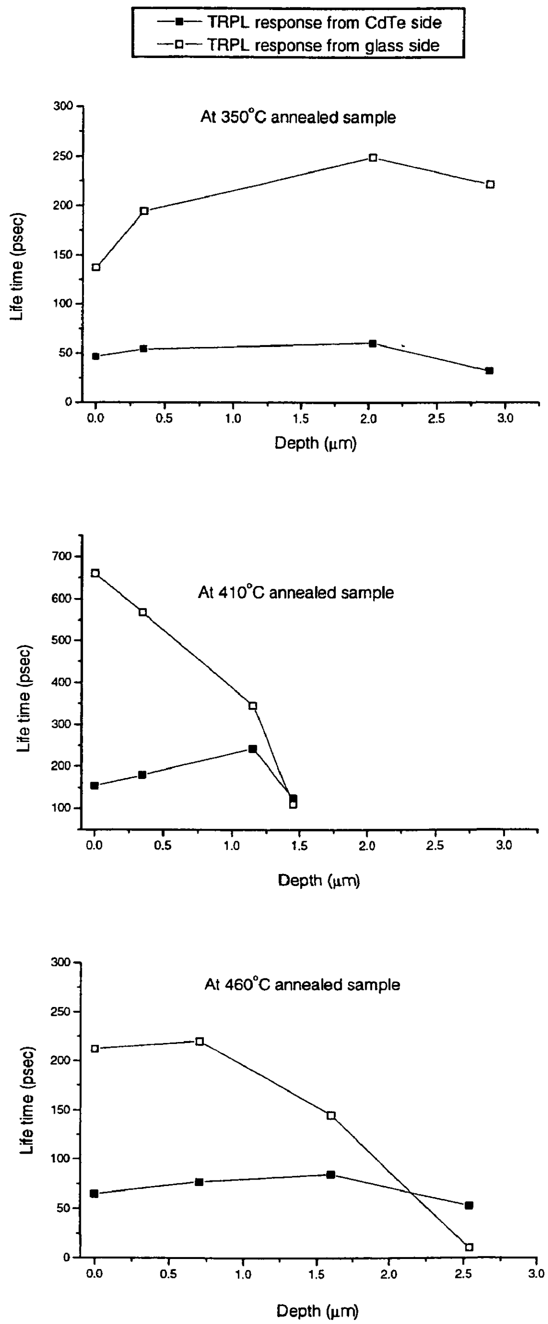

Figure 4.20 The comparison of TRPL responses taken from the CdTe side and the glass side of the samples determine lifetime vs. depth

4.3 Comparison of materials grown by different technique

We also studied PL from CdTe deposited by the CSS technique. CSS deposited CdTe was produced at NREL. The structure of the CSS deposited solar cell is the same as the electrodeposited CdS/CdTe solar cells. The CdTe layer, however is typically much thicker (near 8 μm). Readers can find much more detail about the deposition and processing of these samples in Ref. (51).

We again tried to monitor the S diffusion into the CdTe layer and effects of the $CdCl_2$ treatment on the S diffusion. Samples were again prepared by etching a series of steps into CdTe layer. For this study a CSS sample (which produced high efficiency solar cells) was divided into two pieces. We measured the thickness of the CdTe layer to be 7.2 μm. While one of the pieces was treated with $CdCl_2$ after the CdTe deposition, the other had no $CdCl_2$ treatment. Similar to the work discussed above, a series of steps of various heights was created in a each piece of the CSS sample by using a Br-Methanol solution (2:100, Br:Methanol). The etch composition was somewhat different than used for electrodeposited material. The etch rate of this solution is around 1μm/min. The step heights on each piece of the sample were measured using a surface profiler and are given Tables 4.4 and 4.5. We note that the first step was quite large (almost 6 μm). This was done because the CSS samples were made thicker than electrodeposited samples and the critical region near the interface was buried quite deep. Measurements were made on a similar sample in the 0-6 μm regime. There was no noticeable shift in peak position throughout this first 6 microns.

Table 4.4 Measurement of the step depths on the CSS sample treated with $CdCl_2$.

REGION	Time (min.)	Step Depth (μm)
a	7.0	6.900
b	6.5	6.700
c	5.75	6.200
d	0.0	0.000

Table 4.5 Measurement of the step depths on the CSS sample not treated with $CdCl_2$.

REGION	Time (min.)	Step Depth (μm)
a	7.0	6.800
b	6.5	6.500
c	5.75	6.100
d	0.0	0.000

The PL spectra at low temperature as a function of depth taken from the backside of the CSS sample which had $CdCl_2$ treatment are shown in fig. 4.21. The PL spectrum taken from the unetched region of the sample shows a peak at 1.576 eV and very broad peak at 1.44 eV (fig. 4.21). The peak at 1.44 eV is the deep defect peak previously mentioned, and its position is in the agreement with the PL spectra of the electrodeposited sample in fig. (4.13). The exact identification of the PL peak at 1.576 eV is not completely clear to us, but we can give a few possible explanations. First of all, this peak cannot be a result of excitonic transitions in pure CdTe because as mentioned above, excitonic luminescence in crystalline material occurs between 1.585 to 1.596 eV at low temperature. If we compare this PL spectrum with the PL spectrum of single crystal CdTe, the1.576 eV peak position matches the X-LO phonon replica peak in the spectrum of crystalline CdTe. We could argue that the peak at 1.576 eV is as a result of (X-LO) transition. However, the PL spectrum does not show any no phonon excitonic features. For this reason, this probably is not the correct identification, either. In addition, we believe that this peak cannot be a result of donor-acceptor-pair recombination, based on comparison of the energy of the peak with the energy of DAP transitions reported for CdTe. An excitonic peak from a $CdTe_{1-x}S_x$ phase, could also account for this energy. But for such a thick sample, it is not clear that we should expect a $CdTe_{1-x}S_x$ phase at the back. (Although we note, AES does show S at the back surface as discussed below). From the stand point of this study, however, the identification of the peak is not as important as the fact that it shifts to lower energy as we approach the CdS/CdTe interface.

The band edge PL spectra taken from non-$CdCl_2$ treated sample also shows a shift to lower energy as the PL measurements are made nearer to the interface fig.4.22. The peaks from region c appeared in the same position as obtained in the spectrum of the unetched region (region d). For this reason, we didn't show this spectrum in fig. 4.22. We did not observe the peak at 1.44 eV in both region a and region b.

In both samples, we estimate the S concentration assuming the shift in PL was due to S diffusion. We assume the spectrum from the back side before etching corresponds to nearly pure CdTe. Sulfur concentrations obtained in this way are shown in fig. 4.23. We also made AES measurements of the S concentrations as a function of depth. We used the same measurement technique as discussed in section 4.1.4. AES results as a function of depth for the both pieces ($CdCl_2$ treated piece and non-$CdCl_2$ treated piece) are qualitatively in agreement with PL measurements (fig. 4.23). One interesting aspect of the AES is the presence of a small S concentration at the back surface for the $CdCl_2$ treated piece.

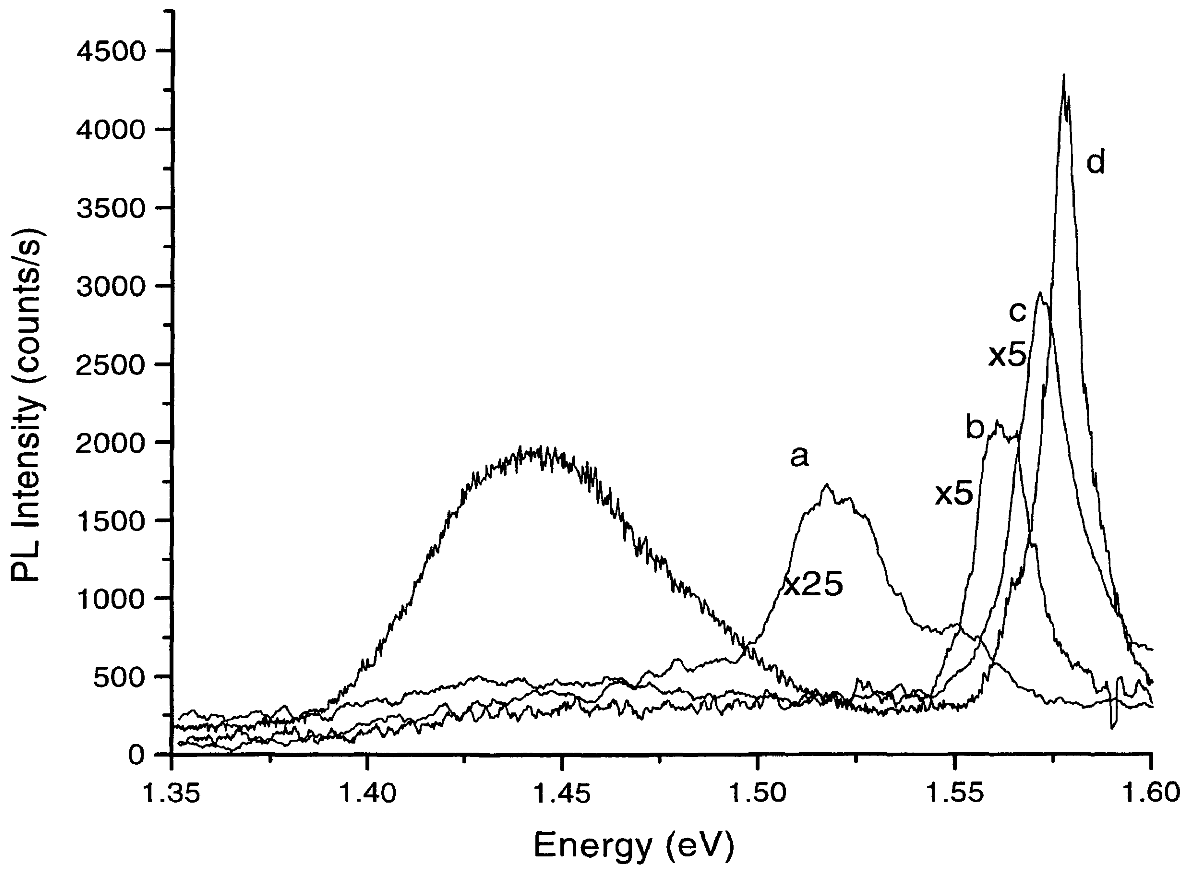

Figure 4.21 The PL spectra of $CdCl_2$ treated piece as a function of step height. Region d corresponds to the unetched CdTe side of the sample while region a corresponds to the CdS interface.

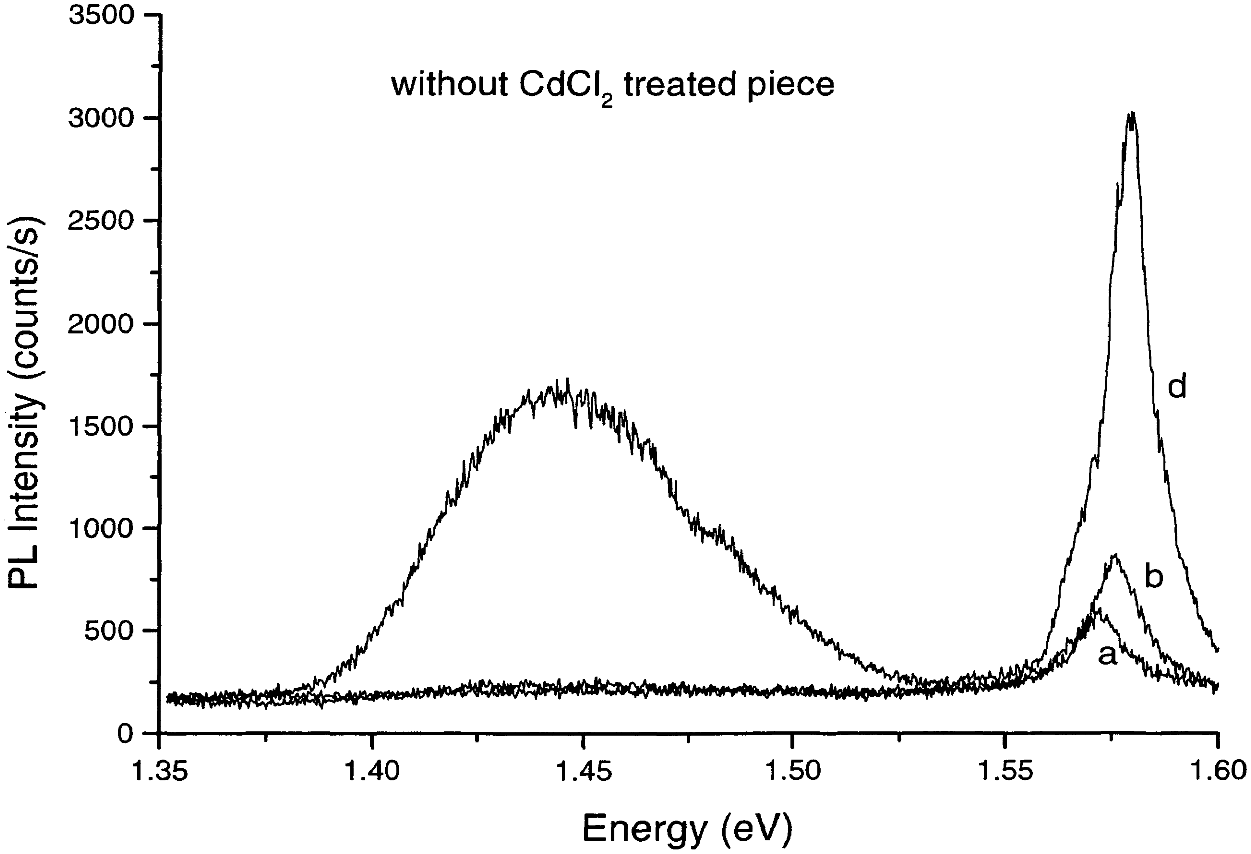

Figure 4.22 The PL spectra of non-$CdCl_2$ treated piece as a function of step height. Region d corresponds to the unetched CdTe side of the sample while region a corresponds to the CdS interface.

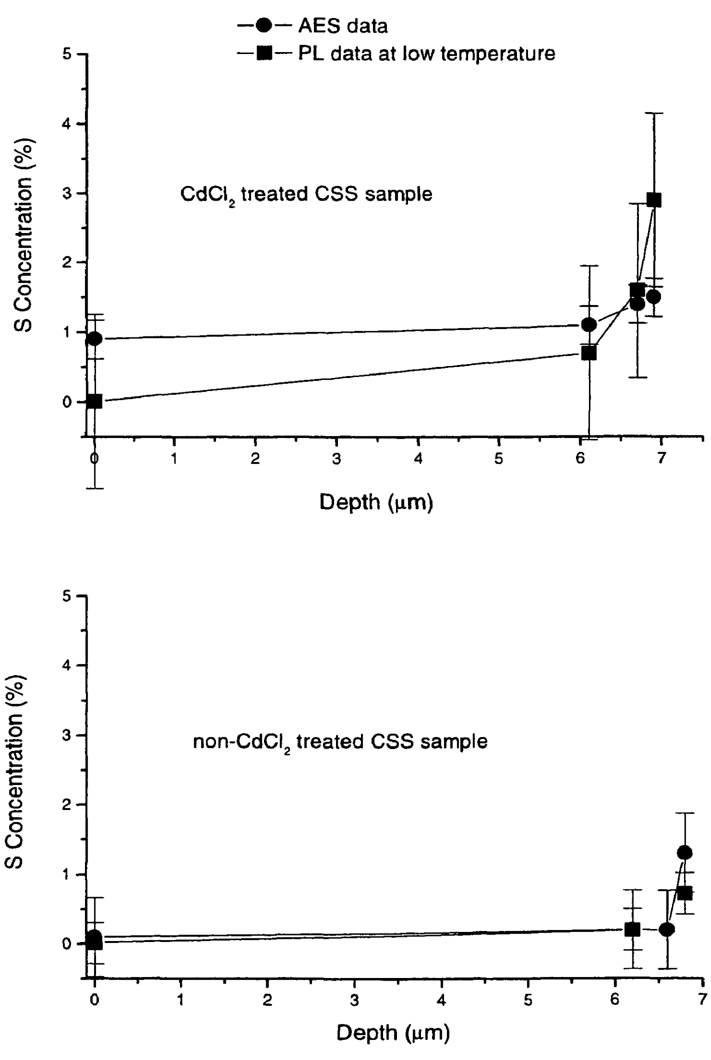

Figure 4.23 The comparison of PL and AES determined S composition vs. depth

4.4 Analyzing CdS optical properties by using PL

CdS thin films are the most commonly used window/contact layer material for high efficiency CdTe polycrystalline thin-film photovoltaic devices. They are also commonly used in CIGS solar cells. Nearly all of the cells discussed above have glass/TO/CdS/CdTe layer configurations. In the case of the CSM electrodeposited samples, after depositing CdS on the SnO_2 coated glass, a $CdCl_2$ treatment is applied to the CdS thin film layer and the layer is then annealed at 450°C for approximately 45-50 min. in N_2 as was discussed above. CdTe is then deposited. A second $CdCl_2$ and anneal treatment is then applied to the CdTe, again, as discussed above.

Since PL measurements were successful in monitoring S diffusion into CdTe from CdS, we wanted to determine if similar signatures of interdiffusion effects in CdS could be seen by PL. A typical PL spectrum taken from a sample annealed at 410 °C after the CdTe deposition is shown in fig. 4.24. The PL measurements were made at low temperature from the glass side of the sample using a 457.8 nm wavelength excitation source. This wavelength has an energy large enough to excite carriers across the CdS bandgap as well as the CdTe band gap. Fig. 4.24 also includes a PL spectrum which we obtained from single crystal (0001) CdS for comparison.

The photoluminescence of crystalline CdS has been studied extensively (52). An energy level diagram taken from Ref.(52) which can be used to explain the PL spectrum of single crystal CdS is shown in fig 4.25. For single crystal CdS, the emission spans the spectral region from 2.25 eV to 2.55 eV. The strongest peak in the PL spectrum of the single crystal is at 2.547 eV. According to the energy-level diagram and Refs. (52), the emission band at 2.547 is due to an exciton related transition (bound exciton). The other peaks at 2.450, 2.434, 2.42, 2.381, 2.345, 2.305, and 2.27 eV arise from a series of shallow level transitions (for example; the peak at 2.381 eV can be due to the transition of an electron from the n=3 exciton level to the acceptor level called exciton bound to acceptor transition).

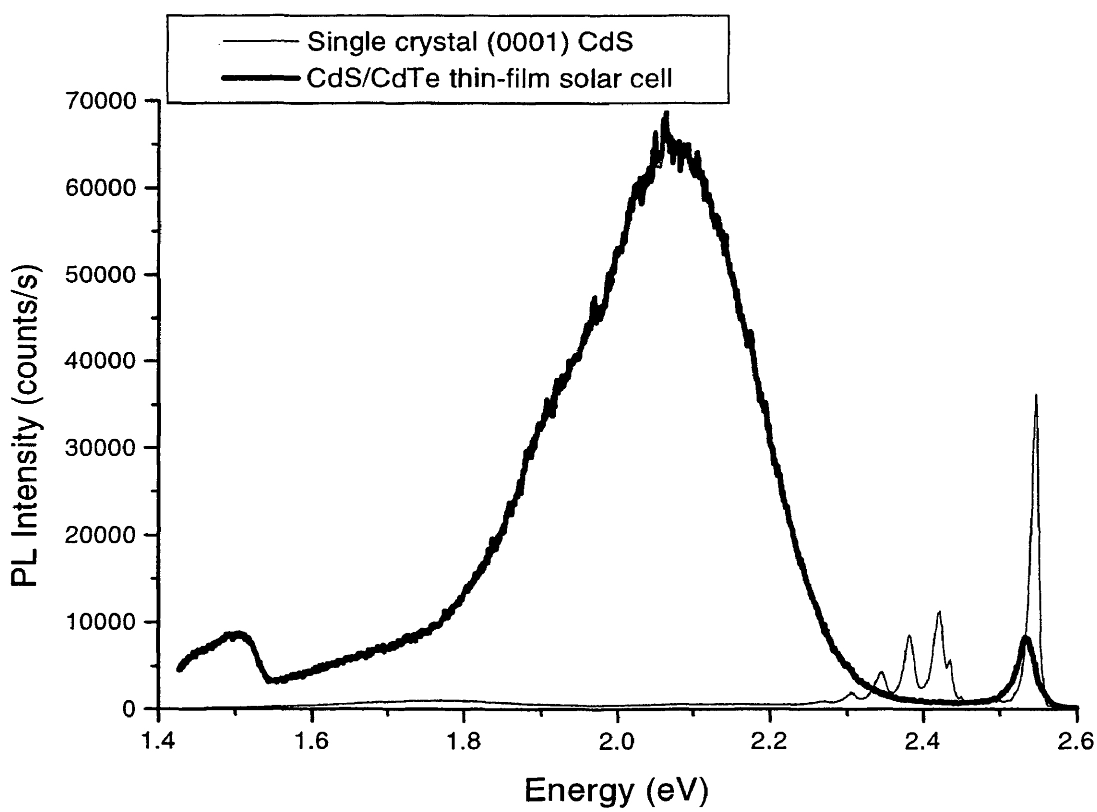

Figure 4.24 PL spectra of single crystal CdS, and CdS/CdTe thin-film solar cell

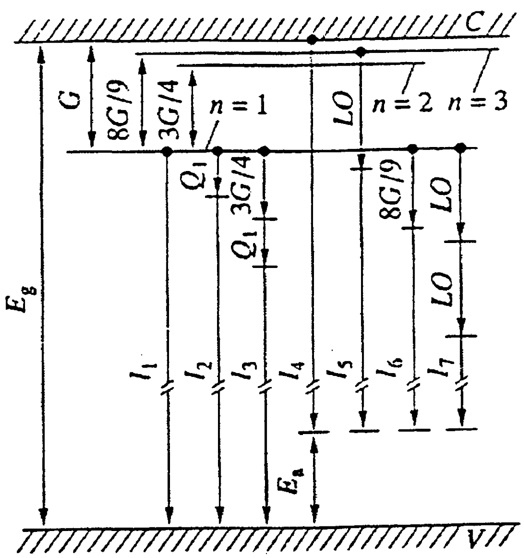

Figure 4.25 The energy levels of bulk CdS at 77 K. (G, which represents the ground state exciton energy, is 36 meV. n is the quantum number of the exciton state. Q_l is the rotation quantum number of the exciton state in the n=1 state. LO, which represents a longitudinal optical phonon level, is 38 meV. E_a, which represents acceptor level, is the 160 meV. Taken from Ref. (52). A more complete explanation of the transition cab be found in this reference)

Since the band edge PL peak at 2.54 eV obtained from PL measurements of the solar cell sample is very close to the peak position (2.547 eV) of the crystalline CdS, we believe that the PL peak at 2.54 eV is also due to exciton related transitions in the cell (fig. 4.24). The PL spectrum of CdS/CdTe solar cell shows a very broad and intense peak at 2.06 eV. This is larger then the band gap of CdTe, hence it must arise from the CdS layer. According to available data on donor and acceptor levels for bulk crystals (53), we believe that the peak at 2.06 eV is due to transitions from donor levels to the valence band. Agata et al. associated this band with Cd interstitials (54), based on an increase in strength in Cd-rich atmosphere, and reduction in strength in S-rich atmosphere.

We observe a shoulder around 1.93 eV in the PL spectrum for the solar cell. This transition has been previously attributed to S vacancies (55). The emission tail at 1.75 eV in the PL spectrum of the cell has been identified as a deep levels introduced by Te in CdS (45). At around 1.5 eV we observe the energy of the CdTe related luminescence features discussed above. This is expected since the CdS is thin and the laser light penetrates through it so electron-hole pairs are created in both CdS and CdTe.

4.4.1 Examination of the effects of annealing temperature on the optical properties of CdS in the CdS/CdTe solar cells

As shown above, interdiffusion between CdTe and CdS occurs during the anneal following CdTe deposition. The amount of interdiffusion is influenced by $CdCl_2$ treatment. We investigated the effects of this annealing step on the PL spectrum of the CdS. In analogy to the CdTe study above, if we annealed and a $CdTe_{1-x}S_x$ phase formed, we would expect a decrease in band gap PL energy (see fig. 4.2). To test this, we prepared three pieces of a standard sample (glass/SnO_2/CdS/CdTe(electrodeposited)), the annealing temperature after CdTe deposition was varied from for 350 °C to 460 °C. A $CdCl_2$ treatment was used after the CdTe deposition. Fig. 4.26 shows the low temperature PL spectra of the three pieces. Measurements were taken from the glass side of the pieces. The PL spectrum of the piece annealed at 350 °C shows the exciton related peak at 2.52 eV. The PL spectrum of the piece annealed at 410 °C (the standard anneal) shows that this peak has shifted to 2.54 eV. This is the opposite of what we might have expected based on diffusion. One possible explanation for the shift come from Ref. (56). Fig. 4.27 which has been reproduced from Ref. (56), shows a shift to higher energy with increasing annealing temperature is associated with a cubic to hexagonal crystalline phase transition that takes place in the CdS film. Since our sample was previously annealed at 450 °C, it is not clear whether this explanation applies. To test this interpretation, the XRD measurements would need to be done on these pieces. This will be performed as future work. Finally we didn't observe any peak around 2.5 eV in the PL spectrum of the 460 °C annealed sample. This loss in the band edge intensity is not understood but could be due to an increase in non-radiative defects.

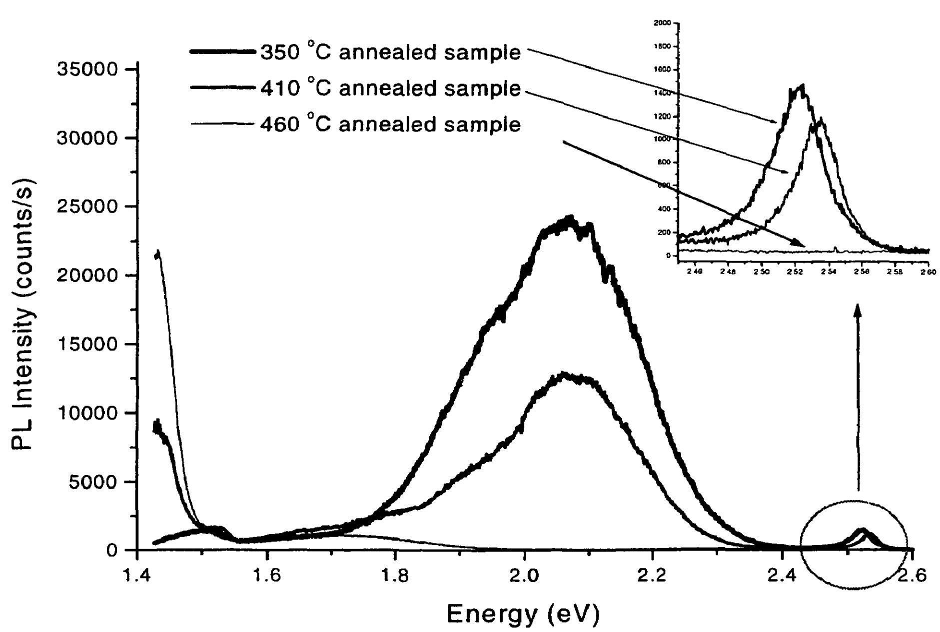

Figure 4.26 The PL spectra of the three pieces annealed at 350 °C410 °C, and 460 °C with $CdCl_2$ treatment

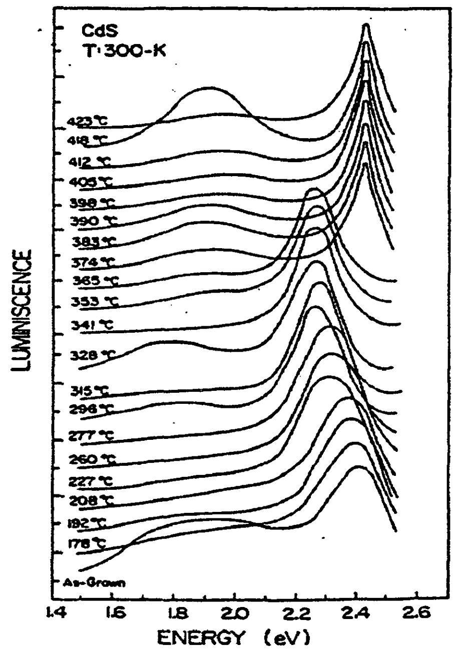

Figure 4.27 PL spectra for the as-grown CdS film, and those annealed at different temperature

In addition to the band edge features, the samples annealed at 350 °C and 410 °C exhibit the broad peak at 2.06 eV and a shoulder around 1.93 eV previously mentioned. While the energies of these features do not appear to shift with anneal temperature, the intensity decreases with annealing. At 460 °C, they are not visible. In ref. (54), these peaks are studied as a function of S-rich and Cd-rich atmospheres. It was suggested that these peaks are the strongest in a S-rich and Cd-poor environment. Based on the simple observation that S leaves CdS during the $CdCl_2$ anneal, we might expect the peak intensity to grow with increased anneal temperature and diffusion, instead we see the intensity decreases. If these peaks are indeed associated with excess S, then our simple picture of S diffusion needs to be modified. In either case, it is unlikely we can use this peak and its intensity as a signature of interdiffusion.

We observe a tail at around 1.7 eV in the PL spectra of all three samples. Within the accuracy of our measurements and fitting, the intensity and the position of the tail does not change with varying anneal temperature. In the PL spectrum of the 460 °C annealed sample, the 1.7 eV feature appears by itself because the ~2.0 eV features are absent. In Ref.(45), features in this energy range are attributed to a defect level arising from the presence of Te. If this is true, this level might provide a PL signature of interdiffusion. However, we observed a result which is going to be discussed in the next section which argues against this belief.

4.4.2 Analyzing the effects of $CdCl_2$ treatment on CdS films

We would also like to analyze the effect of the $CdCl_2$ treatment which is applied to the CdS layer after deposition and before deposition of the CdTe layer. In order to analyze this case, two samples were prepared by CBD procedure discussed above. One of the samples was annealed with $CdCl_2$ after deposition of CdS layer, the other sample was left as-deposited. Then the CdTe layer was deposited and annealed at 410 °C. These two samples were studied by x-ray and this work was previously reported in Ref. (57). Now we discuss PL measurements on the same samples. Fig.4.28 shows the PL spectra of these samples. While the PL spectrum of the $CdCl_2$ treated sample shows a form similar to our typical PL spectrum taken from glass side of the CdS/CdTe solar cell, the PL spectrum of untreated sample shows peaks at 1.74 eV and 1.51 eV. The peaks at 1.51 eV in both PL spectra are CdTe related. The X-ray work on these samples showed a change in lattice constant consistent with 4.4% Te ($CdS_{1-y}Te_y$) diffusion into CdS for the sample with no $CdCl_2$ treatment. The sample which received a $CdCl_2$ treatment; however, showed no detectable ternary formation, suggesting very little Te diffusion. Readers can find more detail on the X-ray measurements in Ref. (11,57). We notice that the PL spectrum for the sample with no $CdCl_2$ shows a strong enhancement of the 1.7 eV peak. This seems to support the work of Ref. (45) mentioned above where the peak was attributed to Te.

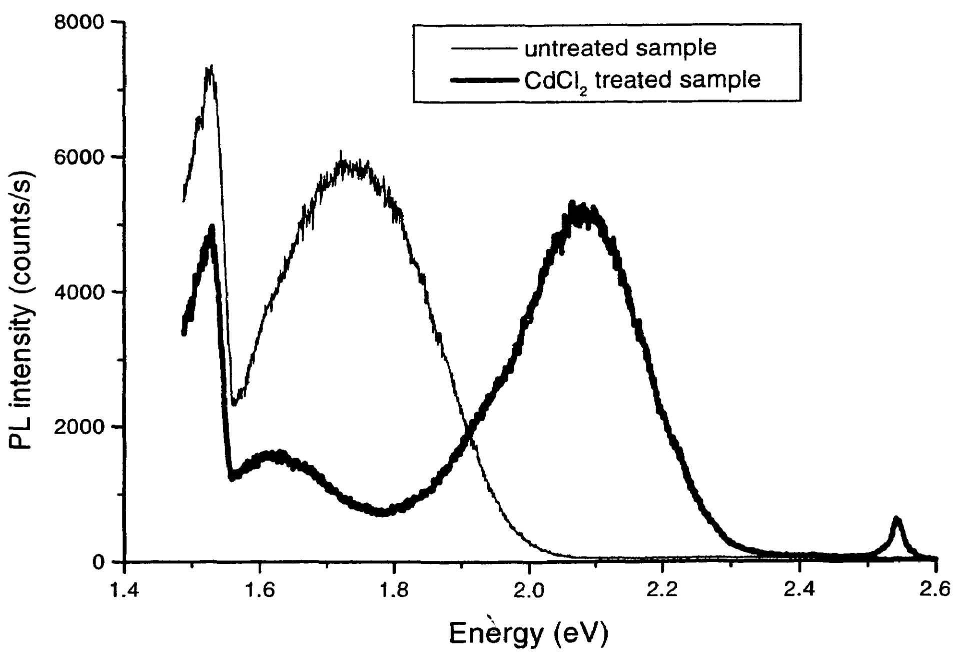

Figure 4.28 The PL spectra of CdTe/CdS films prepared with as-deposited (thin-solid line) and annealed with $CdCl_2$ treatment (thick-solid line)

In the previous section, we did experiments to clarify the origin of the tail at 1.7 eV and whether it is related to Te diffusion or not on the two samples. To test this further, we studied a sample of as-grown CdS with no anneal, $CdCl_2$ treatment, or CdTe layer. Fig. 4.29 shows the PL spectra of the as-deposited CdS compared with the as-deposited CdS with CdTe and subsequent anneal. The PL spectra of the two samples both show a strong 1.7 eV feature. This rules out interpreting this peak is due to Te. It must have an explanation in terms of some other defect.

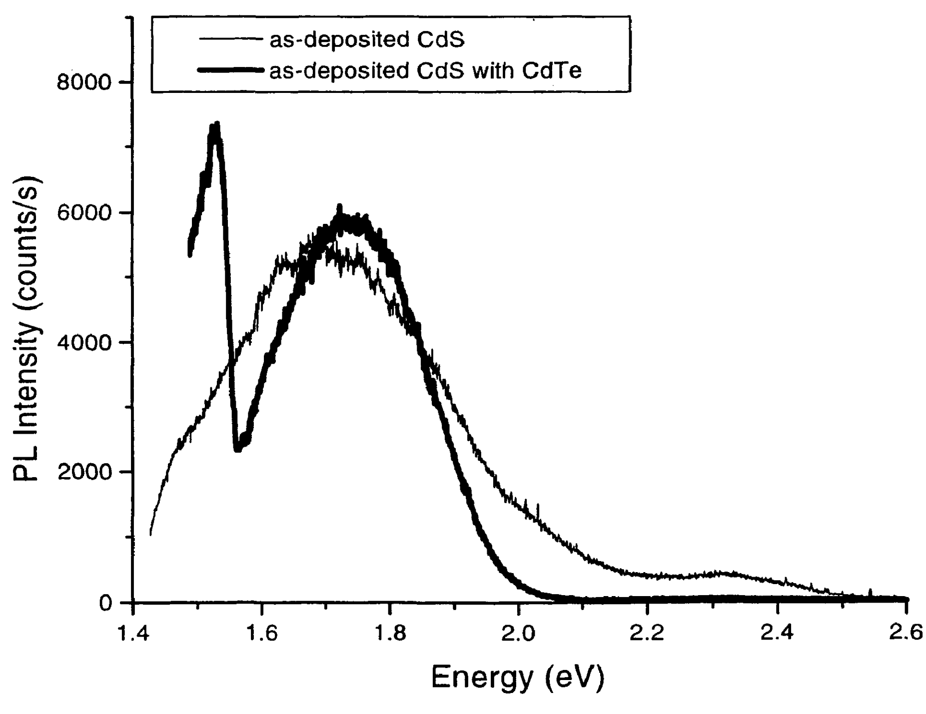

Figure 4.29 The PL spectra of as-deposited CdS and as-deposited with CdTe.

CHAPTER 5
SUMMARY AND CONCLUSION

5.1 Summary and Conclusion

This thesis presents a study of thin film CdS/CdTe solar cells using the optical characterization techniques PL and TRPL in conjunction with other techniques such as AFM, XRD, and AES. In these solar cells the active junction is formed at the interface between an n-type CdS layer and p-type CdTe layer which is basically a pn heterojunction. The annealing process following CdTe deposition is a critical step in the fabrication of high efficiency cells. Annealing temperatures are near 400 °C for maximum efficiency. A $CdCl_2$ treatment is also part of the annealing process. The formation of a $CdTe_{1-x}S_x$ alloy occurs as a result of the annealing process (40-43). Interdiffusion also occurs for CdTe deposition techniques which involve deposition temperatures near 400 °C as a result of the growth process itself. Quite a few studies in addition to ours have shown that interdiffusion across the CdS/CdTe interface produces a thin (200-300nm) layer of $CdTe_{1-x}S_x$ alloy on the CdTe side of the interface (58). The bandgap of the $CdTe_{1-x}S_x$ alloy decreases as S composition increases for the case of x <0.2. Oman (59) reported that S passivates the defects in the CdTe layer. The S diffusion at the interface of CdS/CdTe has a complicated influence on device properties and on cell efficiency. One of the goals of this thesis was to explore this interdiffusion process in much more detail.

We obtained profiles of the S concentration as a function of depth by sequentially removing the CdTe layer using Br-methanol etch solution. For PL measurements, we prepared samples such that a sequence of etching steps of various heights were etched into a single sample. We use PL measurements at low temperature to monitor the shift in the bandgap caused by S diffusion. We applied the relationship between energy gap and S content (20,44,45) to our PL measurements to estimate S content as a function of depth.

There are some important differences among XRD, AES, and PL measurements. Both XRD and AES do a volume average of the properties of the sample. In PL measurements, carriers can move distances comparable to the minority carrier diffusion length before recombining to give off light. If there are small and large band gap regions within a diffusion length of one another, the PL measurements will most likely be skewed toward to the lower bad gap region. Hence, PL tends to be more sensitive to the $CdTe_{1-x}S_x$ phase. Moreover, the S compositions estimated from PL are dependent on our choice of the PL peak position in nearly pure CdTe. Thus the changes in composition are more reliable than absolute composition. Finally by changing wavelength, the penetration depth (and thus sampling volume) of PL can be varied from many microns to a few hundred nanometers. Most of the X-ray measurement done here sample 2-3 microns. AES is quite surface sensitive although by sputtering, depth resolution is achieved.

The amount of S which diffuses into the CdTe layer changes substantially between 350 °C and 460 °C. After annealing the sample at 410°C, the PL spectrum presents two distinct CdTe and $CdTe_{1-x}S_x$ phases within the film, and the $CdTe_{1-x}S_x$ phase varies from less then 1% near the CdTe surface to 4-5% near the interface. This suggests a very inhomogeneous S distribution. We found the maximum S concentration around 5% which is quite close to the S solubility limit at 415 °C of 5.8% reported by Jensen et al (43); however, there is no reported evidence that phase segregation occurs at less than the 5.8% (fig.5.1). Hence, we should have expected diffusion to lead to a broad distribution in S composition and to one broad peak instead of two distinct sets of peaks in PL and XRD.

We know that S diffusion into CdTe preferentially occurs along grain boundaries. During the annealing process, grain regrowth will also affect the S concentration (61). Under the guidance of all this information about the S diffusion, we can give some possible explanation for the inhomogeneous S distribution. For example, when S diffusion along grain boundaries varies from boundary to boundary, the S composition within the individual crystallites will also vary. Another explanation can be that S penetration into the CdTe grain from the grain boundary can create a variation of S content across the grain. From our PL measurements (fig.4.5) on samples annealed at 410 °C, we obtained nearly pure CdTe near the unetched surface and this leads us to believe that pure CdTe and $CdTe_{1-x}S_x$ are separated further spatially, maybe in different crystallites near the unetched surface. As a future project, we are going to use PLE spectroscopy on the CdS/CdTe samples annealed at 410 °C which show two distinct CdTe and $CdTe_{1-x}S_x$ phases in PL spectra. With this discussion in mind, it may not be appropriate to refer to a CdTe " phase" and a $CdTe_{1-x}S_x$ "phase" which implies an equilibrium phase separation. It might be better to think of this as a system with two different S compositions arising from the kinetics of diffusion and regrowth.

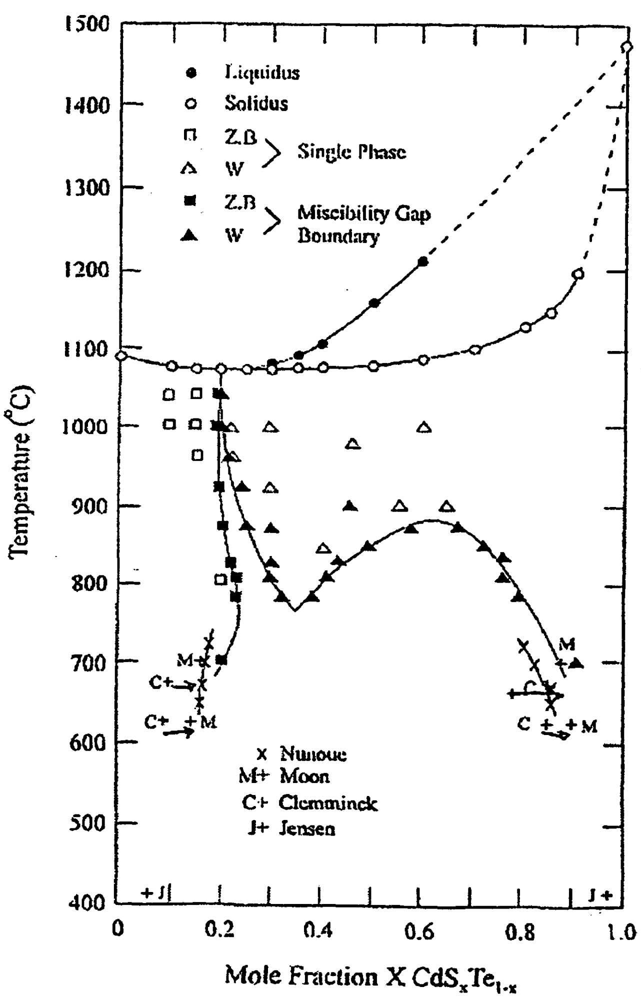

Figure 5.1 Phase Diagram for $CdTe_{1-x}S_x$ alloy, taken from Ref. (60)

Since we were able to monitor the S content as a function of depth in the CdTe layer using low temperature PL, we tried to use PL at room temperature to monitor the S diffusion into CdTe layers. There seems to be an agreement between low temperature PL and room temperature PL but more work needs to be done since the agreement involves a complicated fitting procedure.

After obtaining satisfactory results in monitoring the S composition in the CdTe layer of electrodeposited CdS/CdTe solar cells, we applied the same etching technique to CSS deposited solar cell in order to make a comparison between the two materials and to find S content in the CdTe layer as a function of depth. We found that the amount of S which diffuses into CdTe layer is less in CSS than electrodeposited CdS/CdTe solar cells which is also in agreement with Ref. (62-64). We did not see evidence for multiple compositions.

We also studied the effect of the $CdCl_2$ treatment on interdiffusion in the samples grown by electrodeposition and CSS. For electrodeposition, we found that the intensity of the ternary phase peak relative to the pure CdTe peak grows as the $CdCl_2$ exposure time increased. In CSS samples, the concentration of S at various distances from the CdTe/CdS interface is less in the absence of $CdCl_2$.

Since the interdiffusion CdTe and CdS layers consumes part of the CdS layer, and since CdS absorbs in the blue part of the optical spectrum, in general this layer is made thin to enhance the optical intensity reaching the CdTe layer. The intention is to make the CdS as thin as possible without creating pinholes. Interdiffusion makes it very difficult to control CdS layer thickness. For the thinnest CdS layers, the open circuit voltage is reduced, presumably through the formation of pinholes. We previously found that an annealing process with $CdCl_2$ treatment after CdS deposition improved cell efficiency (57). Motivated by this observation, we tried to understand the optical properties of CdS at far different annealing conditions and whether PL can be used to monitor the effect of interdiffusion on the CdS layer. We analyzed the cells from the glass side of the samples (which allowed optical access to the CdS) using low temperature PL. In the band edge PL, we observed a shift to higher energy as the post CdTe growth annealing temperature varied from 350 °C to 460 °C. This cannot be attributed to Te diffusion. We suspect a change of the structure of CdS from cubic to hexagonal (56) could cause a change in the optical properties of the cell.

Our final conclusion is that the room and low temperature PL as optical characterization techniques can give valuable information about the CdS/CdTe interface. By coupling the PL measurement with microscopic optical techniques such as NSOM, we may be able to eliminate the need for etching and provides a truly non-destructive way of monitoring the interdiffusion and profiling the S concentration.

REFERENCES CITED

1. J.A.Hutchby, R.J.Markunas, M.L.Timmons, P.K.Chiang and S.M.Bedair, 18^{th} IEEE PVSC (1985) p.20
2. J.I.Pankove, Optical Process in Semiconductors (Englwood Cliffs N.J:Prentice-Hall 1971)
3. Sheng S.Li, Semiconductor Physical Electronics, (Plenum Press, 1993)
4. A.J.Strauss, Revue de Physique Appliques Nov.21(1980) 167
5. T.R.Condelerio, S.L.Hester, T.U.Townsend and D.J.Shipman 22^{nd} IEEE PVSC (1991) p.493
6. Jasun Lee, N.C.Giles, D.Rajavel, and C.J.Summers, Phys. Rev. 49, 1668(1994)
7. J.R.Tuttle, J.S.Ward, A.Duda, T.A.Berens, M.A.Contreras, K.Ramanathan, A.L.Tennant, J.Keane, E.D.Cole, K.Emery and R.Noufi, Mat. Res. Soc. Symp. Proc., 426, 143 (1996)
8. J.R.Sites, 20th IEEE PVSC (1988), p.1604
9. H.Ohyama, T.Aramoto, S.Kumazawa, H.Higuchi, T.Arita, S.Shibutani, J.Nakajima, M.Tsuji, A.Hanafusa, T.Hibino, K.Omira and M.Murozono, 26^{th} IEEE PVSC (1997) p.343
10. T.L.Chu, S.S.Chu, J.Britt, G.Chen, C.Ferekides, N.Shultz, C.Wang, C.Q.Wu, 11^{th} Eur. Solar Energy Conf. (1992) p.988
11. W.Song, D.Mao, Y.Zhu, J.Tang, and J.Trefny, 25^{th} IEEE PVSC (1996) p.343
12. L.Kazmerski and K.A.Emery, 2^{nd} World Renewable Energy Congress Proc.,(1992) UK [10]
13. D.Albin and S.H.Risbud, Thin Solid Films 147,203 (1987)
14. D.Lincot and R.O.-Borges, J.Electrochem. Soc. 139, 1880 (1992)

15. R.B.Hall, R.W.Birkmire, E.Eser, T.L.Hench and J.D.Meakin, , 14th IEEE PVSC (1980) p.706

16. J.Skarp, Y.Koshinen, S.Lindfors, A.Rautiainen and T Suntola, 10th Eur. Solar Energy Conf. (1991) p.567

17. A.Rhotagi, R.Sudharsanan, S.A,Ringel and M.H. MacDougal, Solar Cells, 30,109 (1991)

18. S.P.Albright, B.Ackerman, J.F.Gordan, IEEE Trans. Electron Devices ED-37, 434 (1990)

19. A. Rhotagi, Int. J. Solar Energy 12, 37 (1992)

20. K.Ohata, J.Sarate and T.Tamaka, Japan J.Appl Phys 12, 1641(1973)

21. P.M.Amirtharaj, Handbook of Optical Constants of Solids II, p.655, (1991)

22. R.K.Ahrenkiel, Solid-State Electronics 35, 239 (1992)

23. R.K.Ahrenkiel, Semiconductors and Semimetals , Vol. 39, Chapter 2, p.39, (1993)

24. B.D.Cullity, Elements of X-Ray Diffraction, 2nd edition, (Addison Wesley 1978)

25. Surface Physics class notes given by Dr. Timothy Ohno (Fall 96)

26. K.O.Bogers et al. J.Electrochem. Soc. 140, 3464(1993)

27. T.C.Chu et al. J.Electrochem. Soc.139, 2443(1992)

28. I.Kon et al. J. Mater. Sci. 7, 193(1996)

29. B.R.Lanning et al., Int. J.Solar Energy, 12, 247(1992)

30. D.Lincot et al. J.Electrchem., 139,1880(1992)

31. P.C.Rieke, Chem. Mater. 5, 43(1993)

32. Yuming Zhu, PhD Thesis, (1997)

33. Scott Pozder, MSc Thesis, (1994)

34. W.Song private communication

35. D.Albin et al., Mat. Res. Soc. Symp. Proc. 410, 45(1996)

36. D.W.Niles, X.Li, P. Sheldon J.Appl. Phys. 77, 4489(1995)

37. T.A.Gessert, et al. J. Vac. Sci. Tech. A14,806(1996)

38. J.Tersoff Phys. Review Lett. 56, 2755(1986)

39. R.W.Birkmire, B.E. McCandless, and S.S.Hegedus, Int. J. Solar Energy, 12, 145(1992)

40. D.Mao, L.H.Feng, Y.Zhu, J.Tang, W.Song, R.Collins, D.L.Williamson, and J.U.Trefny in 13th NREL Photovoltaics Program Review Proc., AIP Confrence Proc. 353, p352 (1996)

41. R.G.Dhere, S.E.Asher, K.M.Jones, M.M.Al-jassim, H.R.Moutinho, D.Rose, P.Dippo, and P.Sheldon in 13th NREL Photovoltaics Program Review Proc., AIP Confrence Proc. 353, p392 (1996)

42. B.E.McCandless, R.W.Birkmire, D.G.Jensen, J.E.Phillips, and I.Youm in NREL/SNL Photovoltaics Program Review Proc., Confrence Proc. 394, p647 (1996)

43. D.G.Jensen, B.E.McCandless, and R.W.Birkmire, Proc.25th IEEE PVSC (1996) p.773

44. David Albin private communication

45. O.de Melo, M.Melendez lira, I.Hernandez Calderon, L.Benos and A.Moroles Acevedo, 1st WCPEC Proc., Hawaii, 1994, 369-372

46. D.E.Cooper, J.Bajaj, and P.R.Newman, J. of Crystal Growth 86(1998)544-551

47. D.T.F.Marple, Physical Review 150,728 (1966)

48. D.H.Levi et al., Proc.24th IEEE PVSC (1994) p.127

49. D.H.Levi et al., Proc.26th IEEE PVSC (1997) p.351

50. R.K.Ahrienkel, B.M.Keyes, L.Wang, Proc.22th IEEE PVSC (1991) p.940

51. D.Albin et al. MRS Symp. Proc. Vol.148(1998)215

52. S.D.Raevskii,and A.V.Koval, Inorganic Materials, 32, 1262(1996)

53. B.A.Kulp, Phys.Rev. 125, 1865(1962)

54. M.Agata et al., Solid State Comm. 76, 1061(1990)

55. J.J.Ramseden, S.Weber, and M.Gratzel, J. Appl. Phys., 66, 6(1989)

56. H.A.Calderon et al. J.Vac. Sci.Tech A14,4(1996)

57. W.Song at al. MRS Symp. Proc. spring 1996

58. B.E.McCandless and R.W.Birkmire, Solar Cells, 31,527(1991)

59. D.M.Oman et.al, Appl.Phys. Lett., 67, 1896(1995)

60. K. Durose et al., Invited talk for EMRS meeting (June 1998)

61. B.Qi, D.Kim, D.L.Williamson, and J.U.Trefny, J.Electrochem. Soc. 143, 517 (1996)

62. P.R.Edwards, D.P.Halliday and K.Durose, European PVSC , 2083(1997)

63. B.E.McCandless and R.W.Birkmire 26th IEEE PVSC (1997) p.307

64. S.A.Galloway, P.R.Edwards and K.Durose, Inst. Phys. Conf. Ser. 157, 579(1997)